STEALTH POLY(LACTIC-CO-GLYCOLIC ACID)-DIIODINATED BORON DIPYRROMETHENE NANOPARTICLES TO IMPROVE TUMOUR SELECTIVITY IN PHOTODYNAMIC CANCER THERAPY

VOON SIEW HUI

FACULTY OF MEDICINE
UNIVERSITY OF MALAYA
KUALA LUMPUR

2016

STEALTH POLY(LACTIC-CO-GLYCOLIC ACID)-DIIODINATED BORON DIPYRROMETHENE NANOPARTICLES TO IMPROVE TUMOUR SELECTIVITY IN PHOTODYNAMIC CANCER THERAPY

VOON SIEW HUI

THESIS SUBMITTED IN FULFILMENT OF THE REQUIREMENTS FOR THE DEGREE OF DOCTOR OF PHILOSOPHY

FACULTY OF MEDICINE
UNIVERSITY OF MALAYA
KUALA LUMPUR

2016

UNIVERSITY OF MALAYA

ORIGINAL LITERARY WORK DECLARATION

Name of Candidate: VOON SIEW HUI

Registration/Matric No: MHA 110049

Name of Degree: DOCTOR OF PHILOSOPHY

Title of Project Paper/Research Report/Dissertation/Thesis ("this Work"):

STEALTH POLY(LACTIC-CO-GLYCOLIC ACID)-DIIODINATED BORON-DIPYRROMETHENE NANOPARTICLES FOR IMPROVED ANTICANCER PHOTODYNAMIC THERAPY

Field of Study: Pharmacology

I do solemnly and sincerely declare that:

(1) I am the sole author/writer of this Work;
(2) This Work is original;
(3) Any use of any work in which copyright exists was done by way of fair dealing and for permitted purposes and any excerpt or extract from, or reference to or reproduction of any copyright work has been disclosed expressly and sufficiently and the title of the Work and its authorship have been acknowledged in this Work;
(4) I do not have any actual knowledge nor do I ought reasonably to know that the making of this work constitutes an infringement of any copyright work;
(5) I hereby assign all and every rights in the copyright to this Work to the University of Malaya ("UM"), who henceforth shall be owner of the copyright in this Work and that any reproduction or use in any form or by any means whatsoever is prohibited without the written consent of UM having been first had and obtained;
(6) I am fully aware that if in the course of making this Work I have infringed any copyright whether intentionally or otherwise, I may be subject to legal action or any other action as may be determined by UM.

Candidate's Signature Date:

Subscribed and solemnly declared before,

Witness's Signature Date:

Name:

Designation:

ABSTRACT

Poor solubility and a lack of tumour selectivity are among the main issues limiting the clinical use of photosensitisers. Thus, various nanostructures have been reported as delivery agents for photosensitisers in an attempt to overcome these obstacles. However, these delivery agents suffer from premature clearance by the reticuloendothelial system (RES) and non-specific interactions with normal cells due to their hydrophobic surface. This study attempted to circumvent these problems via the application of a low molecular weight chitosan (25 kDa) "stealth" coating onto a nanoparticle-photosensitiser construct, using the poly(lactic-co-glycolic acid)-diiodinated boron dipyrromethene (PLGA-I_2BODIPY) nanoparticle as a model. The chitosan coating altered the PLGA-I_2BODIPY nanoparticle surface to become more hydrophilic and neutral charged without changing their size (average diameter of 147 nm) and morphology. In comparison with the uncoated control, the coated nanoparticles reduced burst release of I_2BODIPY, increased cellular uptake predominantly at lysosomes and enhanced photocytotoxicity in 4T1 murine and MDA-MB-231 human breast cancer cells. PLGA-Chitosan-I_2BODIPY nanoparticles also reduced serum protein adsorption and uptake by macrophages compared to the uncoated control. In 4T1 tumour bearing mice, the PLGA-Chitosan-I_2BODIPY nanoparticles demonstrated better tumour selectivity and significantly reduced accumulation in tissues involved in RES such as lymph node, spleen and liver (by 10.2-, 2.1- and 1.3-fold, respectively), as well as non-tumour organs such as skin and eyes (by 22.7- and 4-fold, respectively) as compared to non-coated control. The PLGA-Chitosan-I2BODIPY and PLGA-I_2BODIPY nanoparticles also showed increased therapeutic efficacy compared to free I_2BODIPY. In conclusion, low molecular weight chitosan (25 kDa) is a promising "stealth coating" to evade premature RES clearance and improved tumour selectivity of PLGA nanoparticles.

ABSTRAK

Ketelarutan terhad dan kekurangan pemilihan barah adalah antara isu utama yang menghadkan penggunaan fotosensitiser secara klinikal. Maka, pelbagai nanostruktur telah dilaporkan sebagai agen penghantaran untuk fotosensitiser sebagai usaha untuk menangani halangan-halangan ini. Walau bagaimanapun, agen-agen penghantaran ini biasanya menghadapi masalah penyingkiran awal oleh sistem reticuloendothelial (RES) dan interaksi-interaksi tidak spesifik dengan sel-sel normal disebabkan oleh permukaannya yang hidrofobik. Di sini, kajian penyelidikan ini telah dijalankan bagi percubaan untuk megatasi masalah-masalah ini dengan menggunakan kitosan dengan berat molekul rendah (25 kDa) sebagai salutan "stealth" ke atas model nanopartikel-fotosensitiser, iaitu "poly(lactic-co-glycolic acid)-diiodinated boron dipyrromethene" (PLGA-I_2BODIPY). Salutan kitosan telah meningkatkan ciri hidrofilik dan mengurangkan caj permukaan nanopartikel PLGA-I_2BODIPY tanpa mengubah saiz (purata diameter 147 nm) atau morfologi nanopartikel. Berbanding dengan nanopartikel kawalan ("control") tanpa salutan, nanopartikel yang bersalut mempamerkan pengurangan pelepasan I_2BODIPY dalam jumlah besar, meningkatkan pengambilan sel terutamanya dalam lisosom, dan meningkatkan foto-sitotoksisiti dalam sel-sel barah payudara bagi mencit 4T1 dan manusia MDA-MB-231. Nanopartikel PLGA-Chitosan-I_2BODIPY juga mengurangkan penyerapan protein serum dan pengambilan oleh makrofaj berbanding dengan nanopartikel kawalan tanpa salutan. Dalam mencit yang diinduksikan 4T1 barah, nanopartikel PLGA-Chitosan-I_2BODIPY menunjukkan pemilihan barah yang lebih baik; pengurangan pengumpulan secara ketara dalam tisu RES juga diperhatikan berbanding dengan bahan kawalan tanpa salutan, termasuk nod limfa, limpa dan hati (dengan 10.2-, 2.1- dan 1.3 kali ganda masing-masing) dan organ bukan barah seperti kulit dan mata (dengan 22.7- dan 4 kali ganda masing-masing). PLGA-Chitosan-I_2BODIPY dan PLGA-I_2BODIPY nanopartikel juga menunjukkan

peningkatan keberkesanan antibarah berbanding dengan I_2BODIPY sahaja. Keputusan-keputusan ini menunjukkan bahawa kitosan dengan berat molekul rendah (25 kDa) adalah salutan “stealth” yang menjanjikan bagi nanopartikel PLGA untuk mengelakkan penyingkiran awal oleh RES dan juga meningkatkan pemilihan barah.

ACKNOWLEDGEMENTS

I would never have been able to finish my dissertation without the guidance of my supervisors, help from the head of department and friends, and support from my family.

I would like to express my gratitude to my supervisors, Prof. Dr. Chung Lip Yong and Dr. Kiew Lik Voon, and my project consultant, Dr. Lee Hong Boon, for their excellent guidance, caring, patience, patiently corrected my writing and financially supported my research. I must acknowledge the Head of Department (Pharmacology), Prof. Dr. Nor Azizan Abdullah, for her generosity, providing me with a comfortable work station with an excellent atmosphere for doing research.

I would like to thank Kue Chin Siang, who as a labmate, was always willing to help and give his best suggestions. I would also like to thank my former coursemates Loh Ping Yeap, Chong Si Zhe, Lisa Chai, Teoh Phaik Ju, Loi Cheng Swee, Sim Boon Chai, William Cheong, Tan Boon Chiew and Loo Shu Cheng for always cheer me up with all the funny messages in the chat group. Also not forget my school friends, Sharon Chong, Jennifer Ho, Pui Mei Phing, Tay Boom Seng, Gan Eng Seng, Chen Eng Pao, Kane Hansel Bong, Liu Sai Kwong, Tan Boon Tiong, Kalvin Chong, Chai Chu Ann and Jong Kuet Yong, for spamming humorous text messages in our chat group almost every day. Life would have been dull without them.

I would also like to thank my mother for her constant and loving support over the years.

In conclusion, I recognise that this research would not have been possible without the financial assistance of High Impact Research Grants, Ministry of Higher Education Malaysia (UM.C/625/1/HIR/MOHE/MED/17 and UM.C/625/1/HIR/MOHE/MED/33) and MyPhD scholarship.

TABLE OF CONTENTS

Abstract iv

Abstrak v

Acknowledgements vii

Table of Contents viii

List of Figures xiii

List of Tables xv

List of Symbols and Abbreviations xvi

List of Appendices xviii

CHAPTER 1: INTRODUCTION 1

1.1 Overview 1

1.2 Aim and Objectives 4

CHAPTER 2: LITERATURE REVIEW 6

2.1 Photodynamic Therapy (PDT) 6

2.1.1 History and development 6

2.1.2 Mechanism 7

2.1.3 Limitation of PDT 9

2.2 Roles of Nanoparticles in PDT 11

2.2.1 Selective drug delivery 11

2.2.2 The fundamentals of EPR effect 12

2.2.3 History and Development of EPR effect 14

2.2.4 Future perspective on passive targeting 15

2.2.5 Nanoparticles in PDT 23

2.2.5.1 Liposomes 23

2.2.5.2 Micelles 24
2.2.5.3 Polymer-based Nanoparticles 29
2.2.5.4 Lipoprotein Nanoparticles 34
2.2.5.5 Inorganic Nanoparticles 35
2.2.6 Problems in drug delivery development based on EPR effect 39
2.2.6.1 Opsonization and phagocytosis 40
2.3 Stealth coating of nanoparticle drug delivery systems 42
2.3.1 Peglyation for stealth coating and its limitation 43
2.3.2 Limitations of PEG coating 43
2.3.2.1 Interference with cellular uptake and endosomal escape of nanoparticles 43
2.3.2.2 Anti-PEG antibodies and immune reponses 44
2.3.2.3 PEG-associated cytoplasmic vacuolation 44

CHAPTER 3: MATERIALS AND METHODS 46

3.1 Materials, reagents and solvents 46
3.2 Equipments 46
3.3 Photosensitisers 47
3.4 Production of low molecular-weight chitosans 47
3.5 Characterisation of low molecular-weight chitosans 48
3.5.1 Determination of average molecular weight of chitosans 48
3.5.2 Estimation of chitosan solubility 48
3.6 Preparation of I_2BODIPY loaded PLGA (PLGA-I_2BODIPY) nanoparticles 49
3.7 Preparation of chitosan coated PLGA-I_2BODIPY (PLGA-Chitosan-I_2BODIPY) nanoparticles 49

3.8 Characterisation of PLGA-I_2BODIPY and PLGA-Chitosan-I_2BODIPY nanoparticles 51
3.8.1 Process yield 51
3.8.2 I_2BODIPY loading and encapsulation efficiency 51
3.8.3 Particle size and zeta potential 52
3.8.4 Particle size and morphology 52
3.9 Biocompatibility of PLGA-Chitosan-I_2BODIPY and PLGA-I_2BODIPY nanoparticles: Haemolysis Test 53
3.10 Evaluation of Protein Adsorption to Particle Surface 53
3.11 Photophysical and photochemical characterisation of free I_2BODIPY, PLGA-I_2BODIPY and PLGA-Chitosan-I_2BODIPY nanoparticles 54
3.11.1 UV-visible and fluorescence emission spectra 54
3.11.2 Chemical detection of singlet oxygen 54
3.12 *In vitro* I_2BODIPY release in phosphate buffer saline (PBS) and plasma 55
3.13 *In vitro* photocytotoxicity of PLGA-Chitosan-I_2BODIPY and PLGA-I_2BODIPY nanoparticles 56
3.14 Cellular uptake of PLGA-Chitosan-I_2BODIPY and PLGA-I_2BODIPY nanoparticles 57
3.15 Intracellular localization of PLGA-Chitosan-I_2BODIPY and PLGA-I_2BODIPY nanoparticles 58
3.16 Animal model 59
3.16.1 Toxicity profiles of free I_2BODIPY, PLGA-Chitosan-I_2BODIPY and PLGA-I_2BODIPY nanoparticles 59
3.16.2 *In vivo* biodistribution studies in 4T1 tumour-bearing mice 59
3.16.3 *In vivo* PDT efficacy studies in 4T1 tumour-bearing mice 60
3.17 Statistical analysis 62

CHAPTER 4: RESULTS.....63

4.1 Production and characterisation of low molecular weight chitosans.....63

4.2 Characterisation of PLGA-I_2BODIPY and PLGA-Chitosan-I_2BODIPY nanoparticles.....65

4.2.1 Process yield, I_2BODIPY loading and encapsulation efficiency, and chitosan coating characterisation.....65

4.2.2 Particle size, size distribution and zeta potential.....65

4.2.3 Particle size and morphology.....68

4.2.4 Biocompatibility of PLGA-Chitosan-I_2BODIPY and PLGA-I_2BODIPY nanoparticles: Haemolysis Test.....70

4.2.5 Evaluation of Protein Adsorption to Particle Surface.....71

4.3 Photophysical and photochemical characterisation.....72

4.3.1 UV-visible and fluorescence emission spectra.....72

4.3.2 Singlet oxygen detection by a chemical method.....75

4.4 *In vitro* I_2BODIPY release in PBS and plasma.....76

4.5 *In vitro* photocytotoxicity of PLGA-Chitosan-I_2BODIPY and PLGA-I_2BODIPY nanoparticles.....79

4.6 Cellular uptake of PLGA-Chitosan-I_2BODIPY and PLGA-I_2BODIPY nanoparticles.....82

4.7 Intracellular localization of PLGA-Chitosan-I_2BODIPY and PLGA-I_2BODIPY nanoparticles.....86

4.8 Animal model.....88

4.8.1 Toxicity profiles of free I_2BODIPY, PLGA-Chitosan-I_2BODIPY and PLGA-I_2BODIPY nanoparticles.....88

4.8.2 *In vivo* biodistribution studies in 4T1 tumour-bearing mice.....89

4.8.3 *In vivo* PDT antitumour efficacy studies in 4T1 tumour-bearing mice.....93

CHAPTER 5: DISCUSSION 97

CHAPTER 6: CONCLUSION, GENERAL LIMITATIONS AND FUTURE PERSPECTIVES 106

6.1 Conclusion 106

6.2 General limitations 106

6.3 Future perspectives 106

References 109

List of Publications and Papers Presented 134

Appendices 137

LIST OF FIGURES

Figure 2.1: The photosensitisation process illustrated by a modified Jablonski diagram. 9

Figure 2.2: Passive targeting of nanoparticles via EPR effect 13

Figure 2.3: Liposomes 24

Figure 2.4: Polymeric micelles 26

Figure 2.5: PEG-lipid micelles 27

Figure 2.6: Cremophor EL 29

Figure 2.7: Chemical structure of polylactic-co-glycolic acid). 31

Figure 2.8: Poly(lactic-co-glycolic acid) (PLGA) nanoparticles 31

Figure 2.9: Dendrimer 33

Figure 2.10: Chitosan nanoparticles 34

Figure 2.11: Lipoprotein nanoparticles 35

Figure 2.12: Silica nanoparticles 37

Figure 2.13: Gold nanoparticles 38

Figure 2.14: Calcium phosphosilicate nanoparticle 39

Figure 3.1: Chemical structure of I_2BODIPY 47

Figure 3.2: Chemical structure of chitosan. 48

Figure 4.1: Debye plot for chitosan of average molecular weight (A) 5, (B) 10, and (C) 25 kDa. 64

Figure 4.2: Particle size distribution PLGA-Chitosan-I_2BODIPY (25 kDa chitosan) and PLGA-I_2BODIPY nanoparticles 66

Figure 4.3: Zeta potential of PLGA-I_2BODIPY nanoparticles upon coating of chitosan (25 kDa) 67

Figure 4.4: Particle size distribution of PLGA-Chitosan and PLGA nanoparticles over 30 days 68

Figure 4.5: Morphology of PLGA-Chitosan-I_2BODIPY and PLGA-I_2BODIPY nanoparticles under scanning electron microscopy.....69

Figure 4.6: Haemolysis at different concentration of PLGA and PLGA-Chitosan (5, 10 and 25 kDa) nanoparticles.....70

Figure 4.7: Protein adsorbed on nanoparticles surface 72

Figure 4.8: UV-visible spectra of PLGA-Chitosan-I_2BODIPY, PLGA-I_2BODIPY nanoparticles and free I_2BODIPY in (A) acetone, (B) methanol and (C) PBS.....74

Figure 4.9: UV-visible, fluorescence excitation and fluorescence emission spectra of (A) PLGA-Chitosan-I_2BODIPY (B) PLGA-I_2BODIPY and (C) free I_2BODIPY in methanol 74

Figure 4.10: Singlet oxygen generation detected by using ADPA as a sensor according to irradiation time.....76

Figure 4.11: *In vitro* release profiles of PLGA-Chitosan-I_2BODIPY and PLGA-I_2BODIPY nanoparticles in PBS at pH 7.4 and 4.8 78

Figure 4.12: *In vitro* release profiles of PLGA-Chitosan-I_2BODIPY and PLGA-I_2BODIPY nanoparticles in plasma 79

Figure 4.13: *In vitro* photocytoxicity of free I_2BODIPY, PLGA-Chitosan-I_2BODIPY and PLGA-I_2BODIPY nanoparticles on (A) 4T1 cells and (B) MDA-MB-231 cells 81

Figure 4.14: Cellular uptake of free I_2BODIPY, PLGA-Chitosan-I_2BODIPY and PLGA-I_2BODIPY nanoparticles in 4T1 cells.....84

Figure 4.15: Cellular uptake of free I_2BODIPY, PLGA-Chitosan-I_2BODIPY and PLGA-I_2BODIPY nanoparticles in RAW246.7 macrophages. 85

Figure 4.16: Intracellular localization of (A) PLGA-Chitosan-I_2BODIPY nanoparticles (20 µM of free I_2BODIPY), (B) PLGA-I_2BODIPY nanoparticles (20 µM of free I_2BODIPY) and (C) free I_2BODIPY (20 µM) in 4T1 cells.....87

Figure 4.17: *In vivo* toxicity profile in BALB/c mice.....89

Figure 4.18: *In vivo* biodistribution studies in 4T1 tumour-bearing mice 92

Figure 4.19: *In vivo* PDT efficacy studies in 4T1 tumour-bearing mice 96

Figure 5.1: Summary of the stealth properties of chitosan coating on PLGA-I2BODIPY that improved tumour selectivity in photodynamic cancer therapy.....104

LIST OF TABLES

Table 2.1: *In Vivo* Studies Reported on Nanostructure-Based Photosensitiser Formulations. 17

Table 2.2: *In Vivo* Characteristics of Nanostructures and Their Regulatory Approval Status for Clinical Use 19

Table 4.1: Composition and physical-chemical parameters of PLGA-Chitosan and PLGA NP 66

Table 4.2: IC_{50} value of tested NP and free I_2BODIPY in 4T1 and MDA-MB-231 cancer cells after different incubation time of 2, 4 and 6 h and PDT 82

LIST OF SYMBOLS AND ABBREVIATIONS

$^1O_2$	:	Singlet oxygen
$^3O_2$	:	Triplet oxygen
ALA	:	Aminolevulinic acid
AlClPc	:	Aluminium chloride phthalocyanine
CME	:	Clathrin-mediated endocytosis
DLI	:	Drug light interval
DMSO	:	Dimethyl sulfoxide
EPR	:	Enhanced permeability and retention
FDA	:	Food and drug administration
HPMA	:	N-(2-hydroxypropyl)methacrylamide
i.v.	:	Intravenous
I_2BODIPY	:	Diiodinated boron dipyrromethene
IC_{50}	:	Half maximal inhibitory concentration
mM	:	Millimolar
MTT	:	3-(4,5-dimethylthiazol-2-yl)-2,5-diphenyltetrazolium bromide
MW	:	Molecular weight
NIPAM	:	N-iso-propylacrylamide
nm	:	nanometre
NP	:	Nanoparticle
O_2-	:	Superoxide anion radical
PBS	:	Phosphate buffered saline
PDT	:	Photodynamic therapy
PEG	:	Polyethylene glycol
PLGA	:	Poly(lactic-co-glycolic acid)

PSD	:	Particle size distribution
PVA	:	Polyvinyl alcohol
RES	:	Reticuloendothelial system
RGD	:	Arginylglycylaspartic acid
ROS	:	Reactive oxygen species
s.c.	:	Subcutaneous
SD	:	Standard deviation
SEM	:	Standard error mean
UV-Vis	:	Ultraviolet-visible
w/v	:	Weight to volume
w/w	:	Weight to weight
λ_{abs}	:	Wavelength absorption maxima
λ_{em}	:	Wavelength emission maxima

LIST OF APPENDICES

Appendix A: Synthesis and Characterisation of Diiodinated-Boron Dipyrromethene ……... 137

Appendix B: Animal Ethics Approval Letter ……. 139

CHAPTER 1: INTRODUCTION

1.1 Overview

Photodynamic therapy (PDT) emerged as a treatment modality for neoplastic and non-malignant lesions of the head and neck, brain, lung, pancreas, bladder, breast, prostate and skin (Agostinis *et al.*, 2011; Dolmans *et al.*, 2003; Fayter *et al.*, 2010; Gao *et al.*, 2010). PDT involved administration of a photosensitiser followed by irradiation at its excitation wavelength (Dolmans *et al.*, 2003; Dougherty *et al.*, 1998). In the presence of molecular oxygen, the excited photosensitisers generate highly reactive singlet oxygen that leads to localized tumour cell death, damage to the microvasculature, and induction of a local inflammatory reaction (Agostinis *et al.*, 2011; Dolmans *et al.*, 2003; Juarranz *et al.*, 2008). The damage caused is highly localized due to the short half-life of singlet oxygen of about 3 μs (Moan & Berg, 1991).

However, the hydrophobic nature of photosensitisers causes them to aggregate in aqueous media, deterring the generation of singlet oxygen (Chen & Zhang, 2006; Kuznetsova *et al.*, 2003) and administration via intravenous route (Trindade *et al.*, 2001). Besides, photosensitisers have poor tumour selectivity and caused adverse generalised photosensitivities in patients (Josefsen & Boyle, 2008a). A widely used photosensitiser, porfimer sodium, causes prolonged skin and eye photosensitivity up to 4 – 12 weeks at its therapeutic dose (Breskey *et al.*, 2013; Triesscheijn *et al.*, 2006).

To improve the outcome of PDT, various nanoparticle delivery systems such as liposomes, polymeric nanoparticles, lipoprotein nanoparticles and inorganic nanoparticles have been evaluated in attempts to improve photosensitiser biodistributions and efficacies (Bugaj, 2011; Master *et al.*, 2013; Voon *et al.*, 2014). These carriers were able to prevent aggregation in blood by protecting the photosensitisers from the hydrophilic environment (Wang *et al.*, 2011a) and thereby

improve their singlet oxygen generation efficiency (Chen & Zhang, 2006). Dissemination of photosensitisers to normal organs was reduced (Konan-Kouakou *et al.*, 2005) and accumulation in tumour tissue was increased via the enhanced permeability and retention (EPR) effect (Chatterjee *et al.*, 2008), or via attachment of specific targeting ligands that direct and bind conjugates to tumour cells (Barth *et al.*, 2011; Gary-Bobo *et al.*, 2011; Kue *et al.*, 2015). This has leads to enhanced antitumour efficacy as well as minimized generalised photosensitivities to the skin and eyes (Solban *et al.*, 2006; Verma *et al.*, 2007). However, these nanoparticles were subjected to opsonisation and premature clearance from the circulation by the reticuloendothelial system (RES), and the Kupffer cells in the liver, due to their hydrophobic and charged surfaces (Carrstensen *et al.*, 1992; Norman *et al.*, 1992; Roser *et al.*, 1998; Salmaso & Caliceti, 2013). This leads to the necessity to design a tumour-targeted nanoparticle with non-immunogenic stealth characteristics.

Since opsonins interact with nanoparticles by van der Waals, ionic and hydrophobic/hydrophilic forces, the surface properties of nanoparticles play a key role in the opsonization process. Hydrophobic and charged particles undergo higher opsonization in comparison with hydrophilic and neutral charged particles (Carrstensen *et al.*, 1992; Müller *et al.*, 1992; Norman *et al.*, 1992; Roser *et al.*, 1998; Salmaso & Caliceti, 2013). In this study, the use of water-soluble low molecular weight chitosan as a hydrophilic "stealth" coating was evaluated on a photosensitiser-nanoconstruct, using poly(lactic-co-glycolic acid)-boron dipyrromethene (PLGA-I_2BODIPY) nanoparticle as a model, to prevent premature clearance from systemic circulation, and thus enhancing the tumour target selectivity and antitumour efficacy of I_2BODIPY. PLGA is a biocompatible and biodegradable co-polymer approved by the US FDA (Lu *et al.*, 2009) and has been widely used for delivery of antitumour agents including photosensitisers (Fadel *et al.*, 2010; Konan-Kouakou *et al.*, 2005; Vargas *et al.*, 2004). Chitosan is a

linear copolymer of glucosamine and *N*-acetylglucosamine with a high degree of *N*-deacetylation. Nanomaterials based on chitosan have emerged as potential tissue engineering scaffolds (Wang *et al.*, 2013), antimicrobial agents (Wang *et al.*, 2003), and drug carriers for proteins, peptides, genes, small molecules and combinational drugs because chitosan has good biodegradability, biocompatibility and non-immunogenicity (Ding *et al.*, 2014; Yang *et al.*, 2014). Despite applications as a food additive (Ilium, 1998) and in wound dressings (Dash *et al.*, 2011; Schipper *et al.*, 1999), chitosan has not been approved for drug delivery (Kean & Thanou, 2010) mainly because its inherent positive charge at physiological pH leads to non-specific interactions with the negatively charged cell membranes, particularly red blood cells and endothelial cells. However, the cationic properties of chitosan allow the adjustment of nanoparticle surface charge by controlling the degree of coating (Cheng *et al.*, 2009; Kafshgari *et al.*, 2015; Kean *et al.*, 2005). This study set out to prove that surface coating of negatively charged PLGA nanoparticles with low molecular weight chitosan could reduce their overall negative charges, thereby, reducing charge-based non-specific interactions. In other words, we set out to explore if low molecular weight chitosan could be used as a stealth coating to evade the immune surveillance system.

Most of studies on chitosan nanomaterials have been performed in *in vitro* system (Yang *et al.*, 2014). Chitosan-modified PLGA nanoparticles were reported to provide sustained drug delivery in an *in vitro* model (Chronopoulou *et al.*, 2013), improve intracellular uptake in tumor cells (Chakravarthi & Robinson, 2011; Kim *et al.*, 2008; Tahara *et al.*, 2009), and be assembled with hydroxyapatite nanoparticles via electrostatic forces to form an injectable colloidal bone tissue filler (Wang *et al.*, 2013). PLGA nanoparticles that were surface-modified with chitosan and alginates were used as biodegradable colloidal gels for injecting human umbilical cord mesenchymal stem cells (Wang *et al.*, 2011), and also to deliver an immunomodulating peptide in a

controlled release manner as a vaccine-like therapeutic *in vivo* (Buyuktimkin *et al.*, 2012). Chitosan-coated dextran nanoparticles that encapsulated insulin and glucose-specific enzymes was used to formulate an injectable nano-network with the oppositely charged alginate-coated nanoparticles as glucose-mediated insulin delivery (Gu *et al.*, 2013). To the best of our knowledge, this is the first study of PLGA nanoparticles coated with *low molecular weight* chitosan for enhancing the tumour selectivity and the stealth effect on the RES system *in vitro* and *in vivo*.

1.2 Aim and Objectives

The aim of this study is to investigate the stealth properties and tumour selectivity of chitosan-coated poly(lactic-co-glycolic acid) (PLGA) nanoparticles as a delivery agent for diiodinated-boron dipyrromethene (I_2BODIPY) as well as the ability of these nanoparticles to improve the antitumour efficacy of I_2BODIPY for photodynamic cancer therapy.

The specific objectives of this study are as follows:

i. To prepare chitosan-coated PLGA-I_2BODIPY and PLGA-I_2BODIPY nanoparticles
ii. To characterize the physicochemical and photochemical properties of chitosan-coated PLGA-I_2BODIPY and PLGA-I_2BODIPY nanoparticles
iii. To investigate the haemo-biocompatibility and protein adsorption on the chitosan-coated PLGA-I_2BODIPY and PLGA-I_2BODIPY nanoparticles
iv. To determine the *in vitro* photocytotoxicity profile, intracellular uptake and localization of chitosan-coated PLGA-I_2BODIPY and PLGA-I_2BODIPY nanoparticles

v. To determine the *in vivo* toxicity profile, biodistribution and antitumour effect of chitosan-coated PLGA-I_2BODIPY and PLGA-I_2BODIPY nanoparticles in tumour-bearing mice

CHAPTER 2: LITERATURE REVIEW

2.1 Photodynamic Therapy (PDT)

2.1.1 History and development

Photodynamic therapy (PDT) emerged as a treatment modality for neoplastic and non-malignant lesions after it was reported by Dougherty *et al.* in 1975 that a combination of red light and porfimer sodium (hematoporphyrin derivatives) could completely eradicate mouse mammary tumour growth. Clinical trials were then conducted in 1978 by Dougherty *et al.* with successful outcome when porfimer sodium was used to treat bladder cancer and skin tumours. Subsequently, clinical trials involved other cancer types were conducted, including breast, colon, prostate, squamous cells, basal cells, endometrium, malignant melanoma, mycosis fungoides, chondrosarcoma and angiosarcoma (Agostinis *et al.*, 2011).

In 1993, porfimer sodium (Photofrin®; Axcan Pharma Inc., Mont-Saint-Hilaire, Canada) was approved for clinical use in Canada to treat bladder cancer (Triesscheijn *et al.*, 2006). At present, a number of anticancer photosensitizing drugs have been approved for clinical use, including Foscan (temoporfin, meta-tetrahydroxyphenylchlorin; Biolitec AG), Visudyne (verteporfin, benzoporphyrin derivative monoacid ring A; Novartis Pharmaceuticals), Levulan (5-aminolevulinic acid; DUSA Pharmaceuticals, Inc.), and most recently, Metvix (methyl aminolevulinate; PhotoCure ASA) (Voon *et al.*, 2014).

PDT has been proven effective in early lung cancer (Kato, 1998), Barrett's esophagus (Hur *et al.*, 2003), bladder cancer (Skyrme *et al.*, 2005), head and neck cancers (Schuller *et al.*, 1985), and skin cancer (Rhodes *et al.*, 2004). PDT is also used to treat prostatic carcinoma, intraperitoneal disseminated ovarian cancer and unresectable mesothelioma (Chatterjee *et al.*, 2008). However, PDT has been less effective with

squamous cell skin carcinoma and melanoma, mainly because the light of wavelengths currently employed are unable to reach the entire tumour as these tumours penetrate deeply into the skin. There were also clinical trials of PDT as an adjunctive therapy for brain tumours to reduce residual tumour burden after surgical resection of tumour.

Recent advancement in laser technology also enables irradiation at difficult-to-reach areas using different light sources including endoscopy, bronchoscopy or other similar apparatus channeling light by optical fibers. PDT is under investigation for early stage nasopharyngeal tumours using a special trans-nasal light delivery system, biliary trees tumours using intra-ductal optical fiber and pancreatic cancer using laparoscopy (Chatterjee *et al.*, 2008).

PDT has several advantages compared to conventional cancer therapy. PDT is localized and can be targeted accurately compared to chemotherapy. Regeneration of normal tissue can be achieved with PDT in contrast to surgical methods due to sparing of extracellular matrix and PDT allows repetitive dosing without cumulative toxicity in contrast to radiotherapy (Chatterjee *et al.*, 2008). Higher cost-effectiveness and cure rates were reported in palliative treatment of head and neck cancer (Hopper *et al.*, 2004) or Barrett's esophagus (Hur *et al.*, 2003) than surgical methods and chemotherapy. Besides, PDT is an outpatient therapy and does not require hospitalisation. PDT also can induce immunity, in contrast to most other cancer therapy, and thus contributes to long term tumour control. Therefore, PDT is useful either as a treatment modality or as an adjuvant therapy for neoplastic and non-malignant lesions.

2.1.2 Mechanism

PDT involves the administration of a light-sensitive photosensitiser followed by irradiation of tumour loci with light of appropriate wavelength to activate the specific photosensitiser. The interaction between light, photosensitisers and oxygen involve a

series of energy transitions in order to generate singlet oxygen as illustrated in Figure 2.1. Upon light irradiation at wavelengths of the photosensitiser absorption maxima, the photosensitiser will transform from its ground state into excited singlet state. This excited singlet state photosensitiser is very unstable and may decay directly back to ground state by emitting fluorescence, which can be used as a photodiagnostic tool clinically. Otherwise, the photosensitiser will undergo intersystem crossing to its more stable triplet state. To return to its ground singlet state, the photosensitiser at the triplet state may either emit phosphorescence or decay without radiation through Type I and Type II reactions (Agostinis *et al.*, 2011; Dolmans *et al.*, 2003).

To obtain a therapeutic photodynamic effect, the photosensitiser needs to transfer its energy to molecular oxygen, which is unique in being a triplet in its ground state ($^3O_2$). This leads to the formation of the highly reactive singlet oxygen ($^1O_2$), which is the main damaging species generated during PDT, and the reaction is referred to as a Type II process. Alternatively, a Type I process can also occur whereby the photosensitiser acquires an electron or hydrogen atom by reacting with an organic molecule in a cellular microenvironment, to form radicals or radical ions which can interact with oxygen to produce superoxide anion radicals (O_2^-). Superoxide itself does not cause oxidative damage to biological system but it can undergo reduction by superoxide dismutase to form hydrogen peroxide (H_2O_2), which can be converted to highly oxidative hydroxyl radical (•OH) by ferrous ion (Fe^{2+}) present in the body. Reactive oxygen species (ROS) generation via Type II chemistry is mechanistically much simpler than Type I. Most photosensitisers are believed to undergo Type II reactions rather than Type I (Agostinis *et al.*, 2011; Castano *et al.*, 2004; Triesscheijn *et al.*, 2006).

Due to the high reactivity and short half-life of singlet oxygen and hydroxyl radicals, the photodynamic damaged caused is highly confined to the location of the

photosensitisers. The half-life of singlet oxygen in biological system is about 3 μs, and hence, limiting its diffusion to only approximately 10 – 55 nm in cells (Agostinis *et al.*, 2011; Dysart & Patterson, 2005; Moan & Berg, 1991). In cancer treatment, PDT can destroy tumour cells directly, damage vasculature surrounding tumour cells and activates immunological responses against tumours (Juarranz *et al.*, 2008).

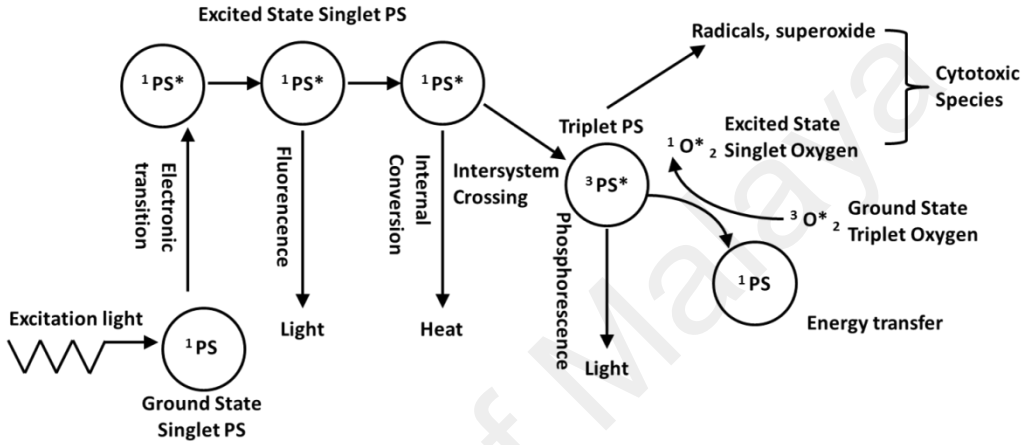

Figure 2.1: The photosensitisation process illustrated by a modified Jablonski diagram.

Upon light irradiation at an appropriate wavelength, ground singlet state photosensitiser (^{1}PS) is transformed to excited singlet state (^{1}PS*). The excited photosensitisers were may undergo intersystem crossing to form excited triplet state (^{3}PS*) and transfer its energy to molecular oxygen ($^3O_2$) to produce singlet oxygen ($^1O_2$), which is the main damaging species in PDT. This diagram is adapted from Castano *et al.* (2004).

2.1.3 Limitation of PDT

PDT has remained at best a fringe cancer treatment option as it is limited by high initial setup cost, lack of standard protocols established by randomised trials, inaccessibility of deep seated tumours, comparable effective cure rates with conventional therapy and skin photosensitivity for prolonged periods following treatment (Chatterjee *et al.*, 2008; Voon *et al.*, 2014). For instance, porfimer sodium

causes skin photosensitivity lasting for up to 4–12 weeks at its therapeutic dose (Triesscheijn *et al.*, 2006). The limitation due to high cost of setup and standardisation of treatment protocols may remain in the initial period until this method of treatment gained greater popularity with the availability of cheaper lasers and optic fiber equipment.

The effectiveness of PDT is mainly determined by the efficiency of singlet oxygen production upon light activation (Chen & Zhang, 2006) and the selective delivery of photosensitiser to the target site at its therapeutic concentrations with minimal uptake by non-tumour organs (Konan-Kouakou *et al.*, 2005). The generation of singlet oxygen depends on the chemistry of the photosensitiser used, light intensity and wavelength as well as the oxygen concentration (Agostinis *et al.*, 2011). Most of the photosensitisers are hydrophobic and form aggregates easily in aqueous media, deterring the singlet oxygen generation (Kuznetsova *et al.*, 2003) and intravenous delivery strategies (Trindade *et al.*, 2001). The low tumour selectivity of photosensitisers also leads to undesired generalised photosensitivity following treatment, especially in the skin and eye (Breskey *et al.*, 2013; Josefsen & Boyle, 2008a; Triesscheijn *et al.*, 2006).

For instance, some boron dipyrromethene (BODIPY)-based systems have been reported to have excellent PDT attributes including favorable extinction coefficients, light-to-dark toxicity ratios, antitumour efficacies *in vivo*, and body clearance (Awuah & You, 2012; Byrne *et al.*, 2009; Kamkaew *et al.*, 2013; Lim *et al.*, 2010; Yogo *et al.*, 2005). Of these, diiodinated-boron dipyrromethene (I_2BODIPY) (Kue *et al.*, 2015; Lim *et al.*, 2010), has all these attributes, and was used as a model photosensitiser in this paper. However, BODIPY are highly hydrophobic and not inherently inclined to localize in tumours (Kue *et al.*, 2015).

Recently, active targeting has been reported to increase the affinity of the photosensitiser for tumour tissue (Hudson *et al.*, 2005; Josefsen & Boyle, 2008b; Kue *et al.*, 2015). These targeting strategies by attaching specific ligands to direct and bind conjugates to tumour cells have led to newer generation of photosensitisers. Another approach to target the photosensitisers to the tumour sites in the body is through passive targeting via EPR effect, by using a nanocarrier.

2.2 Roles of Nanoparticles in PDT

2.2.1 Selective drug delivery

Delivery of photosensitisers is one of the main challenges in PDT as the photosensitisers are highly hydrophobic and lack selectivity to the targeted tumour site. By incorporating photosensitisers into nanoparticles, it can protect the photosensitisers from the aqueous environment without alteration of its activity, allows administration in monomeric form and prevents aggregation in blood which can reduce their singlet oxygen quantum yields (Chen *et al.*, 2006). The nanocarriers should enable selective accumulation of the photosensitisers within the tumour area in therapeutic concentration via an enhanced permeability and retention (EPR) effect with minimal uptake of non-tumour organs in order to enhance the antitumour efficacy and reduce non-specific phototoxicity, especially to the skin and eyes (Chatterjee *et al.*, 2008; Solban *et al.*, 2006; Verma *et al.*, 2007). Ideally, the carrier system should also have minimum immunogenicity to prevent premature clearance from the circulation (Salmaso & Caliceti, 2013).

Accumulation via EPR effect elevates the level of nanostructure-based photosensitisers either in proximity to the tumour tissue or inside the cells upon cellular uptake. Majority of cellular uptake of nanoparticles occur through a process known as clathrin-mediated endocytosis (CME) (Harush-Frenkel *et al.*, 2007; Vasir &

Labhasetwar, 2008; Yameen *et al.*, 2014). The attachment of cancer-targeting moieties such as folic-acid (Idris *et al.*, 2012), F3 peptide (Reddy *et al.*, 2006) or RGD peptide (Kopelman *et al.*, 2005) to the nano-drug carriers can further enhance selectivity for tumours. Chemical modification on the structures of the nano-drug carriers may also confer alternate means for energy transfer to photosensitisers, which enables the use of deep tissue-penetrating light for the activation of the photosensitisers to treat deeply seated tumours (Chatterjee & Yong, 2008; Wang *et al.*, 2011).

2.2.2 The fundamentals of EPR effect

Passive targeting via EPR effect makes use of the anatomical and physiological differences between normal and tumour tissue to facilitate selective delivery of nanoparticles to the targeted tumour area (Figure 2.2) (Misra *et al.*, 2010). The normal vasculature present is insufficient to supply the oxygen and nutrients to the fast-growing and hyperproliferative cancer cells to maintain growth. This causes the tumour cells to secrete growth factors that trigger the rapid development of new irregular blood vessels in a process called angiogenesis (Bates *et al.*, 2002). Unlike the normal vasculature with tight endothelial lining, blood vessels in tumour have discontinuous epithelial lining and lack basal membrane, both of which result in the formation of large gaps between the adjacent endothelial cells (Figure 2.2) (Jain, 1998; Jain & Stylianopoulos, 2010). These large gaps or fenestrations can reach the size ranging from 200 to 2000 nm, depending on the tumour type, environment and localization (Hobbs *et al.*, 1998). When the blood components or nanoparticles reach the abnormal tumour vascular bed, these large fenestrations give little resistance to extravasation to the tumour interstitium. To enhance the permeation of nanoparticles into the tumour area by prolonging their circulation time, the size of nanoparticles should be larger than 6 nm in diameter, which is the threshold of renal clearance (Soo Choi *et al.*, 2007). These represent the *enhanced permeation* component of the EPR effect.

In normal tissues, lymphatic drainage is important to allow continuous flowing and renewal of interstitial fluid as well as to transport extravasated solutes and colloids from tissues back to the circulatory system. Extracellular fluid is constantly drained to the lymphatic vessels at a mean flow velocity around 0.1 – 2 μm/s in normal tissues (Swartz & Fleury, 2007). However, the lymphatic function is impaired in tumours, which leads to minimal uptake of the interstitial fluid and hindered the transport of colloids back to the circulation (Ji, 2005; Padera *et al.*, 2004). Due to the larger dynamic radii of macromolecules and nanoparticles, they are not able to diffuse and be reabsorbed back to the blood circulation like other small molecules that are less than 4 nm (Figure 2.2) (Jain, 1987; Noguchi *et al.*, 1998; Swartz, 2001). Thus, nanoparticles will accumulate in the tumour interstitium for a prolonged period. This denotes the *enhanced retention* portion of the EPR effect.

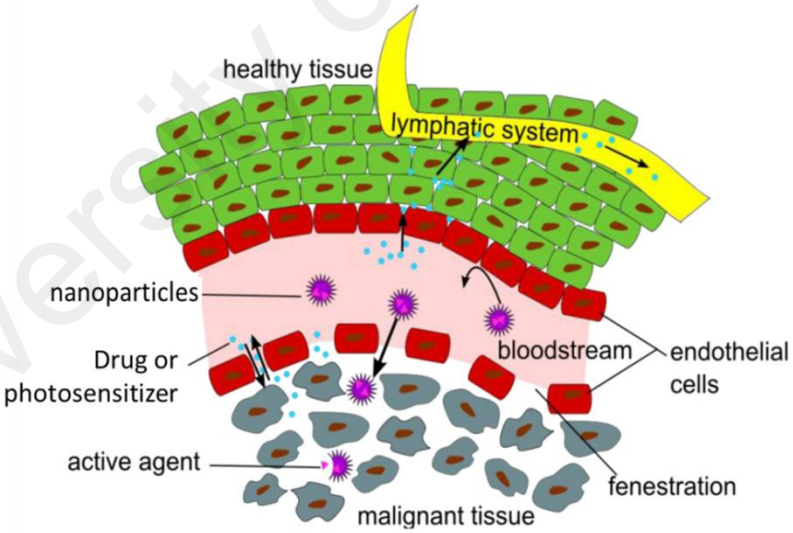

Figure 2.2: Passive targeting of nanoparticles via EPR effect

The selective distribution and accumulation of nanoparticles in tumour via EPR effects results from two distinct phenomena: the extravasation through fenestration of abnormal vasculature of tumour tissues and defective lymphatic drainage. This figure is adapted from Stockhofe *et al.* (2014).

2.2.3 History and Development of EPR effect

More than 30 years ago, Maeda *et al.* had witnessed the phenomenon that certain macromolecules accumulate preferentially at the tumours (Matsumura & Maeda, 1986). In 1979, the first synthesis of the poly(Styrene-co-Maleic Acid)-NeoCarzinoStatin (SMANCS), a polymer conjugate that non-covalently binds to the anticancer protein NeoCarzinoStatin (NCS), was reported to accumulate to a greater extent than unconjugated NCS in tumour tissues (Li & Huang, 2008; Maeda *et al.*, 1979). Besides, this polymer-protein conjugates also prolonged plasma half-life, up to 200 times longer compared to unmodified free NCS or other low molecular weight drugs (Maeda *et al.*, 1984). This has led Maeda *et al.* to further investigate the phenomenon with other plasma proteins of different molecular sizes. Using labelled albumin and other proteins besides the polymer conjugates, they demonstrated that proteins larger than 40 kDa and IgG (160 kDa) could selectively accumulated more in tumour tissues than normal tissues and these proteins remained in tumour tissues for prolonged periods of time (Matsumura & Maeda, 1986). The accumulation of most polymeric macromolecules in tumour tissues was more than 10 – 200 times higher than that in normal tissues, such as skin, muscle, heart and kidney (Duncan, 2003; Fang *et al.*, 2003; Greish *et al.*, 2005; Greish *et al.*, 2004; H. Maeda, 2001; Vicent *et al.*, 2009). This preferential distribution and accumulation of nano-sized macromolucules at tumour area was due to the presence of fenestration in the leaky tumour vasculature and the poor lymphatic drainage in the tissue, a phenomenon known as enhanced permeability and retention (EPR) effect.

In 1993, SMANCS, which is based on the EPR effect, had become the first macromolecular anticancer drug approved for use in clinical settings (Fang *et al.*, 2011). Since then, numerous studies have been reported on delivery of anticancer drugs to different tumour types based on the EPR effects, using liposomes, polymers conjugates and various types of nanoparticles on different tumour types. Table 2.1 gives an

overview on the nanostructure-based photosensitisers that have advanced into the *in vivo* evaluation stage and the animal models employed. The *in vivo* characteristics of the nanostructures in term of biodegradability, clearance, side effects and their regulatory approval status for clinical use are summarised in Table 2.2.

2.2.4 Future perspective on passive targeting

Over the past decades, EPR plays an important role in the delivery of nanomaterials to tumors. However, the degree of interpatient variability and the importance of tumor heterogeneity in the EPR effect in humans are yet to be fully understood (Prabhakar *et al.*, 2013). The individual patients and cancer types benefiting the most from the nanocarriers-mediated drug delivery may need to be identified.

The effectiveness of passive targeting was determined by the physicochemical properties of the nanomaterial and tumor biology. Precise understanding and control of the physicochemical properties of nanomaterials, and possibly fine tuning of the tumour microenvironment may improve the EPR effect in humans (Carmeliet & Jain, 2011; Zhang *et al.*, 2012). In the era of modern cancer biology, assessing the tumour microenvironment in individual patients and predicting their susceptibility to the EPR effect may eventually become the mainstay of therapy when choosing between therapeutic regimens. Despite the difficulties to predict the markers that have better correlations with nanoparticles efficacy in humans, relationships will mostly likely delineate as tumor genotyping and bioassays continue to develop (Bertrand *et al.*, 2014).

The EPR phenomenon affects the distribution of the nanocarrier to the tumour but it may not increase the ability of the drug to reach its pharmacological target site. The optimization of the efficacy of nanocarriers also involves optimal drug release rates (Karnik *et al.*, 2008). Without specific affinity of the nanomaterial for tumor cells, the chemotherapeutic payloads will have difficulties to reach their pharmacological targets

or risk diffusing back into the vasculature (Dreher *et al.*, 2006). Conversely, drugs that have sufficient affinity for their pharmacological target remain trapped in the tumor for prolonged period of time. For instance, the high affinity of docetaxel for the microtubules translates into very low efflux from the tumor; consequently, the elimination half-life of the drug from tumours is approximately 15 – 20 times higher than its elimination from the blood and normal tissue (Bissery *et al.*, 1995). Therefore, the behavior of drugs and their affinity for the intratumoral environment are crucial when designing passively-targeted nanoparticles and the optimal drug release profiles should be optimized on individual basis (Ullal *et al.*, 2011).

Furthermore, most macromolecular drugs, including nucleic acids and some proteins are not able to permeate through the cell membrane readily and reach their pharmacological target (Bertrand *et al.*, 2014). For these cases, modification of the nanocarriers with targeting ligands may increase the affinity of the nanocarriers for tumour cells, increasing its tumour accumulation time and thereby, allow drug-loaded nanocarriers to efficiently enter the cells via receptor-mediated endocytosis.

Table 2.1: *In Vivo* Studies Reported on Nanostructure-Based Photosensitiser Formulations.

Nanostructure	Photosensitiser	Animal model
LIPOSOMES	Photofrin (porfimer sodium); hyprocrellin A; metatetra(hydroxyphenyl) chlorin (mTHPC); Verteporfin	Athymic (nude) rats (strain Cr: NIH-rna) implanted with U87 glioma cells through craniectomy[a]; male Kunming mice transplanted with S-180 sarcoma[b]; female Foxn1$^{nu/nu}$ mice injected subcutaneously with EMT6 cells[c]; male BALB/c mice injected subcutaneously with Meth-A sarcoma cells[d]
MICELLES		
Polymer Micelles	Aluminum chloride phthalocyanine (AlClPc); protophorphyrin IX (PpIX)	Mice with squamous cell carcinoma (SCC7) tumour[e]; Balb/c mice implanted with EMT-6 tumours[f]
PEG-Lipid Micelles	Verteporfin; *meso*-tetraphenylporphine (TPP)	Female C57BL/6 mice injected subcutaneously with LLC cells[g]; male DBA/2 mice implanted with rhabdomyosarcoma (M1) tumour cells[h]
Cremophor® EL	Temocene; azabodipy	DBA/2 mice inoculated with the DBA/2 mastocytoma cell line P815[i]; Balb/c mice inoculated with the Balb/c colon adenocarcinoma cell line CT26.CL25 (ATCC, CRL-2639)[i]; female Balb/c nu/nu mice injected with MDA-MB-231-GFP cells[j]
POLYMER-BASED NANOPARTICLES		
Poly(lactic-Co-Glycolic Acid) (PLGA)	Zinc phthalocyanine; verteporfin	Female albino mice injected with Ehrlich ascites carcinoma cells[k]; male DBA/2 mice implanted with rhabdomyosarcoma (M1) tumour[l]
Dendrimers	Aminolevulinic acid (ALA); phthalocyanine	Male BALB/c mice injected with the LM3 cell line[m] (Casas *et al.*, 2009); female nude mice (BALB/c nu/nu) subcutaneously transplanted with subcutaneous A549 tumour cells[n] (Nishiyama *et al.*, 2009)

Ref: [a](Jiang *et al.*, 1998); [b](Wang *et al.*, 1999); [c](Lassalle *et al.*, 2009); [d](Ichikawa *et al.*, 2004); [e](Koo *et al.*, 2010); [f](Le Garrec *et al.*, 2002); [g](Roby *et al.*, 2007); [h](Zhang *et al.*, 2003); [i](Garc á-D áz *et al.*, 2012); [j](Byrne *et al.*, 2009); [k](Fadel *et al.*, 2010); [l](Konan-Kouakou *et al.*, 2005); [m](Casas *et al.*, 2009); [n](Nishiyama *et al.*, 2009)

Table 2.1 continued

Nanostructure	Photosensitiser	Animal model
POLYMER-BASED NANOPARTICLES (continued)		
Chitosan	Protophorphyrin IX (PpIX); chlorin e_6	Athymic nude mice inoculated with SCC7 cells[o]; athymic nude mice injected with HT-29 human colon adenocarcinoma cells[p,q]
LIPOPROTEIN NANOPARTICLES	Bacteriochlorin e_6 bisoleate (Bchl-BOA)	Female athymic nude mice inoculated with HepG2 cells[r]
INORGANIC NANOPARTICLES		
Silica	Protophorphyrin IX (PpIX); methylene blue; zinc phthalocyanine	Male athymic Nude-Foxn1^{nu} mice subcutaneously implanted with glioblastoma multiforme[s]; female athymic Swiss nude mice and female athymic Naval Medical Research Institute nude mice injected subcutaneously with HCT 116 and A549 cells, respectively[s]; male athymic BALB/c (Balb/C-nu) mice inoculated subcutaneously with Hela cells[t]; female BALB/c nude mice implanted with H22 cells[u]; female Swiss nude mice xenografted with HCT-116 cells[v]
Gold	Silicon phthalocyanine 4; porphyrin-brucine conjugates; Chlorin e_6	NuNu mice subcutaneously injected with basaloid squamous cell carcinoma PE/CA-PJ34 cells[w]; mice with MDA-MB-435 tumour[x]
Calcium Phosphosilicate	Indocyanine green (ICG)	Female C3H/HeJ mice injected with 32D-p210-GFP cells[y]

Ref: [o](Lee *et al.*, 2009); [p](S. J. Lee, H. Koo, D.-E. Lee, *et al.*, 2011); [q](S. J. Lee, H. Koo, H. Jeong, *et al.*, 2011); [r](Marotta *et al.*, 2011); [s](Simon *et al.*, 2010); [t](He *et al.*, 2009); [u](Tu *et al.*, 2012); [v](Gary-Bobo *et al.*, 2011); [w](Cheng *et al.*, 2008); [x](S. Wang *et al.*, 2013); [y](Barth *et al.*, 2011)

Table 2.2: *In Vivo* Characteristics of Nanostructures and Their Regulatory Approval Status for Clinical Use

Nanostructure	Biodegradability	Metabolism & Clearance	Side Effects	FDA Approval Status for PDT use	Regulatory Approval Status for other anticancer drugs
LIPOSOMES	Yes	Vesicle opsonization by serum protein and subsequent uptake by the reticuloendothelial system; Complement-mediated phagocytosis by Kupffer and endothelial cells of the liver as well as other phagocytic cells of the reticuloendothelial system[a]	NA	Yes Clinically approved: Visudyne® (Verteporfin) to treat age-related macular degeneration Phase I & II clinical trials: CGP 55847 (liposomal zinc(II)-phthalocyanine) for cancer treatment [b,c]	Clinically approved: Doxil® (Doxorubicin) [US, EU][d,e] DaunoXome® (Daunorubicin citrate) [US][e,f] Depocyt® (Cytarabine) [US, EU][g] (Glantz *et al.*, 1999) Mepact® (Mifamurtide) [EU][h] Marqibo® (Vincristine sulfate) [On market][i,j]
MICELLES					
Polymer Micelles	No	Degradation of polymer micelles, resulting in the formation of block copolymer unimers, which can be removed via renal excretion if the polymer chains are designed with a lower molecular weight than the critical value for renal filtration less than ~20 – 40 kDa[k]	Slow extravazation; Risk of chronic liver toxicity due to prolonged circulation and slower metabolism of drug which may exhibit toxic side effects[k]	No	Clinically approved: Taxotere® (Docetaxel) [EU, US][f] Phase II clinical trials: SP1049C (Pluronic block-copolymer doxorubicin)[f,l]

Ref: [a](M. Longmire *et al.*, 2008); [b](Isele *et al.*, 1994); [c](Ochsner, 1996); [d](Heidel & Davis, 2011); [e](Wang *et al.*, 2012); [f](Heidel & Davis, 2011); [g](Glantz *et al.*, 1999); [h](Anderson *et al.*, 2010); [i](Rodriguez *et al.*, 2009); [j](Zamboni, 2008); [k](Yokoyama, 2011); [l](Valle *et al.*, 2011)

Abbreviation: NA – not available

Table 2.2 continued

Nanostructure	Biodegradability	Metabolism & Clearance	Side Effects	FDA Approval Status for PDT use	Regulatory Approval Status for other anticancer drugs
MICELLES (continued)					
PEG-Lipid Micelles	NA	NA	NA	No	NA
Cremophor® EL	Slow	May be largely degraded in the blood compartment by serum carboxylesterase-induced degradation, causing a gradual release of the ricinoleic acid residues attached to the triglyceride structure; Hepatobiliary elimination; Less than 0.1% of administered dose via urinary excretion[m]	Associated with severe anaphylactoid hypersensitivity reactions, hyperlipidaemia, abnormal lipoprotein patterns, aggregation of erythrocytes and peripheral neuropathy[m]	No	Clinically approved: Taxol® (Paclitaxel) [US][f] Phase II Clinical Trials: WST09 (TOOKAD) in Cremophor® EL formulation[n] Phase I Clinical Trias: Silicon Phthalocyanine Pc 4 in Cremophor® EL formulation[o]
POLYMER-BASED NANOPARTICLES					
Dendrimers	NA	Renal clearance for dendrimers with diameter 3 – 10 nm[a]	NA	No	Phase III clinical trials: SH L 643A (Gadolinium) for diagnostic imaging[p]
Chitosan	Yes	Mainly degraded by lysozyme through the hydrolysis of the acetylated residues[q]	NA	No	NA

Ref: [m](Gelderblom *et al.*, 2001); [n](Weersink *et al.*, 2005); [o](Kinsella *et al.*, 2011); [p](Herborn *et al.*, 2003); [q](Markovsky *et al.*, 2012)

Abbreviation: NA – not available

Table 2.2 continued

Nanostructure	Biodegradability	Metabolism & Clearance	Side Effects	FDA Approval Status for PDT use	Regulatory Approval Status for other anticancer drugs
POLYMER-BASED NANOPARTICLES (continued)					
Poly(lactic-Co-Glycolic Acid) (PLGA)	Yes	Undergo hydrolysis and biodegrades into lactic and glycolic acids. Lactic acid enters the tricarboxylic acid cycle and is metabolised and subsequently eliminated from the body as carbon dioxide and water. Glycolic acid is either excreted unchanged in the kidney or enters the tricarboxylic acid cycle and is eventually eliminated as carbon dioxide and water[r]	NA	Approved by the US FDA for use in drug delivery[s]	NA
LIPOPROTEIN NANOPARTICLES	Yes	Catabolised by the endothelium-associated lipoprotein lipase , thereby generating free fatty acids, which are taken up by the liver, muscle, and adipose tissues[t]	NA	No	NA

Ref: [r](Muthu, 2009); [s](Makadia & Siegel, 2011); [t](Kwan *et al.*, 2007)

Abbreviation: NA – not available

Table 2.2 continued

Nanostructure	Biodegradability	Metabolism & Clearance	Side Effects	FDA Approval Status for PDT use	Regulatory Approval Status for other anticancer drugs
INORGANIC NANOPARTICLES					
Silica	Slow	Gradual biodegradation results in the formation of water-soluble salts of silicic acid, which are excreted by the kidney; Hepatobiliary excretion[u]	Caused granuloma formation in the organs of the reticulo-endothelial system, such as liver and spleen[u,v]	No	NA
Gold	No	Renal clearance for particles with diameter < 10 nm[a]	NA	No	Phase I clinical trials: AuroShell® (gold nanoparticle) for laser therapy[w]
Calcium Phosphosilicate	No	Hepatobiliary clearance with minimal acute renal involvement[x]	NA	No	NA

Ref: [u](Ivanov *et al.*, 2012); [v](Kumar *et al.*, 2010); [w](Jain *et al.*, 2012); [x](Altinoglu *et al.*, 2008)

Abbreviation: NA – not available

2.2.5 Nanoparticles in PDT

2.2.5.1 Liposomes

Liposomes are spherical, closed membranes composed of concentric phospholipid bilayers with an aqueous inner compartment and have an average diameter of 70 – 100 nm (Kozlowska *et al.*, 2009). Lipophilic photosensitisers were incorporated into the lipid bilayer of liposomes to prevent aggregation in an aqueous environment and improve their solubility (Figure 2.3) (Samad *et al.*, 2007).

Liposome-delivered Photofrin had demonstrated an increase by 2.4 and 6-fold accumulation at tumour tissue in U87 glioma and 9L gliosarcoma nude mice models, respectively, in comparison with Photofrin administered in a dextrose formulation. Tumour tissue necrosis was significantly increased as well in both tumour types after PDT compared to the controls (Jiang *et al.*, 1998; Jiang *et al.*, 1997).

Liposome-hypocrellin A treated S-180 sarcoma Kunming mice also showed higher maximal accumulation in tumour at 12 h by 3.4 fold compared to the group treated with hypocrellin A-DMSO. Enhanced tumour regression in liposome-hypocrellin A treated group was observed at day 7 post-PDT with relative regression percent of tumour, RRP of 87% whereas hypocrellin A-DMSO treatment group only showed RRP of 14% (Wang *et al.*, 1999).

These liposomes of 70 – 100 nm led to an increase in passive accumulation in the tumours via the enhanced permeability and retention effect. However, the main drawback of conventional liposomes is that they are easily taken up by cells of the reticuloendothelial system after systemic administration. This results in their rapid removal from the blood into the liver and spleen, which in turn reduces the accumulation in the tumour tissue (Lasic *et al.*, 1991). Some liposome modifications have been reported to counteract these delivery problems. For instance, polyethylene

glycol has been added to liposomal surfaces to create more stable "sheathed" forms. Such PEGylation may protect liposomes from being recognised by opsonins and taken up by the reticuloendothelial system (Huwyler *et al.*, 2008). However, the increased stability provided by this type of modification of the liposomes may also decrease the liposome-cell interactions and reduce the transfer of the photosensitiser payload into tumour cells (Gijsens *et al.*, 2002).

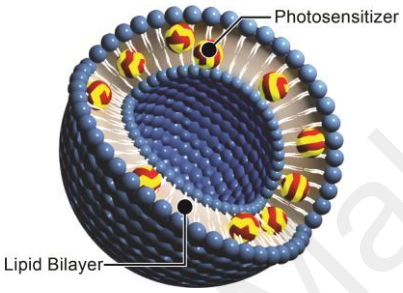

Figure 2.3: Liposomes

Liposomes are spherical, closed membranes composed of concentric phospholipid bilayers with an aqueous inner compartment. Size: 70 – 100 nm. This figure is adapted from Voon *et al.* (2014).

2.2.5.2 Micelles

Micelles are aggregates of surfactant molecules dispersed in a liquid colloid with their hydrophilic head regions are in contact with the surrounding aqueous environment and the hydrophobic tails clumps into the center. They assemble in a spherical form with the size ranging normally within 5 – 100 nm. Micelles are widely used to carry hydrophobic drugs, physically entrapped or covalently bound to the hydrophobic center core, and deliver them to tumour tissue via passive EPR effect or active targeting strategies (Torchilin, 2004; van Nostrum, 2004). Micelles can be divided into two categories depending on the nature of the amphiphilic core: polymeric or lipid micelles.

Polymeric micelles consists of block copolymers whereas lipid micelles are form hydrophilic polymers conjugated to lipids.

(a) ***Polymeric micelles***

Polymer micelles are formed from amphiphilic block or graft copolymers consisting of hydrophilic and hydrophobic monomeric units, which form their corona and core, respectively, in an aqueous solution. These self-assembly structure can deliver the hydrophobic photosensitisers by entrapping them in the centre core and reduce uptake by reticuloendothelial system with the hydrophilic palisades of tethered polymer chain surrounding the photosensitiser-loaded core (Figure 2.4) (Jones & Leroux, 1999; Kataoka *et al.*, 2001; Kwon & Okano, 1996).

In SCC7 tumour-bearing mice treated with pH-responsive methoxy polyethylene glycol-poly(*β*-amino ester) block copolymer micelles (pH-PMs) encapsulating protophorphyrin IX (PpIX), the uptake of PpIX by tumour tissues was 10-fold higher than free PpIX treated group at 48 h post-administration. Strongest fluorescence was observed in tumour tissues while uptake of PpIX-pH-PMs in other non-tumour organs were not significant except in liver and kidney, where PpIX is metabolized. Koo *et al.* suggested that the PpIX-pH-PMs reduced the uptake by RES as in comparison, free PpIX exhibited strong signals mainly in the liver whereas tumour tissues only presented a very weak fluorescence signals that could not be clearly distinguished from the body. In terms of antitumour efficacy, complete tumour ablation occurred in mice treated with PpIXx-pH-PMs while tumour growth continued in free PpIX treated group. Histological examinations revealed that most of the tumour cells in the mice treated with PpIX-pH-PMs were severely damaged or destroyed at day 10 after treatment, while incomplete tumour cell death was observed in the mice treated with free PpIX (Koo *et al.*, 2010).

N-iso-Propylacrylamide (NIPAM) copolymer micelles loaded with alumunium chloride phthalocyanine (AlClPc) were copolymerised with pH-sensitive methacrylic acid for tumour targeting properties and *N*-vinyl-2-pyrrolidone as a non-ionic hydrophilic shield for stealth properties (Le Garrec *et al.*, 2002). This formulation does not increase tumoural uptake of AlClPc over the Cremophor EL formulation (1.8–2% vs. 2.4% AlClPc of injected dose/g, respectively) in mice bearing intradermal EMT-6 tumours. The PDT antitumour efficacies of both formulations were similar where no tumour recurrence was observed in 80% of treated mice. However, these modified NIPAM polymeric micelles served as a good alternative to Cremophor EL for the administration of poorly water-soluble phthalocyanines for PDT due to their low toxicity and strong affinity for AlClPc.

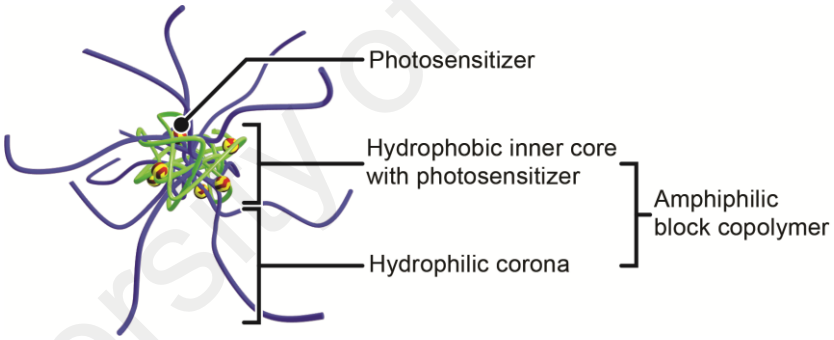

Figure 2.4: Polymeric micelles

Polymer micelles are formed from amphiphilic block or graft copolymers consisting of hydrophilic and hydrophobic monomeric units, which form their corona and core, respectively, in an aqueous solution. Size: 30 – 122 nm. This figure is adapted from Voon *et al.* (2014).

(b) ***Polyethylene Glycol-Lipid Micelles***

Polyethylene glycol-lipid micelles consist of polyethylene glycol conjugated to a relatively short but hydrophobic diacyl phospholipid moiety such as phosphatidyl ethanolamine (Lukyanov & Torchilin, 2004). The hydrophobic photosensitisers (Roby

et al., 2006, 2007; Skidan *et al.*, 2008) bind to the phosphatidyl ethanolamine and the polyethylene glycol provides "stealth" properties to prevent rapid uptake of the micelles by the RES (Figure 2.5) (Klibanov *et al.*, 1990; Senior *et al.*, 1991).

The monoclonal antibodies 2C5 (MAb 2C5) were attached to the polyethylene-glycol-lipid micelles to target surface-bound nucleosomes, which are released from apoptotically dying cancer cells. Meso-tetraphenylporphine (TPP) delivered with these antibody-targeted micelles were found to have 2 – 3 fold improved tumoural accumulation compared to non-targeted micelles in female C57BL/6 mice induced subcutaneously with Lewis lung carcinoma cells. Complete inhibition of tumour growth until day 35 post-PDT treatment was reported in mice treated with TPP-loaded MAb 2C5-polyethylene-glycol-lipid immunomicelles whereas those without antibody targeting micelles only reduced tumour growth by 50%. Treatment with free TPP, on the other hand, only caused slight tumour growth suppression compared to the untreated controls. Histological examination of tumours revealed significantly higher tumour cell death in mice treated with TPP-loaded antibody-targeted micelles (Roby *et al.*, 2007).

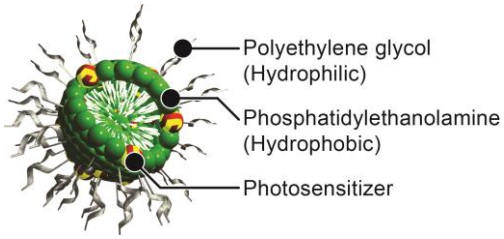

Figure 2.5: PEG-lipid micelles

Polyethylene glycol-lipid micelles consist of polyethylene glycol conjugated to a relatively short but hydrophobic diacyl phospholipid moiety. Size: 13 – 30 nm. This figure is adapted from Voon *et al.* (2014).

(c) ***Cremophor EL***

Cremophor EL is a self-assembling micelle containing glycerol polyethylene glycol ricinoleate. It is used to solubilise hydrophobic photosensitisers and promote their distribution into plasma lipoprotein (Figure 2.6) (Kessel, 1992). Cremophor EL in combination with ethanol was used to solubilise photosensitisers such as TOOKAD (Rück *et al.*, 2005), phthalocyanine (Whitacre *et al.*, 2000), purpurin (Kessel, 1989) and azabodipy-based photosensitisers (Byrne *et al.*, 2009). However, the use of Cremophor EL *in vivo* is associated with anaphylactic hypersensitivity reaction and neurotoxicity which is the major downside of Cremophor EL (Gelderblom *et al.*, 2001). Nevertheless, it is still widely used in early preclinical studies as it conveniently and efficiently emulsifies lipophilic entities.

Temocene incorporated in Cremophor EL micelles was reported to demonstrate better *in vivo* antitumour response than free temocene. After treatment with temocene-loaded Cremophor EL micelles, total remission of tumours was observed for 40 and 60 days in BALB/c mice subcutaneously inoculated with CT26.CL25 tumour cells and DBA/2 mice inoculated with mastocytoma cells P815, respectively (García-Díaz *et al.*, 2012). Cremophor EL micelles were also used to deliver a lead BF2-azadipyrromethene molecule, ADMP06, targeting the mammary tumour vasculature (Byrne *et al.*, 2009). After PDT treatment, 71% of treated nude mice inoculated with MDA-MB-231-GFP cells demonstrated tumour ablation with no recurrence for 6 months.

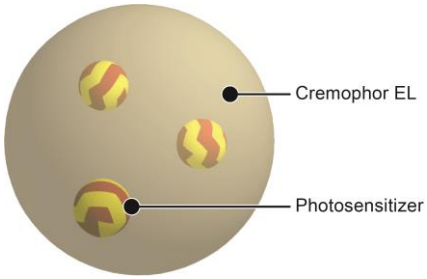

Figure 2.6: Cremophor EL

Cremophor EL is a self-assembling micelle containing glycerol polyethylene glycol ricinoleate. Size: 30 nm. This figure is adapted from Voon *et al.* (2014).

2.2.5.3 Polymer-based Nanoparticles

Polymer-based nanoparticles can have good aqueous dispersions, high drug-loading capacities and sustained release properties. They can also undergo modifications to alter their particle size, surface charge and able to achieve passive or active targeting properties (Hans & Lowman, 2002; Kumari *et al.*, 2010; Hiroshi Maeda, 2001; Mora-Huertas *et al.*, 2010). Polymer-based nanoparticles that have been reported as carriers for PDT agents included synthetic polymers such as poly(lactice-co-glycolide) (PLGA) copolymers and dendrimers, as well as natural polymers such as chitosans.

(a) ***Poly(Lactic-co-Glycolic Acid) (PLGA) nanoparticles***

PLGAs are copolymers of lactic and glycolic acids (Figure 2.1). They were reported to have excellent biocompatibility, biodegradability and mechanical strength. PLGA is one of the most successfully used biodegradable polymers because its hydrolysis leads to metabolite monomers lactic acid and glycolic acid. These two monomers are endogenous and metabolized by the body via Krebs cycle, a minimal systemic toxicity is associated with the use of PLGA for drug delivery applications (Kumari *et al.*, 2010). These structures have been formulated to carry various active agents including vaccines, proteins and macromolecules (Figure 2.7). PLGA is now approved by the US FDA for

the use of drug delivery (Bala *et al.*, 2004; Gilding & Reed, 1979; Jain, 2000; Lowe, 1954; Muthu, 2009; Stevanovic & Uskokovic, 2009). The polymers are commercially available with different molecular weights and copolymer compositions. Depending on the molecular weight and copolymer ratio, their degradation time can vary from several months to several years (Prokop & Davidson, 2008; Vert *et al.*, 1994). The forms of PLGA are identified by the monomers ratio used. For instance, PLGA 50:50 identifies a copolymer with 50% lactic acid and 50% glycolic acid composition.

PLGA nanoparticles are hydrophobic. The body recognizes hydrophobic particles as foreign. The reticuloendothelial system (RES) eliminates these particles from blood stream and accumulates them in the liver or the spleen (Kumari *et al.*, 2010). Therefore, PLGA is often coated with hydrophilic non-ionic polyethylene glycol (PEG) to increase their blood circulation half-life (Owens & Peppas, 2006). PLGA nanoparticles have negative charges which can be shifted to neutral or positive charges by surface modifications including PEGylation of PLGA (Danhier *et al.*, 2010).

Zinc (II) phthalocyanine loaded PLGA nanoparticles were reported by Fadel *et al.* to exhibit enhanced tissue uptake and targeting in photodynamic therapy *in vivo*. Female albino mice implanted with Ehrlich ascites carcinoma cells and treated with PLGA-zinc (II) phthalocyanine had survived significantly longer (mean = 60 days) than those treated with free zinc (II) phthalocyanine (mean = 25 days). Both treatment groups survived longer than the untreated control group (mean = 15 days). At day 14 post-PDT, mice treated with PLGA-zinc (II) phthalocyanine had the mean tumour volume of 1.5 times smaller than those treated with free drug and exhibited a longer tumour growth delay of 39 days (Fadel *et al.*, 2010).

Free verteporfin causes adverse skin photosensitivity (Richter *et al.*, 1991) but when verteprofin was loaded in PLGA nanoparticles, the treated male DBA/2 mice bearing

rhabdomyosarcoma (M1) tumours presented only a very mild and short period of skin photosensitivity as measured by erythema/eschar formation and edema observations 24 h after PDT. Total tumour ablation was observed up to 14 days post-PDT and only 34% of the treated mice showed tumour regrowth.

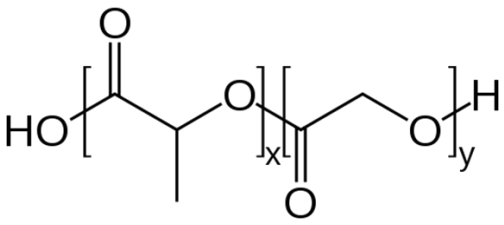

Figure 2.7: Chemical structure of polylactic-co-glycolic acid).

x = number of units of lactic acid; y = number of units of glycolic acid

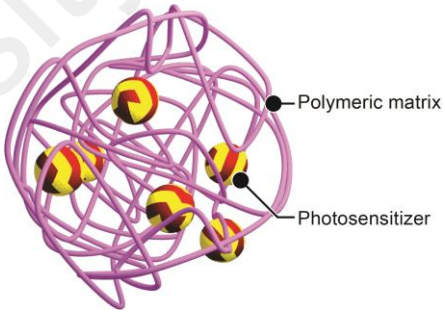

Figure 2.8: Poly(lactic-co-glycolic acid) (PLGA) nanoparticles

Size: 117 – 450 nm. This figure is adapted from Voon *et al.* (2014).

(b) ***Dendrimers***

Dendrimer is a three-dimensional structure composed of a central core molecule with regularly branching units that can be conjugated to drug molecules (Figure 2.8) (Boas &

Heegaard, 2004; Lee *et al.*, 2005; Wolinsky & Grinstaff, 2008). The dendritic branching terminals can be functionalised either with solubilising groups, targeting groups or other moieties. The advantages of these dendrimer-conjugates include high drug loading capacity, alterable particle size and lipophilicity for optimal cellular uptake as well as good tissue biodistribution properties (Lee, 2002; McCarthy *et al.*, 2005).

Casas *et al.* synthesised a dendrimer bearing eighteen aminolevulinic acid residues (18m-ALA) via ester coupling reactions. The 18m-ALA induced sustained production of porphyrin that peaked at 24 h compared to free aminolevulinic acid that peaked at 3 to 4 h in male BALB/c mice. The tumoural accumulation of 18m-ALA was found 7.5 times higher than the free aminolevulinic acid at the same concentration (Casas *et al.*, 2009).

Dendrimeric phthalocyanines complexed with poly-L-lysine-polyethylene glycol polymeric micelles (DPc/m) were evaluated in female BALB/c$^{nu/nu}$ mice implanted with human lung adenocarcinoma A549 cells. A significant reduction in tumour growth rate was observed in mice treated with DPc/m compared to the dendrimer phthalocyanine-treated and untreated control group. In comparison with Photofrin, the PDT effect of DPc/m was significantly greater although the injected dose of DPc/m, based on the phtosenstizing units, was 7.3-fold lower than Photofrin. Furthermore, DPc/m did not induce adversed post-PDT phototoxicity, whereas severe skin and liver damage was found in Photofrin-treated mice (Nishiyama *et al.*, 2009).

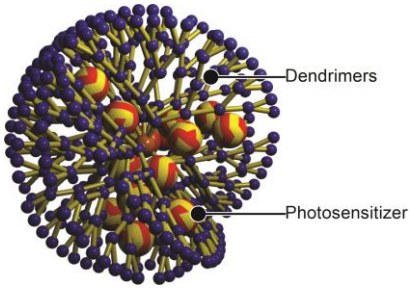

Figure 2.9: Dendrimer

Dendrimer is a three-dimensional structure composed of a central core molecule with regularly branching units that can be conjugated to drug molecules. Size: 50 nm. This figure is adapted from Voon *et al.* (2014).

(c) ***Chitosan nanoparticles***

While synthetic polymers are easily modified to achieve desirable properties, natural polymers are also of interest due to their biodegradability and wide availability. Chitosan is produced from partial deacetylation of the natural polysaccharide, chitin. Chitin is the second most abundant biopolymer after cellulose. It has been widely used in various biomedical and pharmaceutical applications (Park *et al.*, 2010), due to its wide availability, bioavailability and low immunogenicity as well as suitability to undergo chemical modifications (Figure 2.9) (Felt *et al.*, 1998; Ilium, 1998; Kumar *et al.*, 2004).

Glycol chitosan is a chitosan derivative with ethylene glycol groups added to its backbone to enhance its water solubility (Kim *et al.*, 2010). Lee *et al.* had used glycol chitosan to physically encapsulate protoporphyrin IX into nanoparticles. In squamous cell carcinoma (SCC7)-bearing athymic nude mice, the tumoural uptake of protoporphyrin IX-loaded glycol chitosan nanoparticles was 2.3 times higher than free protoporphyrin IX and the total fluorescent photon counts per organ for tumour tissues were 1.49 to 3.-fold higher than in other organs, indicating favourable biodistribution

properties. Tumour volumes showed 44% of reductions in protoporphyrin IX-loaded glycol-chitosan nanoparticles-treated group on day 14 post PDT, whereas the same regimen of free protophorphyrin IX did not produce substantial tumour volume reduction. Besides, histological examination revealed that most of the tumour cells were severely damaged in mice treated with protoporphyrin IX-loaded glycol-chitosan nanoparticles, whereas incomplete tumour cells death was found in mice treated with free protophorphyrin IX (Lee *et al.*, 2009).

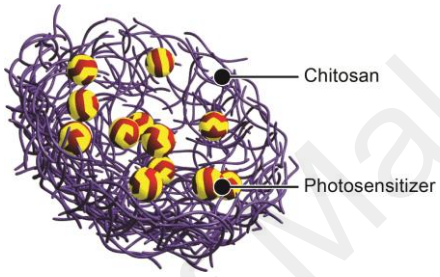

Figure 2.10: Chitosan nanoparticles

Chitosan is produced from partial deacetylation of the natural polysaccharide, chitin. Size: 260 – 350 nm. This figure is adapted from Voon *et al.* (2014).

2.2.5.4 Lipoprotein Nanoparticles

Lipoprotein nanoparticles are composed of cholesterol esters and triglycerides hydrophobic core with naturally occurring apoproteins, phospholipids and cholesterol on the surfaces (Ng *et al.*, 2011). Their ability to evade the reticuloendothelial system and remain in circulation for an extended period forms the criteria of a good drug delivery system (Eisenberg *et al.*, 1973). The hydrophobic core facilitates the incorporation of poorly soluble photosensitisers, and they are amenable to various drug-linking strategies (Figure 2.10) (Ng *et al.*, 2011).

Low-density-lipoprotein (LDL) with particle size less than 30 nm, has an innate cancer-targeting capability due to overexpression of LDL receptors on many cancer

cells including those of colon, adrenal, prostate and breast (Corbin & Zheng, 2007). LDL nanoparticles were used to deliver bacteriochlorin e_6 bisoleate. Significant tumour growth delay of HepG2 liver cancer cells inoculated into female nude mice was observed relative to untreated controls, controls treated with photosensitiser but without irradiation, and controls with irradiation only (Marotta *et al.*, 2011). Treatment with bacteriochlorin e_6 bisoleate-LDL has prevented the doubling of tumour volume in HepG2 tumour-bearing mice up to 60 days post-PDT, whereas the control group exhibited doubling of tumour volume by day 12.

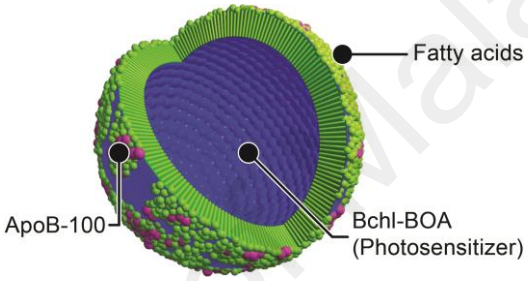

Figure 2.11: Lipoprotein nanoparticles

Lipoprotein nanoparticles are composed of cholesterol esters and triglycerides hydrophobic core with naturally occurring apoproteins, phospholipids and cholesterol on the surfaces. Size: 20 – 30 nm. This figure is adapted from Voon *et al.* (2014).

2.2.5.5 Inorganic Nanoparticles

Nanoparticles for delivery of photosensitisers *in vivo* can be synthesised from non-organic materials such as metals, oxides ceramics and inorganic salts (Rao *et al.*, 2012). These inorganic nanoparticles include silica, gold and calcium phosphosilicate nanoparticles.

(a) ***Silica nanoparticles***

Silica nanoparticles are chemically inert and can be synthesised into various size and shapes, and with different desired matrix porosities and dispersion characteristics.

Specific biomolecules can be attached to the surfaces of silica nanoparticles for targeting properties (Wang *et al.*, 2004). Despite being non-biodegradable, silica nanoparticles do not compromise the photoreactivity of the permanently entrapped photosensitisers as the singlet oxygen generated can diffuse through the porous matrix to reach the surrounding tumour tissues (Figure 2.11) (He *et al.*, 2009). Besides, silica nanoparticles are reported to be tolerated well within the biological systems (Lu *et al.*, 2010; Tarn *et al.*, 2013).

The biodistribution of Protoporphyrin IX silica nanoparticles loaded with dioctadecyl tetramethyl indodicarbocyanine chlorobenzene (DID) as a tracer were studied in glioblastoma tumour-bearing male athymic nude Foxn1 mice, HCT 116 tumour-bearing athymic nude mice and A549 tumour-bearing athymic nude mice. Higher tumoural accumulation of the Protoporphyrin IX-DID-silica nanoparticles than the control DID tracer was observed at each time point in the study (Simon *et al.*, 2010).

The surface charge of silica nanoparticles can be reduced from -29.1 mV to a greater negative charge of -44.0 mV with a phosphonate termination in order to enhance the stability of the nanocarrier system and reduce aggregation. Entrapping methylene blue into these carriers can give a bi-functional hybrid nanoparticle for imaging and PDT when the fluorescence emitted from the tumour site was used as a marker for localized irradiation. Tumour necrosis was developed in the group treated with methylene blue-silica nanoparticles compared to the control group treated with light irradiation alone where the tumours remained intact. The disadvantage of this system is that methylene blue emits a relatively short wavelength and unable to be visualised in deep tissue (He *et al.*, 2009).

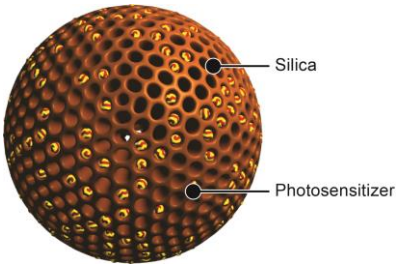

Figure 2.12: Silica nanoparticles

Silica nanoparticles are chemically inert and can be synthesised into various size and shapes, and with different desired matrix porosities and dispersion characteristics. Size: 50 – 118 nm. This figure is adapted from Voon *et al.* (2014).

(b) ***Gold nanoparticles***

Gold nanoparticles are inert, non-biodegradable and can be chemically modified for drug delivery use, including photosensitisers (Zaruba *et al.*, 2010). The particle size range of gold nanoparticles can be tuned from 2 – 100 nm for effective tumour vascular extravasation and tissue permeation and accumulation via the EPR effect (Demberelnyamba *et al.*, 2008). Pegylated gold nanoparticles provide a more stable system by reducing colloid aggregation and prevent RES uptake (Figure 2.12) (Cheng *et al.*, 2008; Greenwald *et al.*, 2003; Liu *et al.*, 2007).

Silicon phthalocyanine conjugated to pegylated gold nanoparticles were found to significantly reduce the delivery time to 2 h in order to reach the tumour in nude mice subcutaneously implanted with the basaloid squamous cell carcinoma, PE/CA-PJ34 cells, compared to 2 days for free silicon phthalocyanine. Conjugation of silicon phthalocyanine to pegylated gold nanoparticles also did not affect its singlet oxygen generation yield (Cheng *et al.*, 2008).

In the same nude mouse model, porphyrin-brucine conjugated gold nanoparticles treated mice showed complete tumour elimination by day 8 post-PDT, with no

detectable relapse. Meanwhile, mice treated with free porphyrin-brucine exhibited only a transient regression in tumour size and regrowth was found after day 18. On the other hand, gold nanoparticles without conjugation with photosensitisers caused slight tumour growth retardation in the treated mice. This could be due to the thermal energy generated by the gold nanoparticles which disrupts the plasma membrane of the target cells that causes cell lysis and consequent cell death (Gamaleia *et al.*, 2010; O'Neal *et al.*, 2004; Rezanka *et al.*, 2008).

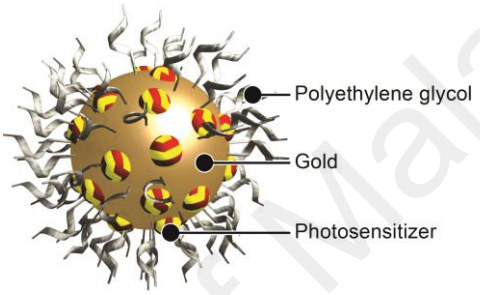

Figure 2.13: Gold nanoparticles

Gold nanoparticles are inert, non-biodegradable and can be chemically modified for drug delivery use, including photosensitisers. Size: 5 – 14.7 nm. This figure is adapted from Voon *et al.* (2014).

(c) ***Calcium phosphosilicate nanoparticles***

Calcium phosphosilicate nanoparticles are reported to be non-toxic, colloidal stable and were used to deliver imaging agents, drugs and other molecules (Figure 2.13). Indocyanine green loaded into these calcium phosphosilicate nanoparticles funtionalised with polyethylene glycol, was found to accumulate at tumour tissues in MDA-MB-231 breast tumour xenografted female nude mice and in BxPC-3 pancreatic tumours xenografted athymic mice (Altinoglu *et al.*, 2008; Barth *et al.*, 2010).

PEGylated calcium phosphosilicate loaded with indocyanine green was used to treated leukemia, a form of blood cancer which is not commonly addressed using PDT.

The nanoparticles were conjugated with antibodies that recognise CD117 receptors, which are overexpressed on leukemic stem cells and important to the pro-growth signaling mechanisms. Irradiation using near-infrared laser was directed at the spleen, 30 min after administration of the nanoparticles into the leukemic C3H/HeJ mice. The treatments were repeated every 3 days. The leukemia burden was monitored in blood collected from tail pricks and analysed for GFP+ leukemic stem cells using flow cytometry. Approximately 29% of leukemia-free survival was reported and this suggests that the *in vivo* efficacy of indocyanine green was enhanced when delivered in this manner (Barth *et al.*, 2011).

Figure 2.14: Calcium phosphosilicate nanoparticle

Calcium phosphosilicate nanoparticles are reported to be non-toxic, colloidal stable and were used to deliver imaging agents, drugs and other molecules. Size: 16 nm. This figure is adapted from Voon *et al.* (2014).

2.2.6 Problems in drug delivery development based on EPR effect

As discussed at section 2.2.2, particle size plays a vital role in EPR-based drug delivery. Surface charge (zeta potential) is also important in determining the EPR effect of the designed nanocarriers (McNeil, 2009). The normal vascular endothelial luminal surface carries a negative charge and thus, nanoparticles with positive charges would tend to bind to the vascular endothelial cells rapidly after administration via intravenous route, before reaching the targeted tumour. This results in a shorter plasma half-life and reduced tumour accumulation of the nanoparticles by EPR effect (Campbell *et al.*, 2002; McNeil, 2009; Nakamura *et al.*, 1998).

Therefore, negatively charged or neutral nanoparticles are expected to have a longer plasma half-life by preventing the rapid binding of the particles to the vascular wall. However, the anionic nanoparticles were reported to show rapid uptake and early clearance by the RES in the liver, lymph node and spleen than that of neutral particles, which in turn reduced their accumulation in the tumour tissue (Li & Huang, 2008). This is also the major drawback of liposomes as they are easily taken up by the RES and results in their rapid removal from the circulation into liver and spleen (Lasic *et al.*, 1991).

In fact, the RES is the major obstacle that prevents the nanoparticles from taking full advantages of the EPR effect (Kao & Juliano, 1981; Senior, 1987). The removal of nanoparticles is initiated by the interactions between the foreign particles and the phagocytic cells in the blood (e.g. monocytes, neutrophils) and tissues (e.g. macrophages, Kupffer cells) (Bartneck *et al.*, 2010; Dobrovolskaia *et al.*, 2008; Pratten & Lloyd, 1986). This process is triggered by the adsorption of plasma proteins called opsonins, such as IgG or complement fragments, onto the particle surface, which induces the recognition of particles by phagocytes through specific membrane receptors (Essa *et al.*, 2011; Moghimi, 1998; Patel & Moghimi, 1998). The opsonized nanoparticles are eliminated eventually by a process called receptor-mediated phagocytosis (Moghimi & Hamad, 2008; Patel & Moghimi, 1998).

2.2.6.1 Opsonization and phagocytosis

Opsinization typically takes place in the blood circulation. Immunoglobulins and components of the complement system such as C3, C4 and C5 are known to be common opsonins and also other blood serum proteins including laminin, fibronectin, C-reactive protein and type I collagen (Frank & Fries, 1991). These opsonins, are thought to come into contact with injected polymeric nanoparticles typically by random Brownian

motion. Once they are sufficiently close to the surface of a particle, attractive forces including van der Waals electrostatic, ionic and, hydrophobic/hydrophilic may involve in the binding of opsonins to the particle surface (Owens & Peppas, 2006).

Following opsonization, clearance occurred through attachment of the phagocytes to the nanoparticle via surface bound opsonins. The bound opsonin proteins undergo conformational changes from an inactive protein present in the blood serum to an activated protein structure that can be recognized by phagocytes. The specific receptors on the phagocytes will thereby interact with these modified opsonins and recognize as a foreign material (Owens & Peppas, 2006; Salmaso & Caliceti, 2013).

Another method of phagocyte attachment is through the non-specific adherence of phagocytes to surface adsorbed blood serum proteins which can leads to phagocytosis as well (Frank & Fries, 1991). This process is due to association of opsonin proteins with a more hydrophobic particle surface. Complement activation is also an alternative method of phagocytic cell attachment. The complement system can be activated by one of several mechanisms including the classical, alternative and lectin pathway (Frank & Fries, 1991; Salmaso & Caliceti, 2013). This will eventually leads to the binding and phagocytosis of the nanoparticles by mononuclear phagocytes.

The final particle clearance process is the ingestion by phagocytes through endocytosis. Following this, the phagocytic cells will secrete enzymes and other oxidative-reactive chemical factors, including superoxide, nitric oxide and hydrogen peroxide, to break down the phagocytosed material (Levine & Deretic, 2007). However, most non-biodegradable polymeric nanoparticles are not able to be degraded by this process. They will be either removed through renal clearance or sequestered and stored in one of the RES organs, depending on their relative size and molecular weight. Molecules with molecular weight around 5000 or less, or dense polymers such as

dendrimers with molecular weight 10,000 or more may be removed by renal system (Owens & Peppas, 2006). Those non-biodegradable particles with molecular weight higher than renal threshold will be sequestered in the RES organs.

Many studies have reported that nanoparticles administered intravenously suffered from premature clearance by the RES, if they are not "stealthed" from opsinization (Gijsens *et al.*, 2002; Kao & Juliano, 1981; Semple *et al.*, 1998; Senior, 1987). In drug delivery, the term "stealth", translated from the "low observable technology" applied to military tactics, refers to nanovehicles that are invisible to the biological system involved in clearance of particles from the bloodstream, namely, RES and Kupffer cells. Hydrophobic and/or charged nanoparticles are subjected to significant opsonization (Sheng *et al.*, 2009; Yamamoto *et al.*, 2001). Therefore, nanoparticles "stealth-coated" with an electrically neutral hydrophilic surface layer may extend their circulation half-life and enhance tumoural accumulation of the nanoparticles (Moghimi *et al.*, 2001).

2.3 Stealth coating of nanoparticle drug delivery systems

Over the past three decades, non-ionic hydrophilic polymers and/or surfactants, particularly polyethylene-glycol (PEG), were used in the studies of surface stabilisation of nanoparticles. In 1977, Abuchowski *et al.* reported that conjugation of 2 kDa or 5 kDa of PEG to bovine liver catalase had decreased the immunogenicity of the protein and prolonged its circulating time in blood (Abuchowski *et al.*, 1977). Since then, PEG (5 kDa) has been widely studied in various nanocarrier systems including liposomes (Allen & Hansen, 1991; Allen *et al.*, 1995; Klibanov *et al.*, 1990), polymeric nanoparticles (Ebrahimnejad *et al.*, 2011; Essa *et al.*, 2011; Shan *et al.*, 2009) and micelles (Bhattarai *et al.*, 2003; Lee *et al.*, 2011).

2.3.1 Peglyation for stealth coating and its limitation

Polyethylene-glycol (PEG) is a well-established "stealth" coating material that has been widely studied in various nanocarrier systems including liposomes (Allen & Hansen, 1991; Allen *et al.*, 1995; Klibanov *et al.*, 1990), polymeric nanoparticles (Ebrahimnejad *et al.*, 2011; Essa *et al.*, 2011; Shan *et al.*, 2009), and micelles (Bhattarai *et al.*, 2003; Lee *et al.*, 2011). It consists of neutral, flexible and hydrophilic material, which can be used to produce a surface layer that reduces the adhesion of opsonins present in the blood serum on the nanoparticles via steric hindrance and hence, "stealth" them from the phagocytic cells (Drobek *et al.*, 2005; Kenausis *et al.*, 2000; Moffatt & Cristiano, 2006; Storm *et al.*, 1995). For instance, liposomal doxorubicin (Doxil®), indicated for the treatment of patients with metastatic breast cancer, ovarian cancer or Kaposi sarcoma, is PEGylated for long term circulation (Zhang *et al.*, 2008a). PEGylated PLA nanoparticles also demonstrated higher plasma concentration at 6 h post-injection, and had significantly lower accumulation in the liver compared to the non-PEGylated PLA nanoparticles (Verrecchia *et al.*, 1995).

2.3.2 Limitations of PEG coating

2.3.2.1 Interference with cellular uptake and endosomal escape of nanoparticles

While PEG has been widely used as "stealth" coating for various nanoparticles, recent studies had reported on its interference with cellular uptake and endosomal escape of extravasated nanoparticles, a phenomenon known as PEG-dilemma (Fella *et al.*, 2008; Hatakeyama *et al.*, 2011; Ishida, Atobe *et al.*, 2006; Ishida *et al.*, 2002; Ishida *et al.*, 2007). For instance, PEGylated Doxil® demonstrated less tumoural accumulation compared to the non-PEGylated liposomes. This indicates that PEG interferes with the interaction between tumour cells and liposomes (Hong *et al.*, 1999). PEGylation of non-viral gene vectors (branched polyethyleneimine (bPEI) or β-cyclodextrin-containing polymer) showed significant reduction in gene expression. From the results of electron

microscopy, non-PEGylated cationic gene vectors entered the cells as large aggregates whereas the PEGylated ones remained small and discrete, both inside and outside the cells. This indicates that PEGylated vectors are less effective in terms of cellular uptake and intracellular vesicle escape (Mishra *et al.*, 2004). Meanwhile, fluorescence resonance energy transfer microscopy also revealed that the PEG layer interfered with endosomal escape of oligonucleotides-loaded liposomes, leading to premature degradation of the oligonucleotides (Remaut *et al.*, 2007).

2.3.2.2 Anti-PEG antibodies and immune reponses

Besides its effects on the cellular uptake and endosomal escape, PEGylation also raises immune reactions and elicits anti-PEG antibodies upon repeated injections. The polymer itself can lead to hypersensitivity indirectly by side products formed during synthesis (Zhang *et al.*, 2014). Accelerated blood clearance of the second dose of PEGylated liposomes was reported resulting from the binding of PEG-specific IgM (Ishida *et al.*, 2005; Ishida, Ichihara, *et al.*, 2006), produced by the first dose of liposomes, and the subsequent activation of the complement system (Hamad *et al.*, 2008), thereby leads to opsonization of PEG with C3 fragments and an increased uptake by Kupffer cells (Ishida *et al.*, 2008; Ishida & Kiwada, 2008). Such immunogenicity of PEG reduces its attractiveness for use in the clinic because it affects the bioavailability of the drug, decreases the therapeutic efficacy of the encapsulated drugs and may cause adverse effects resulting from biodistribution of the drug (Zhang *et al.*, 2014).

2.3.2.3 PEG-associated cytoplasmic vacuolation

PEG-associated cytoplasmic vacuolation in tissues were reported in animals administered PEGylated proteins (Bendele *et al.*, 1998). Vacuolation in renal tubular epithelium was observed as renal clearance is the major excretion pathway for PEGs (Yamaoka *et al.*, 1994). In addition, vacuolation was also found in macrophages, lymph

node and spleens (Zhang *et al.*, 2014). The vacuoles might include PEGs or the accumulation of PEGs results in the vacuolation. Despite severe side effects of the accumulation have not been reported, consequences of life-long therapies with high dosages treatment containing high molecular weight PEG conjugates are hardly predictable. Significant PEG-protein accumulation in the related organs may increase the incidence of patient developing liver toxicity (Bukowski *et al.*, 2002; Gregoriadis *et al.*, 2005), renal failure and diabetes (Zhang *et al.*, 2014).

CHAPTER 3: MATERIALS AND METHODS

3.1 Materials, reagents and solvents

Chitosan powder with molecular weight ranging from 100-300 kDa was purchased from Acros Organics (NJ, USA). Acetic acid, hydrochloric acid (37%), sodium hydroxide and acetone were supplied by Merck (Darmstadt, Germany). Poly(D,L-lactide-co-glycolide), (50:50), MW 38,000 – 54,000), poly(vinyl alcohol) (PVA) (MW 30,000 – 70,000), sodium nitrite ($NaNO_2$) was purchased from Sigma-Aldrich (MO, USA). Deionised water with resistivity of 18.2 ΩS cm^{-1} produced from Barnstead NANOpure® Diamond™ ultrapure water system coupled with Barnstead NANOpure® Diamond™ RO system (MA, USA) was used throughout all syntheses and measurements.

3.2 Equipments

UV-visible absorption spectra were recorded with the cuvette platform of LAMBDA 25 UV/Vis Systems (Perkin Elmer, MA, USA) using 1 cm path length quartz cuvette. All cell culture works were carried out with aseptic technique in an Airstream class II biological safety cabinet (ESCO, Singapore). Cultured cells were incubated in a Forma® direct heat CO_2 incubator (Thermo Fisher Scientific, OH, USA). Photoirradiation for *in vitro* experiments was performed with a light source consisting of a Halotone 300 W halogen lamp (Philips Electronic, Amsterdam, Netherlands). A water column was used to filter off the infrared irradiation and a Roscolux "CalColor 90 Green" filter no. 4490 (>460nm) (Rosco, NY, USA) was placed in the irradiation path before the sample. The irradiation intensity was measured with a calibrated Nova-Oriel power meter (Newport Corp, CA, USA). Other equipment used for specific experiments only is listed under their respective methodology sections.

3.3 Photosensitisers

The photosensitiser diiodinated-boron dipyrromethene (I_2BODIPY) used in this study was prepared and supplied by Prof Kevin Burgess's group from the Department of Chemistry, Texas A&M University, Texas, USA. Its synthesis, purification and NMR characterisation were previously described by Lim *et al.* (2010), Loudet and Burgess (2007) and Yogo *et al.* (2005) (Appendix A). (Yogo *et al.*, 2005). Figure 3.1 showed the chemical structure of I_2BODIPY.

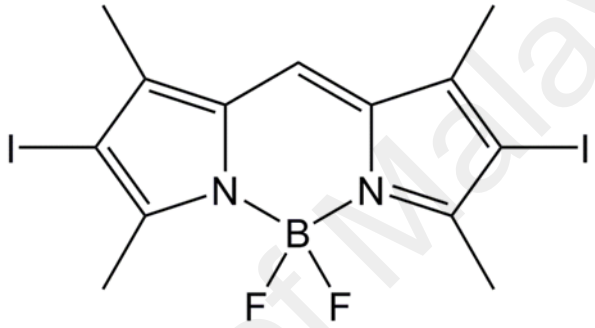

Figure 3.1: Chemical structure of I_2BODIPY

3.4 Production of low molecular-weight chitosans

Low molecular-weight chitosans were prepared as previously described by Tan and Misran (2013) (Tan & Misran, 2013). The 5, 10 and 25 kDa water-soluble chitosans were prepared by adding an appropriate amount of 0.1 M $NaNO_2$ solution dropwise to 1% (w/v) of chitosan (mean MW = 200 kDa). To precipitate the undissolved chitosan, the chitosan solution was adjusted to alkaline pH of 8 – 9. The solution was then filtered to remove the undissolved chitosan. The filtrate was then adjusted to neutral pH and the remaining chitosan was precipitated with acetone. The precipitated chitosan was collected by centrifugation at 2,700 x g for 3 min at 25 ℃ and dried under vacuum.

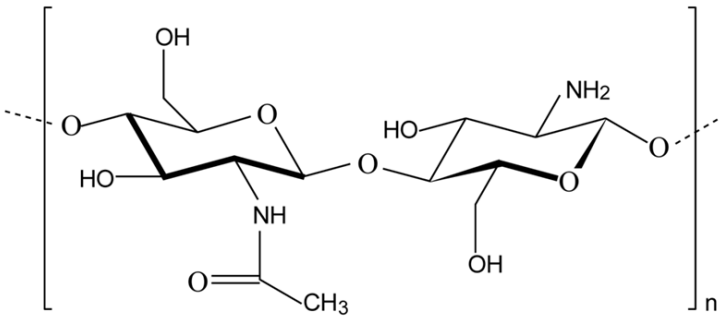

Figure 3.2: Chemical structure of chitosan.

Chitosan consists of a linear copolymer of glucosamine and N-acetylglucosamine.

3.5 Characterisation of low molecular-weight chitosans

3.5.1 Determination of average molecular weight of chitosans

A series of chitosan concentrations were measured to determine the average molecular weight of each type of chitosan using static light scattering method with a Malvern NanoSeries ZetaSizer (Worcestershire, UK) (Chen & Tsaih, 1998). A Debye plot was constructed from the intensity of scattered light versus various concentrations of the chitosan solutions. The reciprocal of molecular weight of the chitosan, represented by the intercept point at y-axis in Debye plot, was used to calculate the average molecular weight of chitosan.

3.5.2 Estimation of chitosan solubility

A series of concentrations of water-soluble chitosan and saturated chitosan were prepared for measuring the spectrophotometric absorption at 274 nm with a Cary 50 UV-Vis Spectrophotometer (Varian, CA, USA). The absorption of diluted chitosan at 274 nm was plotted against the concentration to derive the calibration curve. The UV-Vis absorption of the saturated solution was measured to determine the water-solubility of chitosan by extrapolation of the calibration curve (Tan & Misran, 2013).

3.6 Preparation of I_2BODIPY loaded PLGA (PLGA-I_2BODIPY) nanoparticles

PLGA nanoparticles loaded with I_2BODIPY were prepared using a nano-precipitation technique with minor modifications (Govender *et al.*, 1999). Fifty milligrams of PLGA in 3 ml of acetone was mixed with 10 mg of I_2BODIPY dissolved in 1 ml of acetone and the mixture was stirred for about 5 min. Following this, the solution was added dropwise to 25 ml of aqueous solution containing 1% PVA (w/v) under magnetic stirring. Subsequently, precipitation by self-assembly of nanoparticles was observed. The suspension was then sonicated for 30 min (VCX400 sonicator, Sonics and Materials Incorporation, CA, USA, 19 mm tip, power 400 W, frequency 20 kHz) in melting ice. Overnight stirring of the suspending was carried out in the dark at room temperature to remove traces of acetone. Larger aggregates were removed by centrifugation at 2,700 x g for 30 min. The supernatant containing PLGA-I_2BODIPY nanoparticles were recovered by ultracentrifugation at 102,000 x g for 25 min at 4 ℃ using a 90 Ti Rotor (Beckman Coulter, CA, USA) and then by decanting the supernatant. The pellet was resuspended in water by sonication in a water bath for 30 s and was then washed twice more with water to remove PVA. The washings were centrifuged at 93,000 x g for 20 min at 4 ℃. The pellet was finally resuspended by sonication and maintained at -80 ℃ overnight before being freeze-dried for 36 h. The resulting nanoparticles were then stored in a dessicator at 4 ℃ until further use. Similarly, blank PLGA nanoparticles were prepared by dissolving PLGA in acetone without I_2BODIPY with the rest of the method remaining the same.

3.7 Preparation of chitosan coated PLGA-I_2BODIPY (PLGA-Chitosan-I_2BODIPY) nanoparticles

The prepared PLGA-I_2BODIPY nanoparticles were coated with the water-soluble chitosan of different molecular weight, 5-, 10- and 25 kDa. Subsequently, the 25-kDa chitosan was selected to coat PLGA nanoparticles at concentrations of 0.05, 0.10, 0.30

and 0.50% w/v. The coating was performed by adding 2% w/v of PLGA-I_2BODIPY nanoparticles in deionised water dropwise into the chitosan solutions in deionised water at the ratio of 4:1 under magnetic stirring. The mixture was stirred overnight at room temperature. The suspension was then centrifuged at 13,400 x g for 20 min at 4 ℃, and the supernatant was removed. The coating of chitosan onto blank PLGA nanoparticles was carried out using the same technique. All the chitosan-coated nanoparticle suspensions were stored at 4 ℃ until further use.

The amount of chitosan coating on the PLGA nanoparticles was calculated by quantifying the amount of chitosan remaining in the supernatant that was collected after the preparation of the nanoparticles using ninhydrin assay. Ninhydrin assay is commonly used to detect unreacted primary amines in chitosan through the formation of Ruhemann's purple, which can be quantified using a UV-Vis spectrophotometer (Khan *et al.,* 2002). One milliliter of each of the supernatants and 1 ml of the standard solutions containing chitosan at concentrations of 0.10, 0.15, 0.20, 0.25, 0.30, 0.35 and 0.40 mg/ml were transferred into test tubes. Following this, 1 ml of ninhydrin reagent (1% w/v) was added, and the solutions were boiled in a water bath for 10 min. The absorbance of the solutions was measured using a UV-Vis spectrophotometer at 570 nm. The concentration of chitosan in the supernatants was determined from a calibration plot.

3.8 Characterisation of PLGA-I_2BODIPY and PLGA-Chitosan-I_2BODIPY nanoparticles

3.8.1 Process yield

The percentage of the total mass of nanoparticles obtained after freeze drying over the weight of the initial photosensitiser plus polymer was referred to as the process yield. It was calculated by the equation as follows:

$$\text{Yield (\%)} = (M_{NP} / M_{Total}) \times 100$$

where M_{NP} is the mass of nanoparticles recovered after freeze drying and M_{Total} is the mass of PLGA plus the mass of I_2BODIPY in the formulation. This experiment was performed in triplicate for each formulation (n=3).

3.8.2 I_2BODIPY loading and encapsulation efficiency

Freeze-dried PLGA-I_2BODIPY nanoparticles were dissolved in acetone at 1 mg/ml for acetone extraction of I_2BODIPY to estimate its loading and encapsulation efficiency (Yallapu *et al.*, 2010). The solution was placed on a shaker (OS-20 Orbital Shaker, Boeco, Hamburg, Germany) at 100 rpm for 24 h at room temperature to separate the I_2BODIPY from the nanoparticles in acetone, followed by centrifugation at 9,300 x g and the supernatant was collected. The supernatant was diluted 20 times for the subsequent quantification step. The amount of I_2BODIPY content in the supernatant was measured using a UV-Vis spectrophotometer at 532 nm. The concentration of I_2BODIPY was calculated by means of a standard calibration curve derived from known concentrations of I_2BODIPY (0.39 – 6.25 μg/ml). The I_2BODIPY loading (% w/w) and entrapment efficiency (%) were calculated using the following formula:

$$I_2\text{BODIPY loading (\% w/w)} = (\text{mass of } I_2\text{BODIPY in nanoparticles} / M_{NP}) \times 100$$

$$\text{Entrapment efficiency (\%)} = (\text{mass of } I_2\text{BODIPY in nanoparticles} / M_{t)} \times 100$$

where M_{NP} is the mass of nanoparticles recovered after lypohilised and M_t is the mass of I_2BODIPY used in formulation.

3.8.3 Particle size and zeta potential

The PLGA-I_2BODIPY and PLGA-Chitosan-I_2BODIPY mean particle size and size distribution were measured using a Malvern NanoSeries ZetaSizer (Wochestershire, UK) by applying the dynamic light scattering principle. Fifty microlitres of 1 mg/ml nanoparticle suspension was added to 3 ml of distilled water and sonicated for 30 s for particle size measurement. The size distribution was determined from the polydispersity index (PDI), ranging from 0 to 1 where zero indicates completely monodispersed particles formulations. The PDI up to 0.2 are considered ideal for PLGA nanoparticles (Yallapu *et al.*, 2010).

To examine the nanoparticle stability in stock solution (deionised water), both the chitosan-coated and uncoated nanoparticles dimension were monitored by using a Malvern NanoSeries ZetaSizer over 30 days to detect cluster formation, at ambient temperature and 4 ℃. Clusters of these nanoparticles are formed through aggregation phenomena that cause a shift of the particle size distribution (PSD) towards higher values.

The zeta potential indicates the surface charge of nanoparticles and affects the stability of formulations and their interactions with cellular membranes. It was determined using Malvern NanoSeries ZetaSizer based on the principle of electrophoretic mobility under an electric field.

3.8.4 Particle size and morphology

The nanoparticle morphology and particle size were examined under scanning electron microscope (SEM) (FEI Quanta 250 FEGSEM, OR, USA). Nanoparticles were

air-dried in a desiccator and coated with gold prior to examination by SEM. The scanning voltage ranged from 10 to 20 kV was used in this study.

3.9 Biocompatibility of PLGA-Chitosan-I_2BODIPY and PLGA-I_2BODIPY nanoparticles: Haemolysis Test

A mixture of 100 µl 2% red blood cells (RBC) suspension and 100 µl of PLGA nanoparticles or 5-, 10- and 25-kDa chitosan-coated PLGA nanoparticles were prepared in sterile microcentrifuge tubes to give final concentration ranging from 0 to 10 mg/ml. For positive control, 100 µl Triton X100 (1% v/v) was added to 100 µl of 2% RBC suspension to produce 100% haemolysis. All the samples were incubated for 5 h at 37 ℃ for haemolysis to take place (Kiew *et al.*, 2010; Petersen *et al.*, 2002). The samples were then centrifuged for 10 min at 1,000 x g and the supernatants (100 µl) were transferred to a 96-well plate to determine haemoglobin release by spectrophotometric absorbance at 550 nm using Tecan Infinite® M1000 PRO microplate reader (Zürich, Switzerland). The absorbance values of respective samples were compared to that of the positive control and the percentage (%) of lysis was determined.

3.10 Evaluation of Protein Adsorption to Particle Surface

To determine the amount of protein adsorption on the particle surface, PLGA nanoparticles and 5-, 10- and 25-kDa chitosan-coated PLGA nanoparticles were incubated in DMEM containing 50% fetal bovine serum (FBS) for 1 h at 37 ℃ (Amoozgar *et al.*, 2012). FBS was used because it contains opsonins including immunoglobulins and complements that enhanced phagocytosis and activation of lymphocytic and macrophage cell types (Zheng *et al.*, 2006). The ability of the nanoparticle to reduce the amount of opsonins adsorbed on the particle surface indicates its stealth properties and reduce uptake by macrophages and reticuloendothelial system (RES).

The nanoparticles were washed four times with water by centrifugation at 14,000 x g for 10 min using centrifugal filter tubes (100 kDa nominal molecular weight limit, NMWL). The washed nanoparticles were freeze-dried, and a protein assay using Thermo Scientific Pierce Micro BCA Protein Assay Kit was performed to quantify the amount of adsorbed proteins. A standard curve ranging from 2 – 40 μg/ml was prepared following the instructions from the assay kit.

3.11 Photophysical and photochemical characterisation of free I_2BODIPY, PLGA-I_2BODIPY and PLGA-Chitosan-I_2BODIPY nanoparticles

3.11.1 UV-visible and fluorescence emission spectra

The UV-visible spectra of free I_2BODIPY, PLGA-Chitosan-I_2BODIPY and PLGA-I_2BODIPY nanoparticles (25 μM) in different solvents were measured using a UV-vis spectrophotometer (LAMBDA 25 UV/Vis Systems, Perkin Elmer, MA, USA). UV-vis spectra were collected for wavelength ranging from 300 – 700 nm for PBS and 400 – 700 nm in acetone and methanol. The molar extinction coefficient for each sample was determined.

The fluorescence emission spectra of each sample in methanol were also recorded at 500 – 850 nm, following excitation at their maximal absorption (λ_{max}), using a microplate reader.

3.11.2 Chemical detection of singlet oxygen

Anthracene-9,10-dipropionic acid disodium salt (ADPA) was used as a singlet oxygen detector to determine the generation of singlet oxygen. ADPA is bleached by singlet oxygen to its corresponding endoperoxide which does not absorb in the 350 – 450 nm regions. Thus, the decrease in the ADPA 400-nm absorption band optical density indicates the generation of singlet oxgen in the solution (Roy *et al.*, 2003; Zhang *et al.*, 2007). Three hundred microlitres of ADPA was dissolved in deuterium oxide

(D_2O) to yield a concentration of 5.5 mM. Free I_2BODIPY (12 µM) was dissolved in D_2O or in D_2O solution containing 1% SDS (w/v) or 0.1% Tween 80 (w/v). PLGA-Chitosan-I_2BODIPY and PLGA-I_2BODIPY nanoparticles with 12 µM I_2BODIPY were mixed with pure D_2O. Two-millilitres of each sample was added into 300 µl of ADPA solution for measurement of singlet oxygen generation. Before initiating the measurements, the solution was aerated for 10 min followed by irradiation at 10 mW/cm^2 with light filtered by a Rosculux "CalColor 90 Green" filter no. 4490 (>460nm) (CT, USA) at room temperature for 60 min. Aliquots of 200 µl were removed from the mixture and transferred into a 96-well plate at predetermined time intervals. The optical densities of APDA were measured at 400 nm with a microplate reader. For negative controls, irradiation of ADPA solution in the absence of photosensitisers, using PLGA-Chitosan blank and PLGA blank nanoparticles were performed.

3.12 *In vitro* I_2BODIPY release in phosphate buffer saline (PBS) and plasma

The *in vitro* release test was carried out at pH 7.4 and 4.8 to represent the physiological, and tumoural and lysosomal acidic environments, respectively (Chronopoulou *et al.*, 2013). PLGA-Chitosan-I_2BODIPY and PLGA-I_2BODIPY nanoparticles containing equivalents of 50 µg/ml of I_2BODIPY were suspended in 25 ml of PBS containing 0.1% Tween-80 solution (w/v) at the two different pH. Tween-80 was used in the buffer to maintain a sink condition and to enhance the solubility for I_2BODIPY in the aqueous phase. Subsequently, 1 ml aliquot of each of the nanoparticle suspension was transferred to microcentrifuge tubes. The tubes were sealed and incubated at 37 ℃ at 100 rpm in an orbital shaker (ZHWY 103D, Labwit, Shanghai, China). Triplicates of the samples were centrifuged at 9,300 x g for 10 min and the supernatant containing the released I_2BODIPY was collected at predetermined time intervals. The amount of I_2BODIPY in the released samples was measured at 532 nm

using a UV-Vis spectrophotometer. A standard plot of I_2BODIPY (0 – 20 µg/ml) was prepared under identical conditions.

The *in vitro* release profile of I_2BODIPY in BALB/c mouse plasma was also determined in this study. The PLGA-Chitosan-I_2BODIPY and PLGA-I_2BODIPY nanoparticles were added to 1 ml of preheated plasma solution to give a final concentration of 200 µM (I_2BODIPY equivalent) (Konsoula & Jung, 2008). The assays were performed at 37 ℃ at 100 rpm in an orbital shaker in triplicate. Fifty-microlitres of each sample were taken at predetermined time intervals and centrifuged at 9,300 x g for 10 min. The supernatant was collected and added with 200 µl of acetonitrile to remove the protein content from the plasma. The samples were then vortexed for 1 min and centrifuged at 14,000 x g for 15 min at 4 ℃. The amount of I_2BODIPY in the supernatant (100 µl) was measured spectrophotometrically at 532 nm using a microplate reader.

3.13 *In vitro* photocytotoxicity of PLGA-Chitosan-I_2BODIPY and PLGA-I_2BODIPY nanoparticles

Murine 4T1 and human MDA-MB231 breast cancer cell lines were used to evaluate the *in vitro* photocytotoxicity of PLGA-Chitosan-I_2BODIPY and PLGA-I_2BODIPY nanoparticles. The I_2BODIPY was prepared at 10 mM in DMSO and stored at -20 ℃ before use. Meanwhile, the stock solutions of PLGA-Chitosan blank nanoparticles, PLGA blank nanoparticles, PLGA-Chitosan-I_2BODIPY and PLGA-I_2BODIPY nanoparticles were prepared in PBS at 1 mM equivalent to free I_2BODIPYs. The 4T1 cell line was grown and maintained in RPMI whereas the MDA-MB-231 cell line was grown in DMEM; both types of media were supplemented with 10% fetal bovine serum and 1% penicillin-streptomycin. For assays, both cells lines were seeded into 96-well plates at 4000 cells/well and incubated overnight to allow cells to adhere. Test samples

diluted in respective culture media were added to the cells to give a final concentrations ranging from 0.03 to 3 µM. Following 2 h incubation, cells were washed twice with PBS and culture media was added. Cells were then irradiated with 5.3 J/cm^2 of light from a broad-spectrum halogen light source at a fluence rate of 8.9 mW/cm^2 for 10 min. Subsequently, the treated cells were incubated for 24 h before cell viability was assessed using the MTT assay. Briefly, 20 µl of MTT (5 mg/ml in PBS) was added to each well and incubated for 3 h. The supernatant were then removed and 100 µl of DMSO were added to dissolve the purple formazan crystal formed. The optical densitiy of each well were measured at 570 nm using a microplate reader. The cell viability in response to the treatment of test samples was calculated as percentage (%) of cell viability = (OD treated/OD control) x 100. A set of dark controls without irradiation was performed concurrently.

3.14 Cellular uptake of PLGA-Chitosan-I_2BODIPY and PLGA-I_2BODIPY nanoparticles

The 4T1 murine breast carcinoma cells and RAW 246.7 macrophages were seeded into 96-well plates at 4000 and 5000 cells/well, respectively, and were incubated overnight. 4T1 cells were treated with free I_2BODIPY (20 µM), PLGA-Chitosan-I_2BODIPY and PLGA-I_2BODIPY nanoparticles (20 µM of I_2BODIPY equivalent) for 0, 0.25, 0.5, 1, 1.5, 2, 2.5 and 3 h. For RAW246.7 macrophages, the treatment periods were 0, 0.25, 0.5, 1, 4, 6, 8 and 24 h. Following incubation, the content of each well was removed and the cells were washed twice with PBS. Subsequently, 200 µl of acetonitrile: water (4:1) was added to each well and incubated for 30 min at room temperature to lyse the cells and extract I_2BODIPY (Lim *et al.*, 2014). Next, 100 µl of the extract from each well was transferred to a 96-well plate and the optical densities at absorbance 532 nm was measured using a microplate reader. The concentration of I_2BODIPY was determined from a standard curve (3.125 – 50 µM). The protein content

of the cells were measured with a Pierce BCA protein assay (Thermo Scientific, IL, USA) on the cell lysate obtained by solubilising the cells with M-PER® Mammalian Protein Extraction Reagent (Thermo Scientific, IL, USA). Uptake was expressed as the amount of I_2BODIPY (nmol) normalised to per milligram (mg) of total cell protein (Tahara *et al.*, 2009).

Confocal microscopy was also used to observed the uptake of the free I_2BODIPY (20 μM), PLGA-Chitosan-I_2BODIPY and PLGA-I_2BODIPY nanoparticles following incubation of 2 h for 4T1 cells, 6 and 24 h for RAW246.7 macrophages according to the results obtained from the quantitative uptake study described above.

3.15 Intracellular localization of PLGA-Chitosan-I_2BODIPY and PLGA-I_2BODIPY nanoparticles

The intracellular localization of the free I_2BODIPY, PLGA-Chitosan-I_2BODIPY and PLGA-I_2BODIPY nanoparticles was analysed by confocal microscopy using dual staining techniques (Lim *et al.*, 2010). Twenty micromolar of test samples were added to the 4T1 cells grown on coverslips and incubated for 2 h. The cells were then rinsed twice with PBS to remove free photosensitisers or free nanoparticles. Subsequently, the cells were stained with organelle-specific fluorescence probe. Mitochondria, endoplasmic reticula and lysosomes were stained with 100 nM Mito Tracker Red 580, 100 nM ER-Tracker Blue-White DPX and 500 nM LysoTracker Blue DND-22, respectively. The cells were incubated with the stain for 15 to 30 min at room temperature. Following incubation, cells were rinsed with PBS to remove free dyes, and the stained cells were observed using a LEICA TCS SP5 II confocal microscope configured with a 60 x oil objective (Leica Microsystem, Wetzlar, Germany). Organelle-specific fluorescence probes were respectively excited at wavelength of 330-385 nm to illuminate ER-Tracker and LysoTracker, 460-490 nm for Mito Tracker Red

580 and 520-550 nm for the photosensitiser (I_2BODIPY). The intracellular localization of the test samples was determined by comparing the fluorescence topographic profile with the topographic profile of each organelle-probe generated from a longitudinal transcellular axis.

3.16 Animal model

Female wild-type BALB/c mice of 8 – 10 weeks old were purchased from InVivos Pte Ltd., Singapore for *in vivo* studies. The mice were maintained in the satellite animal facility at the Department of Pharmacology, Faculty of Medicine, University of Malaya. They were kept in a controlled environment of 12 h light-dark cycle with free access to food and water. Enrichment was also provided according to the Animal Experimental Unit (AEU) standard practice in University of Malaya. All animal experiments were conducted in accordance with protocols and ethics approved by the Faculty of Medicine Institutional Animal Care and Use Committee, University of Malaya (FOM IACUC) (Ethics Reference no. 2014-09-11/PHAR/R/VSH).

3.16.1 Toxicity profiles of free I_2BODIPY, PLGA-Chitosan-I_2BODIPY and PLGA-I_2BODIPY nanoparticles

The *in vivo* toxicity profiles of free I_2BODIPY, PLGA-Chitosan-I_2BODIPY and PLGA-I_2BODIPY nanoparticles, blank PLGA-Chitosan and blank PLGA nanoparticles were determined following intravenous administration of these samples to the mice via tail vein at a dose equivalent to 30 or 60 mg/kg of I_2BODIPY. Potential toxicity was observed for 20 days based on symptoms such as inactivity, ruffled fur, behavior changes, and loss of body weight (Kue *et al.*, 2015).

3.16.2 *In vivo* biodistribution studies in 4T1 tumour-bearing mice

To perform 4T1 tumour transplantation, the fur of the BALB/c mice was shaved followed by orthotopic injection of murine 4T1 breast cancer cells (5×10^5 cells) in 0.1

ml of RPMI medium into the mammary fat pad of the mice. When the tumour reached an average volume of approximately 150 mm^3 (Lee *et al.*, 2009; Simon *et al.*, 2010), the mice were randomly divided into 3 groups. The first two groups were administered with PLGA-Chitosan-I_2BODIPY and PLGA-I_2BODIPY nanoparticles (at 10 mg/kg of I_2BODIPY equivalent, drug loading = 10% w/w) dissolved in normal saline to give a volume of 0.2 ml, respectively, via intravenous tail vein injection. The third group was administered with free I_2BODIPY (10 mg/kg). The I_2BODIPY was dissolved in a cocktail of 2.5% ethanol and 2.5% Cremophor EL. The mixture was then further dissolved in saline to reach a volume of 0.2 ml and was administered by intravenous tail vein injection. The mice (n=3) were sacrificed at predetermined time-points (0, 0.25, 1, 6, 24 and 48 h post-administration of free photosensitiser or nanoparticles). Major organs including tumour tissue, lymph nodes, spleen, kidney, liver, lung, skin and eyes were harvested and imaged using an In Vivo MS FX PRO (Carestream Molecular Imaging, CT, USA) with an excitation filter at 530 nm and an emission filter at 550 nm. Fluorescence intensities of each organ and tissue were quantified using Carestream Molecular Imaging software 5.0 (CT, USA). Mice treated with saline under identical conditions were used as a control.

3.16.3 *In vivo* PDT efficacy studies in 4T1 tumour-bearing mice

4T1 tumour transplantation was carried out as described in section 3.16.2. When the tumours reached an average volume of 150 mm^3, the mice were intravenously injected via tail vein with saline, free I_2BODIPY (10 mg/kg), PLGA-Chitosan-I_2BODIPY or PLGA-I_2BODIPY nanoparticles (at 10 mg/kg of I_2BODIPY equivalent), blank PLGA-Chitosan or PLGA nanoparticles (90 mg/kg, the equivalent to PLGA-Chitosan-I_2BODIPY and PLGA-I_2BODIPY nanoparticles that contain 10 mg/kg of free I_2BODIPY). PLGA-Chitosan-I_2BODIPY and PLGA-I_2BODIPY nanoaparticles were prepared in saline to a volume of 0.2 ml per injection. Meanwhile, free I_2BODIPY was

dissolved in a cocktail of 2.5% ethanol and 2.5% Cremophore EL. The mixture was then dissolved in saline to a volume of 0.2 ml per injection. The mice were randomly divided into 9 groups (n = 7) with different treatments, as follows: (1) PLGA-Chitosan-I_2BODIPY nanoparticles (irradiation at 1 h post-injection), (2) PLGA-Chitosan-I_2BODIPY nanoparticles (irradiation at 3 h post-injection), (3) PLGA-I_2BODIPY nanoparticles (irradiation at 1 h post-injection), (4) PLGA-I_2BODIPY nanoparticles (irradiation at 3 h post-injection), (5) free I_2BODIPY (irradiation at 1 h post-injection), (6) free I_2BODIPY (irradiation at 3 h post-injection), (7) blank PLGA-Chitosan nanoparticles (irradiation at 1 h post-injection), (8) blank PLGA nanoparticles (irradiation at 1 h post-injection), (9) saline (irradiation at 1 h post injection). A control group that was treated with saline mixed with a cocktail of 2.5% ethanol and 2.5% Cremophor EL (irradiation at 1 h post-injection) was also included in this study. The mice were then kept in the dark until irradiation. Before irradiation, the mice were anesthesised by administrating a cocktail of 90 mg/kg ketamine and 10 mg/kg xylazine. The solid tumour was then irradiated for 10 min (100 J/cm^2, fluence rate = 160 mW/cm^2) using a Lumacare LC-122A fiber optic light delivery system (standard fiber optic probe model LUM V, 400−700 nm, Lumacare Medical Group, CA, USA, with a 500/585 nm bandpass filter from Omega Optical, catalogue no. XF 3105) emitting light at 530 nm. A barrier was created between the light source and the tumour using a 4 mm thick glass slide (1.0 mm × 1.2 mm) (Sail Brand, Jiangsu, China, catalogue no. 7101), in order to avoid direct photothermal effect on the tumour. Illumination was directed at the tumour and the other parts of the body were covered with a black blanket to minimise unwanted PDT effect on non-tumour parts of the body. After PDT, the mice were kept in dark and tumour size changes were monitored 3 times per week. Tumour volumes were measured with a caliper and calculated as tumour volume, mm^3 = (L × W^2/2), where L is the longest dimension and W is the shortest dimension (Tomayko &

Reynolds, 1989). Tumour volumes did not exceed 1000 mm^3 throughout this study for ethical reasons. A set of dark controls without irradiation was performed concurrently (Kue *et al.*, 2015).

3.17 Statistical analysis

In vitro and *in vivo* experiments were performed to compare the efficacy of free I_2BODIPY, PLGA-Chitosan-I_2BODIPY and PLGA-I_2BODIPY nanoparticles. Statistical analysis was carried out using SPSS. One-Way ANOVA with Dunnett's Multiple Comparisons were used to compare means among the three groups of samples. Student's t-test was used to assess differences between two groups. The mean differences were considered statistically significant when the *p* value was less than 0.05 (*).

CHAPTER 4: RESULTS

4.1 Production and characterisation of low molecular weight chitosans

Chitosan were fragmented into lower molecular weights of 5, 10 and 25 kDa by oxidative degradation with sodium nitrite (Tan & Misran, 2013). Static light scattering method was used to determine the average molecular weight the chitosan produced. The intensity of scattered light is proportional to the average molecular weight and the concentration of the sample. For molecules which do not have angular dependence in their scattering intensity, their molecular weight determination can be made at a single angle (Rayleigh scatterers) using the Debye plot derived from the following Rayleigh equation:

$$\frac{KC}{R_\theta} = \left[\frac{1}{M} + 2A_2C\right]\frac{1}{P_\theta}$$

where K = optical constant, C = concentration, M = molecular weight, R_θ = Rayleigh ratio, A_2 = 2nd virial coefficient, P_θ = shape factor.

For Rayleigh scatterers, P_θ = 1, and the equation is simplified to

$$\frac{KC}{R_\theta} = \left[\frac{1}{M} + 2A_2C\right] \qquad (y = b + mx)$$

Therefore, a plot of KC/R_θ versus C would give a straight line and the intercept at zero concentration will be 1/M.

Hence, the reciprocal of molecular weight of the chitosan (1/kDa), represented by the intercept point at y-axis in Debye plot, was used to calculate the average molecular weight of chitosan (Figure 4.1).

The chitosan with molecular weight of 5-, 10- and 25-kDa were produced at a yield of 8, 30 and 60%. Increasing molecular weight had reduced the water solubility of

chitosan. The water solubility was 21.31, 9.41 and 5.60 g/L for 5-, 10- and 25-kDa mean-molecular weight chitosan solutions, respectively.

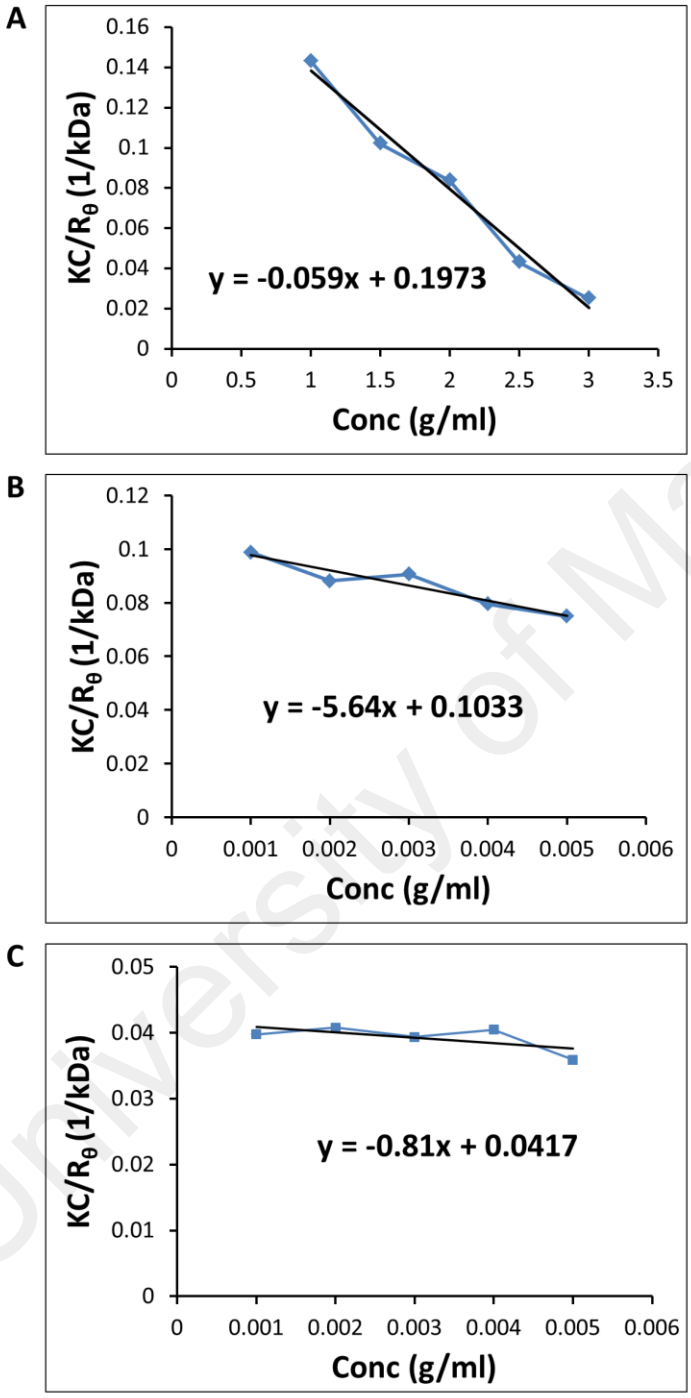

Figure 4.1: Debye plot for chitosan of average molecular weight (A) 5, (B) 10, and (C) 25 kDa.

The reciprocal of molecular weight of the chitosan (1/kDa) is represented by the intercept point at y-axis in Debye plot. Thus, the molecular weight of the chitosan is calculated as (A) 1/0.1973 = 5 kDa, (B) 1/0.1033 = 10 kDa, and (C) 1/0.0417 = 24 kDa.

4.2 Characterisation of PLGA-I_2BODIPY and PLGA-Chitosan-I_2BODIPY nanoparticles

4.2.1 Process yield, I_2BODIPY loading and encapsulation efficiency, and chitosan coating characterisation

PLGA-I_2BODIPY nanoparticles were produced via nanoprecipitation technique at a yield of 73%, with 10% I_2BODIPY loading amount (wt%) and 50% entrapment efficiency. The synthesis of blank PLGA nanoparticles also gave the same yield. The amount of chitosan coating on the nanoparticles was approximately 25 ± 1.9, 40 ± 1.6 and 60 ± 1.7% (w/w, n=3) for the 5-, 10- and 25-kDa chitosan concentration used to coat the particles.

4.2.2 Particle size, size distribution and zeta potential

The particle size and distribution of the prepared PLGA-I_2BODIPY nanoparticles was determined using a Malvern NanoSeries ZetaSizer. The average diameter of the nanoparticles was approximately 150 nm. Coating the nanoparticles with chitosan of different molecular weights did not cause significant changes in the average particle size. The polydispersity index (PDI) which indicates the particle size distribution was less than 0.06 (Table 4.1). The value of PDI was close to zero showing that the nanoparticles were monodispersed. Over 80% of the PLGA-I_2BODIPY and PLGA-Chitosan-I_2BODIPY nanoparticles prepared were in the range of 106 – 190 nm (Figure 4.3). This indicates the nanoparticles had a narrow size distribution, thus constituting a monomodal system (Scholes *et al.*, 1993).

Table 4.1: Composition and physical-chemical parameters of PLGA-Chitosan and PLGA NP

Sample	PLGA-Chitosan-I_2BODIPY NP			PLGA-I_2BODIPY NP	PLGA-Chitosan NP	PLGA NP
	0.5% w/v 5 kDa Chitosan	0.5% w/v 10 kDa Chitosan	0.5% w/v 25 kDa Chitosan		0.5% w/v 25 kDa Chitosan	
Diameter (nm)	143.9 ± 2.17	146.2 ± 0.17	146.9 ± 0.76	149 ± 1.22	145.7 ± 0.35	146.2 ± 0.21
PDI	0.059 ± 0.05	0.059 ± 0.02	0.046 ± 0.02	0.056 ± 0.01	0.077 ± 0.02	0.038 ± 0.02
Zeta Potential (mV)	-13.39 ± 0.07	-8.52 ± 0.16	-5.32 ± 0.05	-32.2 ± 0.12	-5.19 ± 0.02	-29.2 ± 0.66

Data are expressed as mean ± SD (n=6). PDI < 0.2 is considered good for PLGA NP.

(NP = nanoparticles, PDI = polydispersity index)

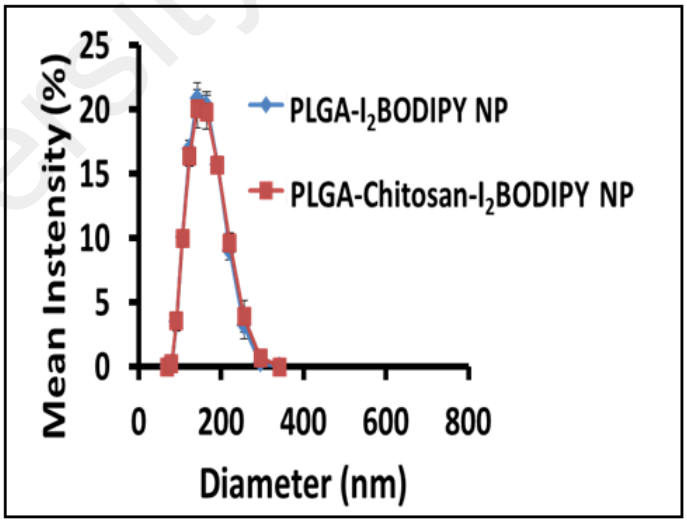

Figure 4.2: Particle size distribution PLGA-Chitosan-I_2BODIPY (25 kDa chitosan) and PLGA-I_2BODIPY nanoparticles

The zeta potential indicates the surface charge of the nanoparticles. The PLGA-I_2BODIPY nanoparticles were negatively charged with a zeta potential of -32 mV. The zeta potential of PLGA-I_2BODIPY nanoparticles became less negative upon coating with chitosan of increasing molecular weight (Table 4.1) and concentrations (Figure 4.4). PLGA-I_2BODIPY nanoparticles coated with 0.5% (w/v) of 25 kDa chitosan gave a zeta potential of -5 mV, which is close to neutral to prevent premature clearance by the RES.

Despite the low surface charge, both the chitosan-coated and uncoated nanoparticles were stable in the system and did not aggregate. The size distribution of the chitosan-coated and uncoated nanoparticles did not vary over a period of 30 days, whether at ambient temperature or at 4 ℃ in deionised water (Figure 4.5).

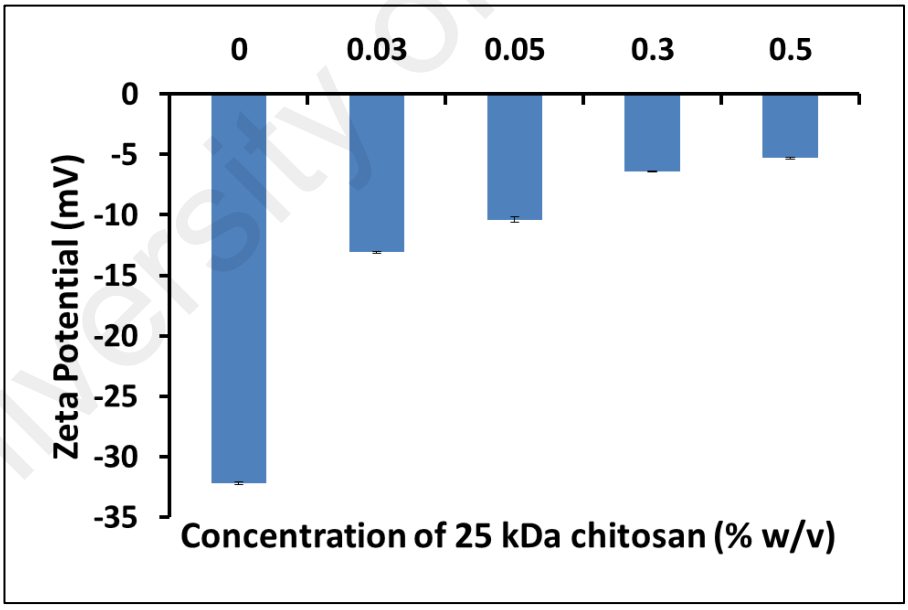

Figure 4.3: Zeta potential of PLGA-I_2BODIPY nanoparticles upon coating of chitosan (25 kDa)

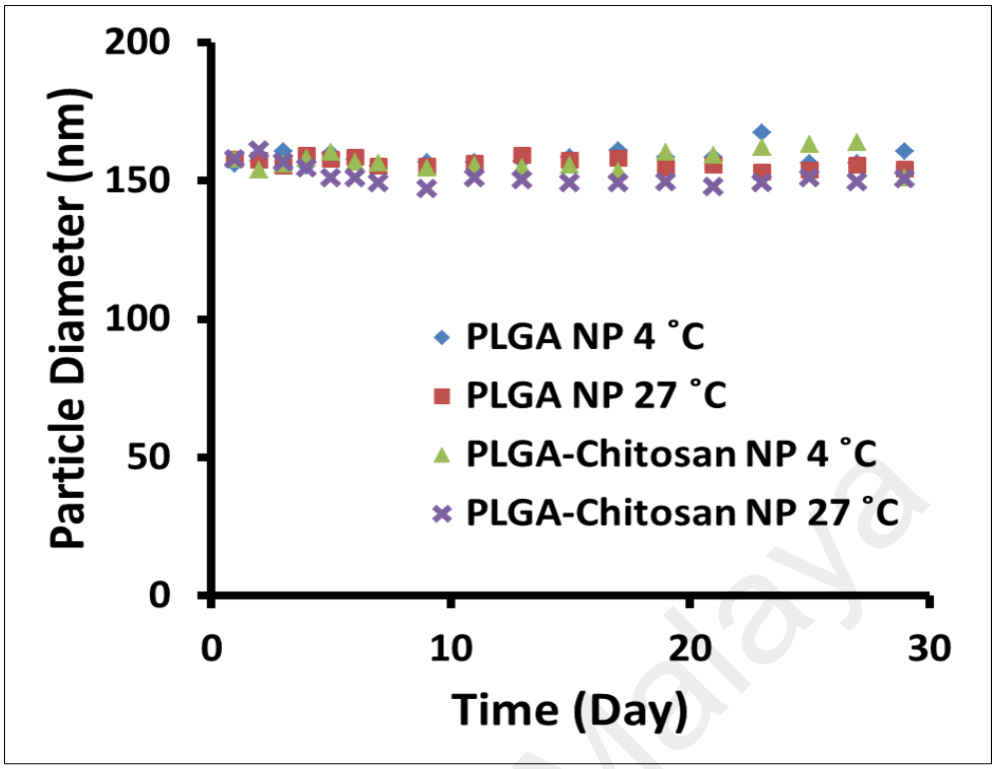

Figure 4.4: Particle size distribution of PLGA-Chitosan and PLGA nanoparticles over 30 days

Nanoparticles remained stable and did not aggregate when kept at 27 ℃ and 4 ℃

4.2.3 Particle size and morphology

The PLGA-Chitosan-I_2BODIPY and PLGA-I_2BODIPY nanoparticles appeared as discrete spheres with smooth surfaces when observed under scanning electron microscopy (Figure 4.6). No significant changes were found in the particle size range or the morphology upon coating of chitosan onto the PLGA-I_2BODIPY nanoparticles, suggesting that the coating layer was too thin to be detected in the analysis. This observation is in agreement with previous reports (Chakravarthi & Robinson, 2011; Chronopoulou *et al.*, 2013).

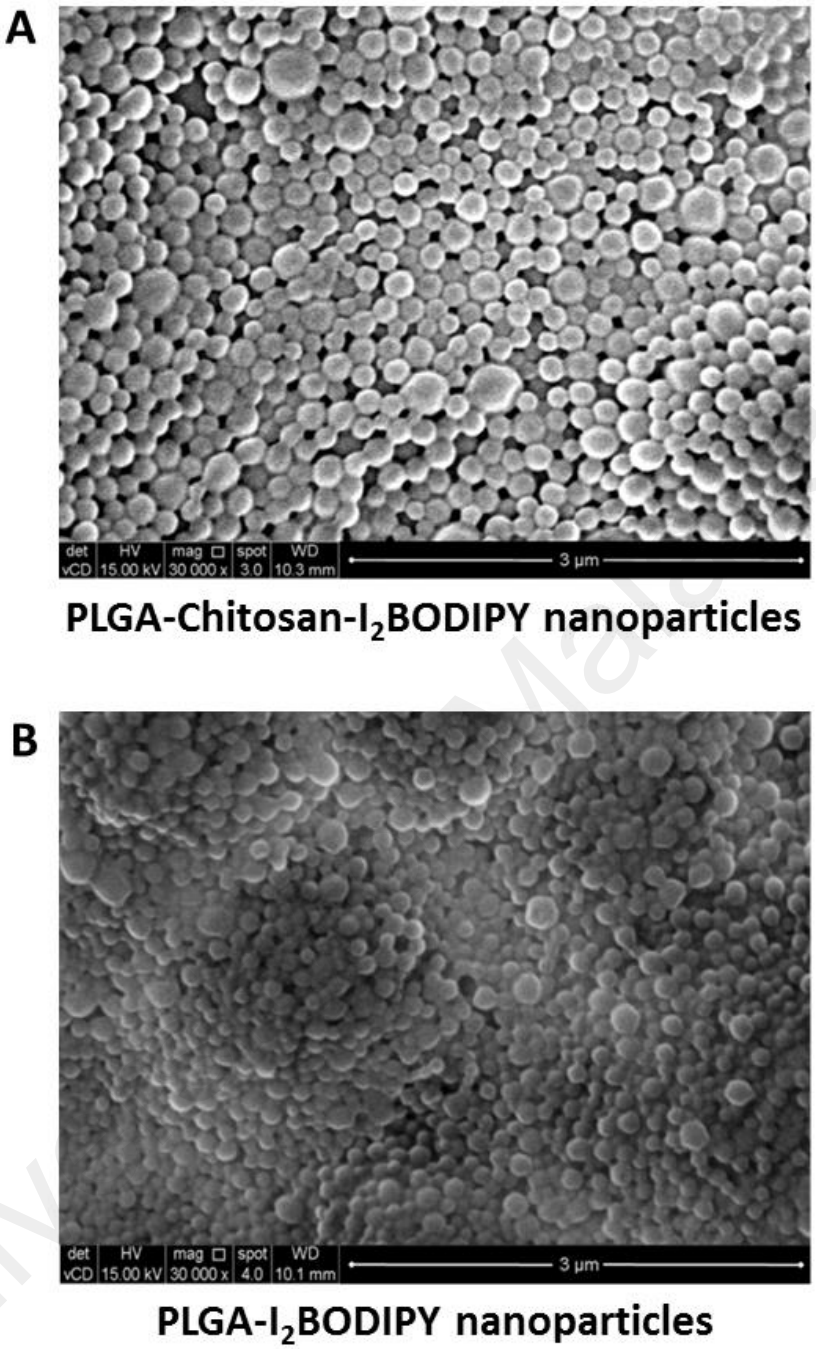

Figure 4.5: Morphology of PLGA-Chitosan-I_2BODIPY and PLGA-I_2BODIPY nanoparticles under scanning electron microscopy

4.2.4 Biocompatibility of PLGA-Chitosan-I_2BODIPY and PLGA-I_2BODIPY nanoparticles: Haemolysis Test

Evaluation of haemo-biocompatibility is essential to prevent complications such as haemolytic anemia when the nanoparticles are administered *in vivo*. After the nanoparticles were incubated with the red blood cells for 5 h, a small degree of haemolysis was observed with a plateau haemolysis value of approximately 13% for chitosan-coated PLGA nanoparticle (chitosan molecular weight of 5, 10 and 25 kDa) and PLGA nanoparticles (Figure 4.7) at concentrations from 2.5 – 10 mg/ml. This value is tolerable since substances are classified as non-haemolytic when less than 15% of the red blood cells are lysed in the assay (Petersen *et al.*, 2002; Richardson *et al.*, 1999). Furthermore, approximately 2 mg of the nanoparticles injected into the mice in the animal study later would be rapidly diluted by the total blood volume in circulation (estimated to be 2 ml) (Perrault & Chan, 2010) to a level which an insignificant degree of haemolysis is expected. Based on the encouraging haemo-biocompatibility data, PLGA-chitosan and PLGA nanoparticles were considered suitable for intravenous administration in mice.

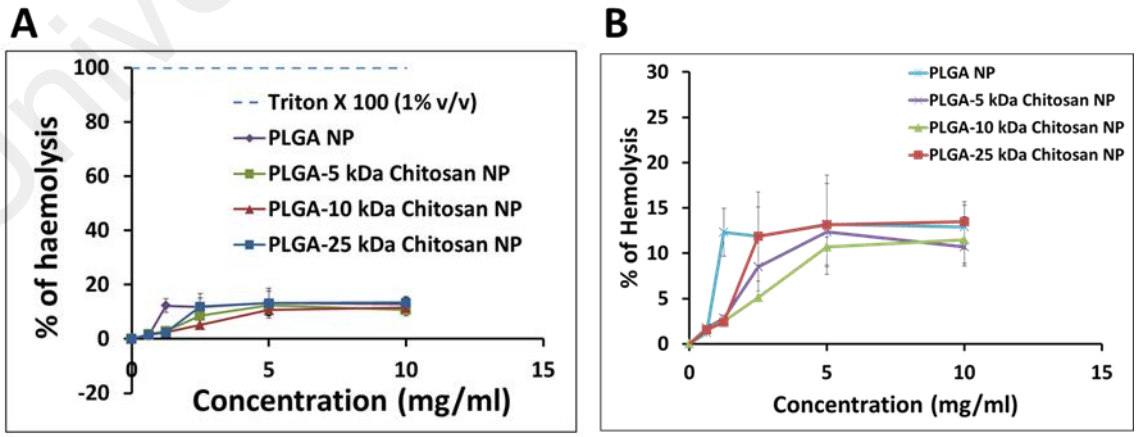

Figure 4.6: Haemolysis at different concentration of PLGA and PLGA-Chitosan (5, 10 and 25 kDa) nanoparticles

(A) Triton X 100 (1% v/v) was used as positive control. (B) Same set of data was presented without showing Triton X 100 as positive control for better clarity of the results. PLGA-Chitosan nanoparticles (5, 10 and 25 kDa chitosan) and PLGA nanoparticles are classified as non-haemolytic as haemolysis was around 13% (less than 15%). Data represents mean ± SD (n=3).

4.2.5 Evaluation of Protein Adsorption to Particle Surface

The amount of serum protein that was adsorbed on the PLGA nanoparticles decreased with increasing molecular weights (5, 10 and 25 kDa) of the chitosan coating on the nanoparticles (Figure 4.8). The amount of serum protein adsorbed to 1 mg of PLGA-Chitosan (25 kDa) nanoparticles was approximately 2-fold lower ($p < 0.05$, One-Way ANOVA) than the blank uncoated PLGA nanoparticles and 1.5 to 1.6-fold lower than the PLGA nanoparticles coated with 5- and 10-kDa chitosan, respectively (Figure 4.8). This result indicates that chitosan coating on the PLGA nanoparticles may reduce surface opsonization and hence, prevent premature clearance from blood circulation through the reticuloendothelial system and the Kupffer cells in the liver (Salmaso & Caliceti, 2013). The difference between the amounts of protein adsorbed by the nanoparticles coated with 5- and 10-kDa chitosan was not statistically significant. Thus, PLGA-Chitosan (25-kDa) nanoparticles, which exhibited the lowest measured protein adsorption and surface charge close to neutral (-5 mV) (section 4.2.2), were used in the subsequent photophysical and photochemical characterisations, *in vitro* drug release evaluation, as well as cell- and animal-based studies.

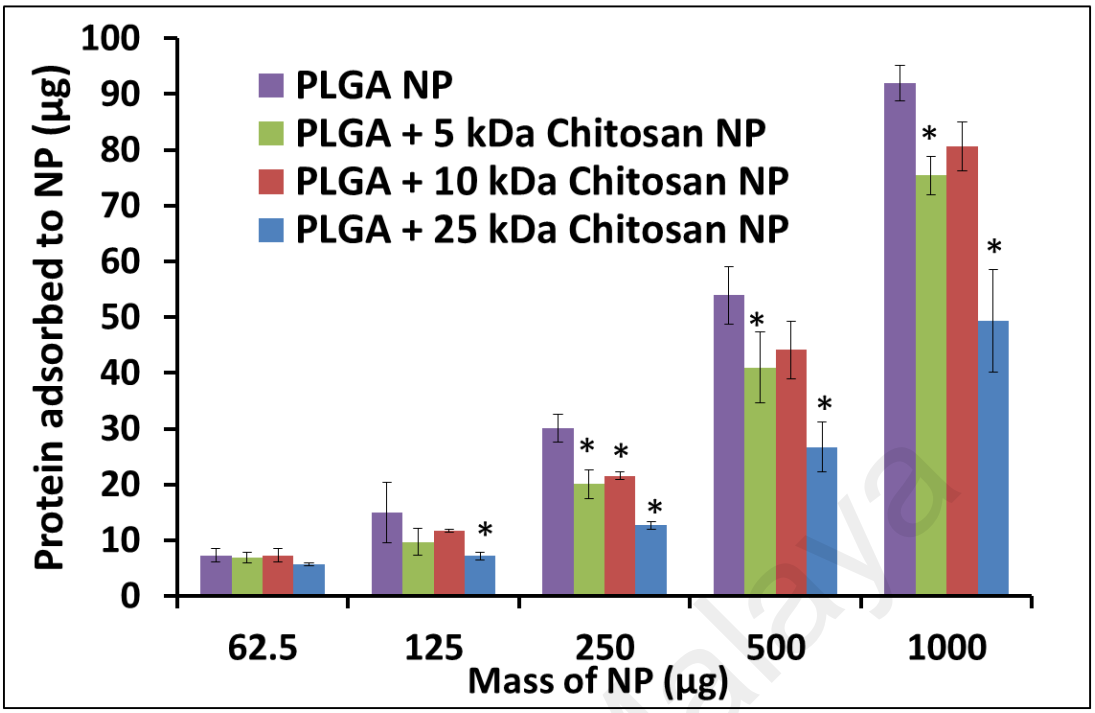

Figure 4.7: Protein adsorbed on nanoparticles surface

The amount of serum protein adsorbed onto PLGA-Chitosan (25 kDa) nanoparticles was lower than that for blank PLGA and PLGA-Chitosan nanoparticles (5 and 10 kDa). Data represents mean ± SD (n=3).* $p < 0.05$ using one-way ANOVA. (NP = nanoparticles)

4.3 Photophysical and photochemical characterisation

4.3.1 UV-visible and fluorescence emission spectra

The methanol and acetone extract of I_2BODIPY (25 µM) from the chitosan-coated and uncoated nanoparticles were found to exhibit a similar UV-vis absorbance peak at 532 nm to that of free I_2BODIPY (Figure 4.9). Besides, the fluorescence emission spectra of I_2BODIPY extracted from the PLGA-Chitosan-I_2BODIPY and PLGA-I_2BODIPY nanoparticles produced an emission peak similar to free I_2BODIPY at 552 nm after light excitation at 532 nm in methanol (Figure 4.10). These results indicate that

the process of encapsulation with PLGA and chitosan coating did not alter the original photophysical properties of I_2BODIPY in organic solvents. In PBS, free I_2BODIPY showed the lowest molar extinction coefficients with no absorbance peak observed. Conversely, PLGA-Chitosan-I_2BODIPY and PLGA-I_2BODIPY nanoparticles produced sharp peaks at 492 and 479 nm (Figure 4.9). This may be due to the aggregation of free I_2BODIPY because of their hydrophobic nature. The entrapping of I_2BODIPY with PLGA-Chitosan or PLGA nanoparticle had probably prevented the aggregation of I_2BODIPY in aqueous solvent and restored the light absorption of I_2BODIPY.

Also, the fluorescence excitation spectra were found to resemble the corresponding absorption spectra in methanol for the free I_2BODIPY and the I_2BODIPY extracted from the nanoparticles (Figure 4.10). This suggests that I_2BODIPY in PLGA-Chitosan or PLGA nanoparticles did not aggregate in aqueous solution, which is consistent with those of other studies that demonstrate that in cases of aggregation, the fluorescence excitation and UV-visible absorption spectra are not overlapping. The observed shift to a shorter wavelength may be due to the increased polarity of the solvent (Schmid, 2001) and entrapment of I_2BODIPY in a polymeric carrier (John & George).

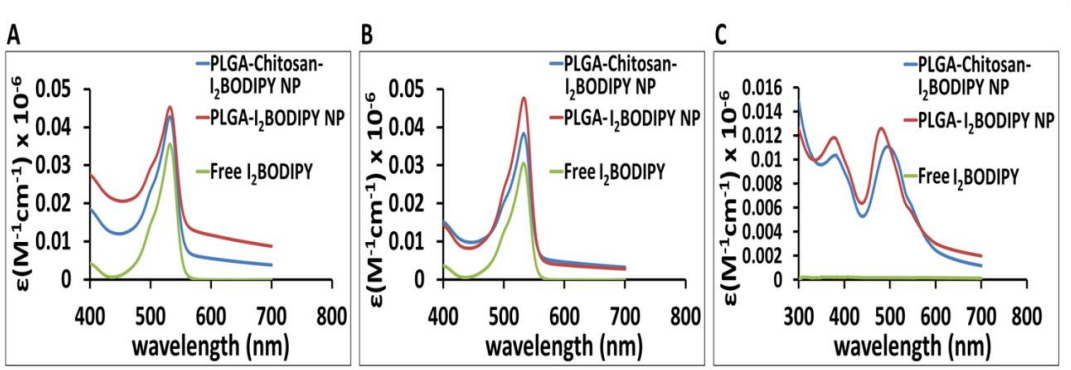

Figure 4.8: UV-visible spectra of PLGA-Chitosan-I_2BODIPY, PLGA-I_2BODIPY nanoparticles and free I_2BODIPY in (A) acetone, (B) methanol and (C) PBS

UV-visible absorption spectra of PLGA-Chitosan-I_2BODIPY, PLGA-I_2BODIPY nanoparticles (25 µM of free I_2BODIPY) and free I_2BODIPY (25 µM) were similar in (A) acetone and (B) methanol. PLGA-Chitosan-I_2BODIPY, PLGA-I_2BODIPY nanoparticles showed higher absorbance peak and molar extinction coefficient in (C) PBS than free I_2BODIPY which did not show any absorbance peak.

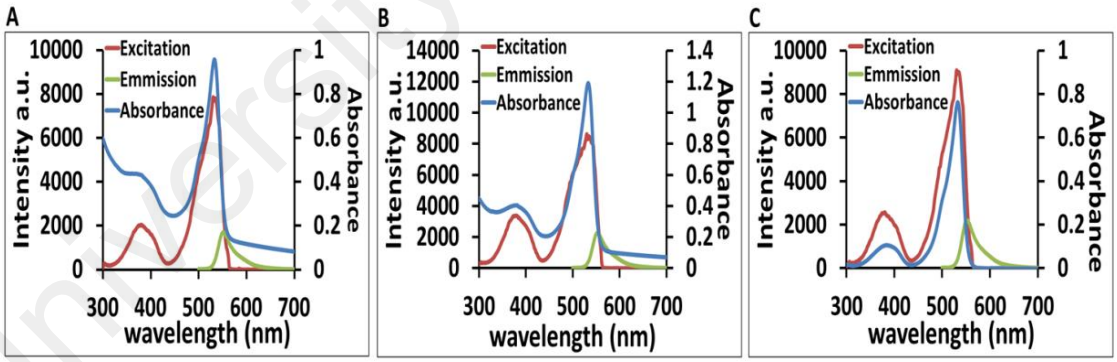

Figure 4.9: UV-visible, fluorescence excitation and fluorescence emission spectra of (A) PLGA-Chitosan-I_2BODIPY (B) PLGA-I_2BODIPY and (C) free I_2BODIPY in methanol

(A) PLGA-Chitosan-I_2BODIPY, (B) PLGA-I_2BODIPY nanoparticles (25 µM of free I_2BODIPY) and (C) free I_2BODIPY (25 µM) have the same UV-visible absorption, fluorescence emission and fluorescence excitation spectra.

4.3.2 Singlet oxygen detection by a chemical method

The generation of singlet oxygen was confirmed by using a chemical detector disodium salt of 9,10-anthracenedipropionic acid (ADPA). When a solution of I_2BODIPY dissolved in 1% SDS or 0.1% Tween 80 in PBS was added to the ADPA and photo-irradiated, a marked decrease in optical density at 400 nm (the absorption maximum for ADPA) was observed, indicating rapid generation of singlet oxygen as a function of time to light exposure. The optical density was also found to decrease in a manner similar to that of free I_2BODIPY in surfactant (either in SDS or Tween 80) when the PLGA-Chitosan-I_2BODIPY and PLGA-I_2BODIPY nanoparticles in D_2O were irradiated with light during the first 10 min, followed by a slower rate of decrease (Figure 4.11). Meanwhile, blank PLGA-Chitosan, blank PLGA nanoparticles and the hydrophobic I_2BODIPY in D_2O did not show any changes in optical density (Figure 4.11). These suggest that entrapment of I_2BODIPY in nanoparticles reduced aggregation of the photosensitiser molecules and enabled generation of singlet oxygen in aqueous environment. The nanocarriers PLGA and PLGA-Chitosan alone did not generate singlet oxygen.

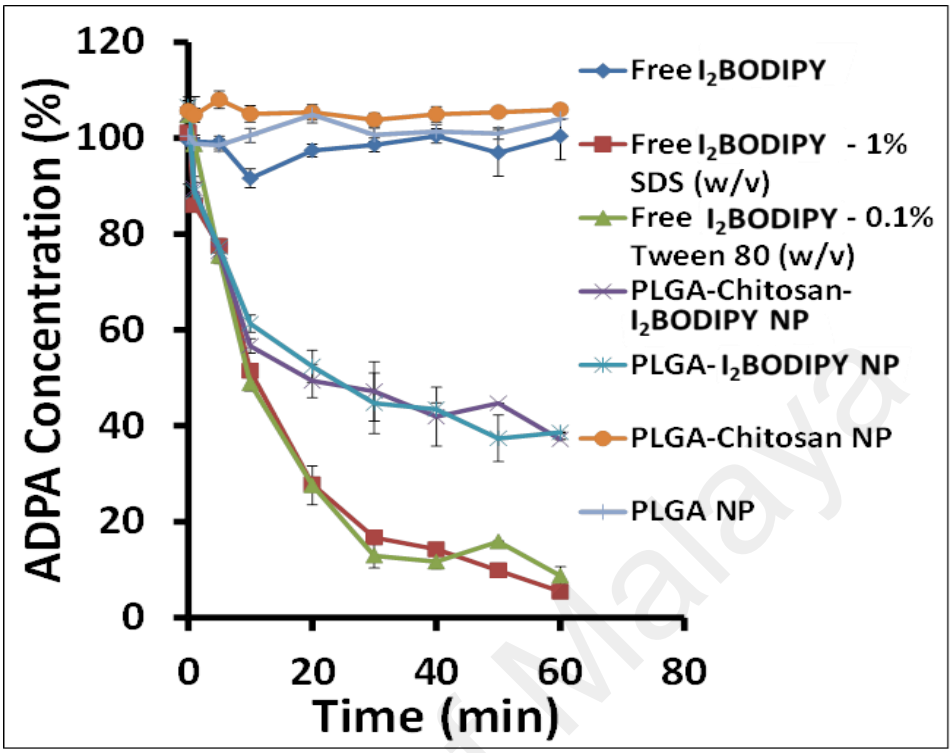

Figure 4.10: Singlet oxygen generation detected by using ADPA as a sensor according to irradiation time.

PLGA-Chitosan-I_2BODIPY and PLGA-I_2BODIPY nanoparticles in PBS and free I_2BODIPY in surfactant generated singlet oxygen but not free I_2BODIPY in PBS. Data represents mean ± SD (n=3).

4.4 *In vitro* I_2BODIPY release in PBS and plasma

At the physiological pH of 7.4, initial burst release followed by a sustained release of I_2BODIPY was observed for chitosan-coated PLGA nanoparticles at a lower amount and slower rate compared to the uncoated nanoparticles (Figure 4.12). During the first 6 h, the initial rapid release of I_2BODIPY at pH 7.4 was reduced by approximately 2-fold when the PLGA-I_2BODIPY nanoparticles were chitosan-coated. Conversely, in acidic environments at pH 4.8, the initial release of I_2BODIPY from chitosan-coated PLGA

nanoparticles increased by about 3-fold compared to that released at pH 7.4. The low burst release (less than 20%) from the chitosan-coated nanoparticles at 6 h is not giving a therapeutic effect. This is because singlet oxygen can only be generated upon activation by light. Irradiation was applied directly to the tumor in the *in vivo* antitumor assays.

The initial burst release was observed for 3 days followed by controlled release which was best fitted with zero-order kinetics ($r^2 = 0.98 \pm 0.003$ for PLGA nanoparticle pH 7.4; $r^2 = 0.94 \pm 0.002$ for PLGA-Chitosan nanoparticle pH 7.4; $r^2 = 0.92 \pm 0.002$ for PLGA nanoparticle pH 4.8; $r^2 = 0.96 \pm 0.005$ for PLGA-Chitosan nanoparticle pH 4.8). There was an insignificant difference in release rate ($p > 0.05$) between the formulations (release rate $K_0 = 0.03 \pm 0.02$) for a short period of 12 days. The kinetic release (zero-order) reflects a sustained PLGA degradation that leads to the release of I_2BODIPY. The kinetic release does not fit well into first order, Higuchi model and Hixson-Crowell model.

On day 12, the I_2BODIPY level released from chitosan-coated nanoparticles at pH 4.8 was 1.5-fold higher than that released at pH 7.4. Meanwhile, similar release rate was observed for the uncoated PLGA-I_2BODIPY nanoparticles at both pH 4.8 and 7.4. The early burst release may be due to the I_2BODIPY that was deposited or loosely bound to the surface of nanoparticles. This was followed by a sustained release when I_2BODIPY were slowly diffused out of the nanoparticle after polymer degradation (Yallapu *et al.*, 2010).

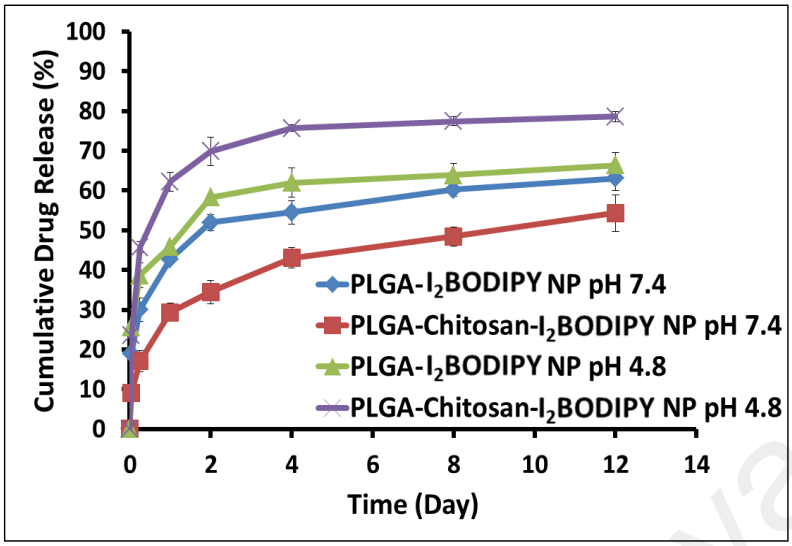

Figure 4.11: *In vitro* release profiles of PLGA-Chitosan-I_2BODIPY and PLGA-I_2BODIPY nanoparticles in PBS at pH 7.4 and 4.8

PLGA-Chitosan-I_2BODIPY NP (chitosan 25 kDa, 0.5% w/v) showed a slower release of I_2BODIPY compared to PLGA-I_2BODIPY NP at pH 7.4 in PBS (0.1% w/v Tween 80), even though more I_2BODIPY was released at a faster rate from PLGA-Chitosan-I_2BODIPY NP compared to PLGA-I_2BODIPY NP at pH 4.8. Data represents mean ± SD (n=3).

The release profile in plasma demonstrated similar rapid burst release of I_2BODIPY from PLGA-chitosan and PLGA nanoparticles during the first 6 h, which was approximately 20%. Subsequently, a 5% decrease in the sustained release of I_2BODIPY from PLGA-Chitosan-I_2BODIPY nanoparticles compared to the rate of PLGA-I_2BODIPY nanoparticles was observed up until day 12, which was approximately 32% for PLGA-Chitosan-I_2BODIPY and 37% for PLGA-I_2BODIPY nanoparticles, respectively ($p < 0.05$, Student's t-test, Figure 4.13).

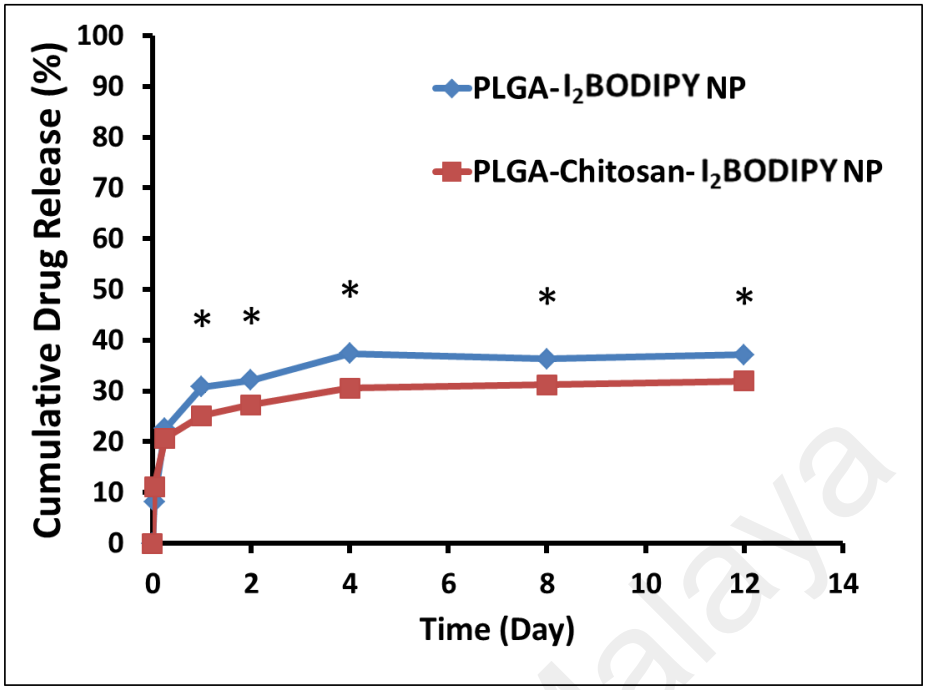

Figure 4.12: *In vitro* release profiles of PLGA-Chitosan-I_2BODIPY and PLGA-I_2BODIPY nanoparticles in plasma

In murine plasma, the release of I_2BODIPY from PLGA-Chitosan-I_2BODIPY NP (chitosan 25 kDa, 0.5% w/v) was significantly lower than that of PLGA-I_2BODIPY NP up to day 12. Data represents mean ± SD (n=3). * $p < 0.05$ using Student's t-test. (NP = nanoparticles)

4.5 *In vitro* photocytotoxicity of PLGA-Chitosan-I_2BODIPY and PLGA-I_2BODIPY nanoparticles

To determine the photocytotoxicity of PLGA-Chitosan-I_2BODIPY and PLGA-I_2BODIPY nanoparticles, murine 4T1 and human MDA-MB-231 breast cancer cell lines, were incubated with the nanoparticles and free I_2BODIPY for 2 h, washed twice with PBS then irradiated with a light dose of 5.3 J/cm^2. The cell viability following treatment was determined 24 h later using the MTT assay (Figure 4.14). Without

irradiation, no cytotoxicity was observed in 4T1 or MDA-MB-231 cells treated with free I_2BODIPY, the chitosan-coated and uncoated nanoparticles loaded with I_2BODIPY and the blank PLGA-Chitosan or PLGA nanoparticles (data not shown). However, the cell viability significantly decreased when the cells treated with PLGA-Chitosan-I_2BODIPY or PLGA-I_2BODIPY nanoparticles were photo-irradiated. PLGA-Chitosan-I_2BODIPY nanoparticles were found to be more photocytotoxic with lower IC_{50} than the PLGA-I_2BODIPY nanoparticles and free I_2BODIPY (Table 4.2). Meanwhile, 4T1 and MDA-MB-231 cells treated with blank PLGA-Chitosan or PLGA nanoparticles showed no photocytotoxicity (Figure 4.14, Table 4.2).

When the incubation time was increased from 2 to 4 and 6 h, both the PLGA-Chitosan-I_2BODIPY and PLGA-I_2BODIPY nanoparticles showed increased photocytotoxocity in 4T1 and MDA-MB-231 tumour cells in 4T1 and MDA-MB-231 tumour cells, but the difference between the cytotoxicity of the two became less noticeable (Figure 4.14, Table 4.2). Free I_2BODIPY also showed increased photocytotoxicity with increasing incubation time from 2 to 4 and 6 h (Figure 4.14, Table 4.2).

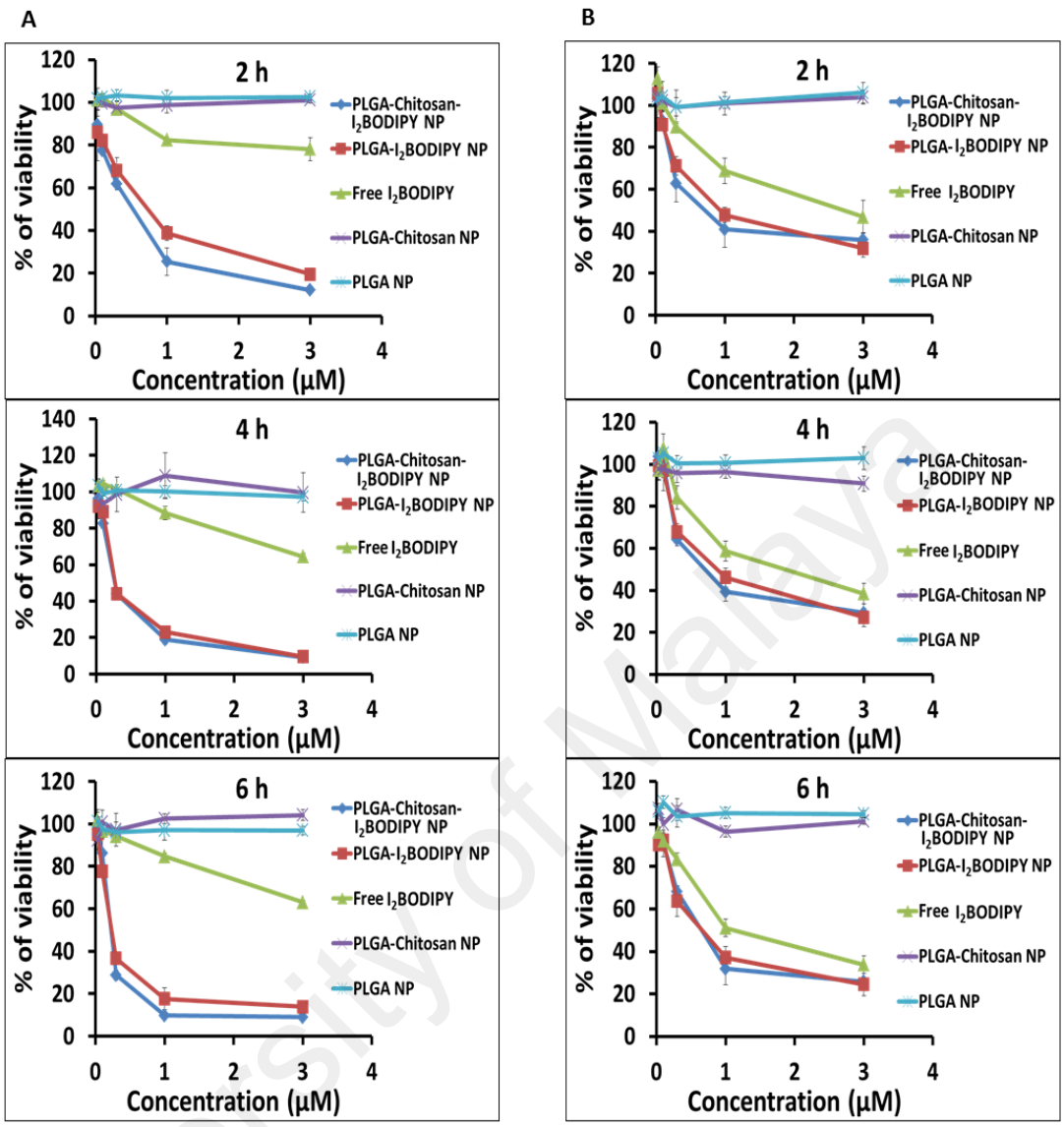

Figure 4.13: *In vitro* photocytoxicity of free I_2BODIPY, PLGA-Chitosan-I_2BODIPY and PLGA-I_2BODIPY nanoparticles on (A) 4T1 cells and (B) MDA-MB-231 cells

Viability of (A) 4T1 cells and (B) MDA-MB-231 cells treated with free I_2BODIPY, PLGA-Chitosan-I_2BODIPY or PLGA-I_2BODIPY nanoparticles, blank PLGA-chitosan and PLGA nanoparticles. After 2, 4 and 6 h of incubation, cells were washed twice with PBS, followed by irradiation with 5.3 J/cm^2 of light from a broad-spectrum halogen light source, at a fluence rate of 8.9 mW/cm^2 for 10 min. Data represents mean ± SEM (n=3). *$p < 0.05$ using One-Way ANOVA.

Table 4.2: IC_{50} value of tested NP and free I_2BODIPY in 4T1 and MDA-MB-231 cancer cells after different incubation time of 2, 4 and 6 h and PDT

Samples	IC_{50} (μM)					
	4T1			MDA-MB-231		
	2 h	4 h	6 h	2 h	4 h	6 h
PLGA-Chitosan-I_2BODIPY NP	0.37	0.31	0.26	0.76	0.80	0.62
PLGA-I_2BODIPY NP	0.55	0.33	0.29	0.99	0.86	0.63
Free I_2BODIPY	> 10	> 10	> 10	3.30	2.03	1.34
Blank PLGA-Chitosan NP	-	-	-	-	-	-
Blank PLGA NP	-	-	-	-	-	-

(NP = nanoparticles; "-" no photocytotoxicity observed)

4.6 Cellular uptake of PLGA-Chitosan-I_2BODIPY and PLGA-I_2BODIPY nanoparticles

The cellular accumulation kinetics of the chitosan-coated and uncoated PLGA-I_2BODIPY nanoparticles were studied in 4T1 murine breast cancer cells and RAW246.7 murine macrophages. The molar amount of I_2BODIPY taken up by the cells was determined after incubation with the PLGA-Chitosan-I_2BODIPY or PLGA-I_2BODIPY nanoparticles (20 μM of free I_2BODIPY equivalent) in the dark. Confocal microscopy was also used to qualitatively assess the uptake of the studied nanoparticles and free I_2BODIPY.

In 4T1 cancer cells, the chitosan-coated PLGA-I_2BODIPY nanoparticles exhibited the highest rate and amount of uptake compared to the uncoated PLGA-I_2BODIPY

nanoparticles and free I_2BODIPY (Fig. 4.15). After 0.5 h of incubation, the 4T1 cellular uptake of PLGA-Chitosan-I_2BODIPY nanoparticles increased significantly ($p < 0.05$, One-Way ANOVA) and reached a plateau of approximately 75% of the initial amount added (based on the concentration of I_2BODIPY) in 3 h. This uptake amount was higher by approximately 1.5- and 3-fold than those of PLGA-I_2BODIPY nanoparticles and I_2BODIPY, respectively. These results suggest that the coating of PLGA-I_2BODIPY nanoparticles with low molecular weight chitosan enhanced the cellular uptake of I_2BODIPY compared to PLGA-I_2BODIPY nanoparticles and free I_2BODIPY in 4T1 cells.

Conversely, the chitosan-coated PLGA-I_2BODIPY nanoparticles significantly reduced the rate and amount of RAW246.7 macrophage uptake compared to PLGA-I_2BODIPY nanoparticles and free I_2BODIPY (Figure 4.16). During the first 8 h, the uptake of PLGA-Chitosan-I_2BODIPY nanoparticles was approximately 4 and 5 times lower than the uptake levels of PLGA-I_2BODIPY nanoparticles and free I_2BODIPY, respectively, which is only approximately 12% of the initial amount added. The uptake amount of PLGA-Chitosan-I_2BODIPY nanoparticles by the macrophages remained the lowest up to 24 h of incubation period (36% of initial amount), which was approximately 1.7- and 1.9-fold lower than that of PLGA-BOPDIPY nanoparticles and free I_2BODIPY, respectively. These indicate that chitosan coating on the nanoparticles exhibited “stealth” properties and significantly reduced uptake of the nanoparticles by macrophages (Salmaso & Caliceti, 2013).

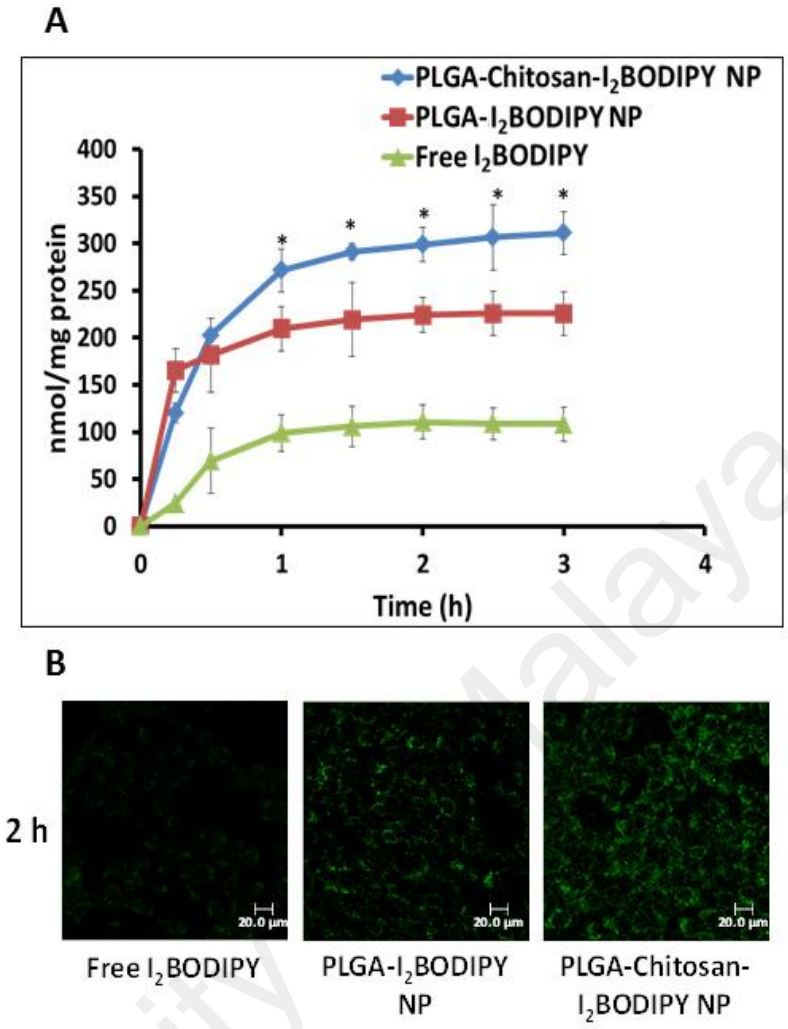

Figure 4.14: Cellular uptake of free I_2BODIPY, PLGA-Chitosan-I_2BODIPY and PLGA-I_2BODIPY nanoparticles in 4T1 cells.

(A) Intracellular uptake profiles of free I_2BODIPY (20 µM), PLGA-Chitosan-I_2BODIPY and PLGA-I_2BODIPY NP (20 µM equivalent of I_2BODIPY) in 4T1 cells. The uptake of PLGA-Chitosan-I_2BODIPY NP increased significantly after 0.5 h incubation and reached a plateau at 3 h. The uptake was higher than those of PLGA-I_2BODIPY NP and free I_2BODIPY by 1.4 and 2.9 times, respectively. * $p < 0.05$ using One-Way ANOVA. (B) Confocal images of 4T1 cells were taken after 2 h incubation with the samples (I_2BODIPY is in green).

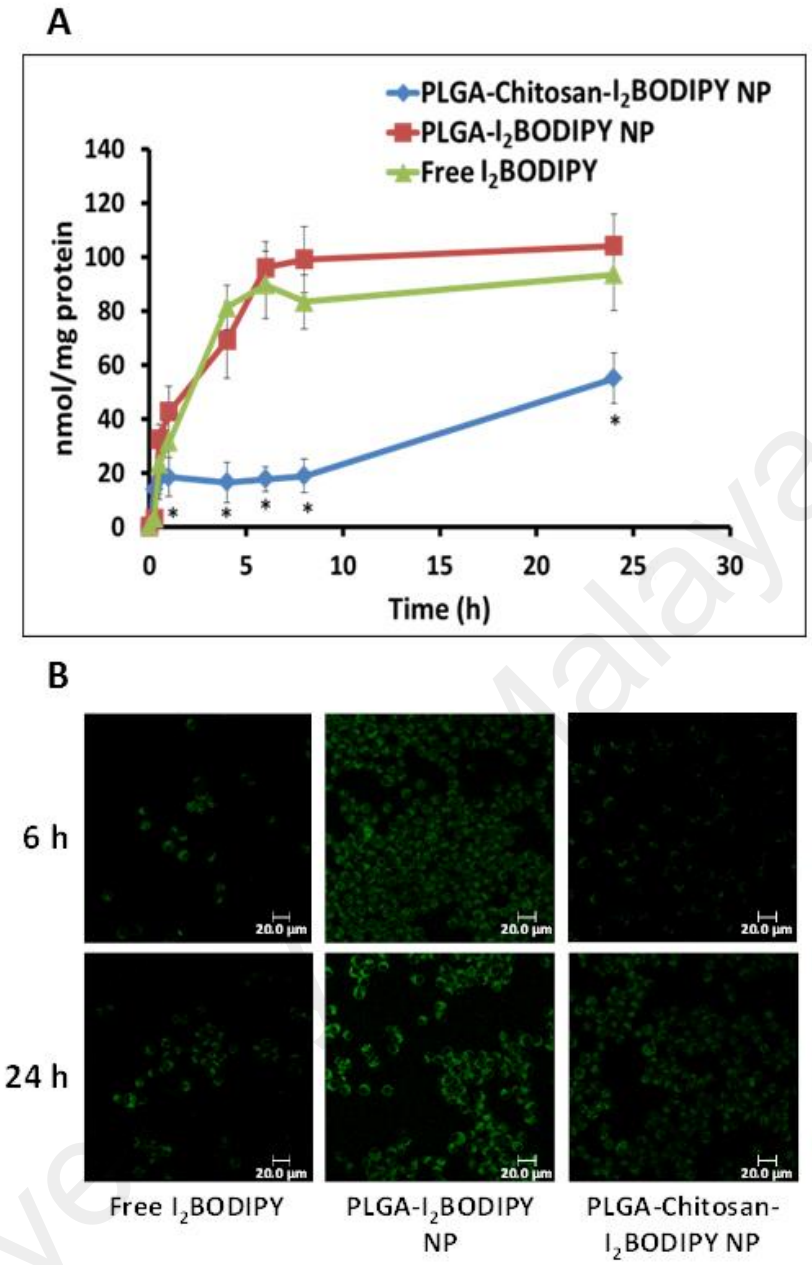

Figure 4.15: Cellular uptake of free I_2BODIPY, PLGA-Chitosan-I_2BODIPY and PLGA-I_2BODIPY nanoparticles in RAW246.7 macrophages.

(A) Intracellular uptake profile of free I_2BODIPY (20 µM), PLGA-Chitosan-I_2BODIPY and PLGA-I_2BODIPY NP (20 µM equivalent of I_2BODIPY) in RAW246.7 macrophages. During the first 8 h, the uptake PLGA-Chitosan-I_2BODIPY NP was approximately 4 and 5 times lower than PLGA-I_2BODIPY NP and free I_2BODIPY, respectively. The uptake amount of PLGA-Chitosan-I_2BODIPY NP remained the lowest

up to 24 h of incubation period, which was approximately 1.7 to 1.9 times lower than the amounts of PLGA-BODIPY NP and free I_2BODIPY.* $p < 0.05$ using One-Way ANOVA (B) Confocal images of RAW246.7 macrophages were taken after 6 and 24 h incubation with the samples (I_2BODIPY is in green). (NP = nanoparticles).

4.7 Intracellular localization of PLGA-Chitosan-I_2BODIPY and PLGA-I_2BODIPY nanoparticles

The intracellular localization of free I_2BODIPY, PLGA-Chitosan-I_2BODIPY and PLGA-I_2BODIPY nanoparticles was observed and analysed using confocal microscopy. Images of the samples co-stained with organelle-specific probes were captured and their localization topographic profiles were compared (Figure 4.17). The topography profiles revealed that both PLGA-Chitosan-I_2BODIPY and PLGA-I_2BODIPY nanoparticles localized primarily to lysosomes and partially to the mitochondria and endoplasmic reticulum (Figure 4.17A-B). Meanwhile, free I_2BODIPY localized mainly to the lysosomes and mitochondria compared to endoplasmic reticulum (Figure 4.17C). The localization of nanoparticles to lysosomes indicated that cellular internalisation of nanoparticles occurred mainly through endocytosis (Harush-Frenkel *et al.*, 2007; Yameen *et al.*, 2014). Staining of nuclei and plasma membrane was not found among the samples studied. This result suggests that free I_2BODIPY, PLGA-Chitosan-I_2BODIPY and PLGA-I_2BODIPY nanoparticles did not cause direct DNA damage or reaction with plasma membranes.

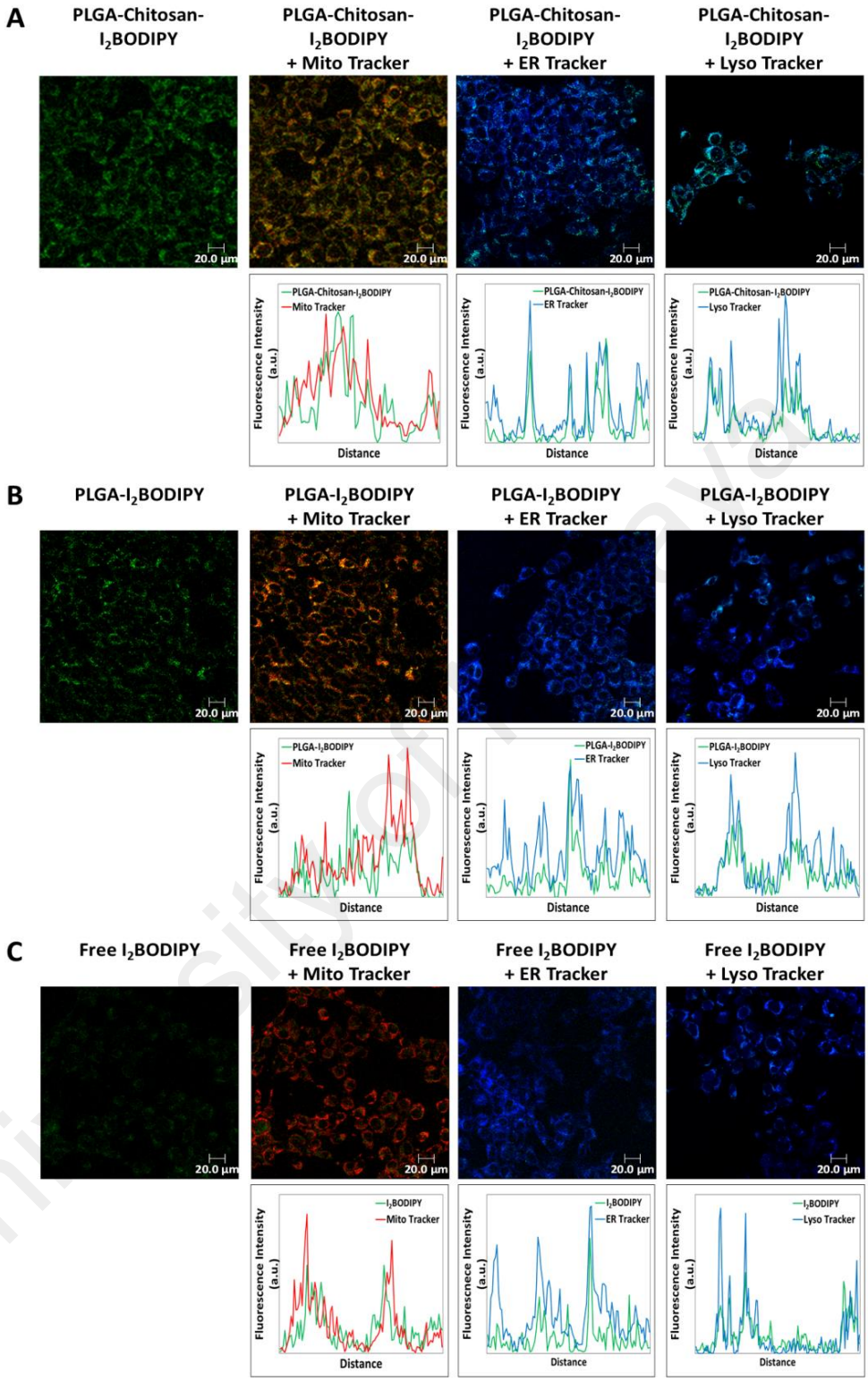

Figure 4.16: Intracellular localization of (A) PLGA-Chitosan-I_2BODIPY nanoparticles (20 µM of free I_2BODIPY), (B) PLGA-I_2BODIPY nanoparticles (20 µM of free I_2BODIPY) and (C) free I_2BODIPY (20 µM) in 4T1 cells.

Confocal fluorescence images and the respective fluorescence topographic profiles of 4T1 cells co-stained with free I_2BODIPY or PLGA-Chitosan-I_2BODIPY or PLGA-I_2BODIPY NP and organelle-specific probes are shown. Mitochondria were labelled with 100 nM Mito Tracker Red 580, which was excited at 460-490 nm (red). Endoplasmic reticula were labelled with 100 nM ER-Tracker Blue-White DPX and excited at 330-385 nm (blue). Lysosomes were labelled with 500 nM LysoTracker Blue DND-22 and excited at 330-385 nm (blue). I_2BODIPY was excited at 520-550 nm (green). Topographic profiles revealed that both PLGA-Chitosan-I_2BODIPY and PLGA-I_2BODIPY NP localized primarily in the lysosomes and free I_2BODIPY localized mostly in lysosome and mitochondria. Objective magnification x60 (oil immersion). (NP = nanoparticles)

4.8 Animal model

4.8.1 Toxicity profiles of free I_2BODIPY, PLGA-Chitosan-I_2BODIPY and PLGA-I_2BODIPY nanoparticles

The chitosan-coated and uncoated PLGA-I_2BODIPY nanoparticles and free I_2BODIPY (30 and 60 mg/kg of I_2BODIPY equivalent), blank chitosan-coated and uncoated nanoparticles at equivalent dose were administered intravenously to the mice via the tail vein injection. The *in vivo* toxicity was evaluated with the Berlin test of typical symptoms, such as inactivity, ruffled fur, diarrhea, behavior changes, and loss of body weight (Koudelka *et al.*, 2010). No death or symptoms of toxicity were observed in mice receiving up to 60 mg/kg (I_2BODIPY equivalent) of chitosan-coated and uncoated PLGA-I_2BODIPY nanoparticles and free I_2BODIPY (Figure 4.18). Thus, free I_2BODIPY, PLGA-Chitosan-I_2BODIPY and PLGA-I_2BODIPY nanoparticles did not cause toxicity to mice at doses up to 60 mg/kg.

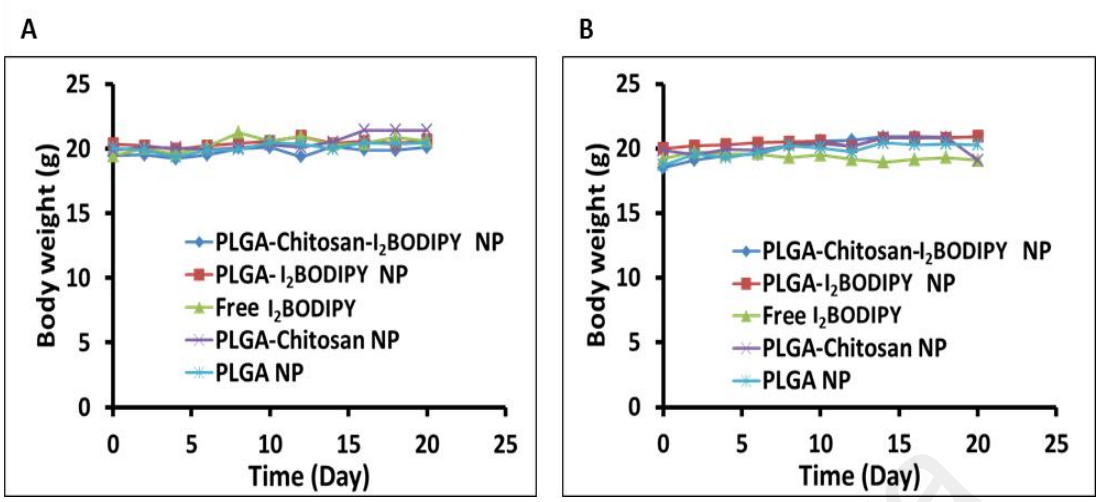

Figure 4.17: *In vivo* toxicity profile in BALB/c mice

Free I_2BODIPY, PLGA-Chitosan-I_2BODIPY, PLGA-I_2BODIPY, blank PLGA-Chitosan and blank PLGA nanoparticles were not toxic to mice at (A) 30 mg/kg and (B) 60 mg/kg of equivalent doses to I_2BODIPY. Healthy 7−8 weeks old BALB/c female mice were administered intravenously via tail vein respectively with the samples. The mice were then kept in the dark and observed for 20 days. Data represents average body weight (g) with two mice per treatment group.

4.8.2 *In vivo* biodistribution studies in 4T1 tumour-bearing mice

The biodistribution of free I_2BODIPY, chitosan-coated and uncoated PLGA-I_2BODIPY nanoparticles was monitored in 4T1 tumour-bearing mice for up to 48 h. Both PLGA-Chitosan-I_2BODIPY and PLGA-I_2BODIPY nanoparticles showed significant and prolonged accumulation in tumours compared with free I_2BODIPY (Figure 4.19A-B). At 1 h post administration, the fluorescence intensity of tumours in mice treated with PLGA-Chitosan-I_2BODIPY and PLGA-I_2BODIPY nanoparticles was approximately 4.5 times higher (2.7 ± 0.4 ($\times 10^6$) and 2.7 ± 0.2 ($\times 10^6$), respectively) than the intensities of those treated with free I_2BODIPY 6.2 ± 0.1 ($\times 10^5$) ($p < 0.05$, One-Way ANOVA). The accumulation of nanoparticles remained high until 3 h post administration, at which point the tumour fluorescence intensities of mice treated with

PLGA-Chitosan-I_2BODIPY and PLGA-I_2BODIPY nanoparticles were 7 times (2.0 ± 0.4 ($\times 10^6$)) and 8 times (2.8 ± 1.0 ($\times 10^6$)) higher, respectively, compared to the group treated with free I_2BODIPY (2.8 ± 0.1 ($\times 10^5$)) that showed a decrease in tumour accumulation from 1 h ($p < 0.05$, One-Way ANOVA). At 6 h post administration, no significant difference was observed between the tumour fluorescence intensities of mice treated with PLGA-Chitosan-I_2BODIPY nanoparticles or free I_2BODIPY. Meanwhile, PLGA-I_2BODIPY exhibited significantly higher tumour accumulation at 6 h and showed no significant difference at 24 h onward compared to chitosan-coated nanoparticles and free I_2BODIPY. These results indicate that selective tumour accumulation and prolonged retention of I_2BODIPY occur when I_2BODIPY was entrapped in PLGA and PLGA-Chitosan nanoparticles. Because the maximal accumulation of PLGA-Chitosan-I_2BODIPY and PLGA-I_2BODIPY nanoparticles occurred at 1 and 3 h post administration, subsequent *in vivo* antitumour efficacy studies was carried out at a drug-light interval of 1 and 3 h.

Although PLGA-I_2BODIPY nanoparticles showed the longest retention in tumours, the nanoparticles also accumulated in the liver, spleen and kidney during the first 3 h post administration and also in the lung and lymph nodes at 6 h. At 3 h post administration, a large amount of fluorescence intensity was observed in the liver and lung (approximately 5.3- and 7.2-times higher than the level in tumour tissue, respectively). However, this accumulation dissipated in the subsequent monitoring period. Meanwhile, in comparison with PLGA-I_2BODIPY nanoparticles, chitosan-coated nanoparticles exhibited 1.3-, 10.2- and 2.1-fold lower accumulation levels in the liver, lymph nodes and spleen, respectively (peak at 1 h post administration), even though the levels were still considerably high compared to that in tumour tissue. The lower levels of accumulation in liver, lymph nodes and spleen probably resulted from the "stealth" properties of the chitosan coating, which are expected to play a vital role in

avoiding rapid clearance of the nanoparticles by the RES more efficiently than the uncoated PLGA-I_2BODIPY nanoparticles. This finding is parallel with the results from the cellular uptake study where approximately 4- to 5-fold lower uptake by macrophages was observed when the nanoparticles were coated with chitosan (Figure 4.16).

Moreover, PLGA-Chitosan-I_2BODIPY nanoparticles also showed very minimal accumulation in non-tumour organs such as the lung, kidney, skin and eye of the treated mice, where the fluorescence intensities of the tumour tissue were 2.7, 3.2, 19.7 and 58.2 times higher than the intensities of these organs, respectively (at 1 h post administration). Compared to uncoated PLGA-I_2BODIPY nanoparticles, the accumulation of chitosan-coated PLGA-I_2BODIPY nanoparticles was reduced greatly by 28, 2.2, 22.7 and 4 times in lung, kidney, skin and eye, respectively (at 3 h post administration). These results indicate that chitosan-coated PLGA nanoparticles display higher tumour selectivity and lower rates of accumulation in non-tumour organs (tumor/skin ratio = 19.7; tumor/eyes ratio = 58.2 at 1 h) than the uncoated PLGA nanoparticles (tumor/skin ratio = 3.9, tumor/eyes ratio = 9.0 at 1 h), suggesting that the former may cause less photosensitivity in normal tissues after treatment, especially in the skin and eyes.

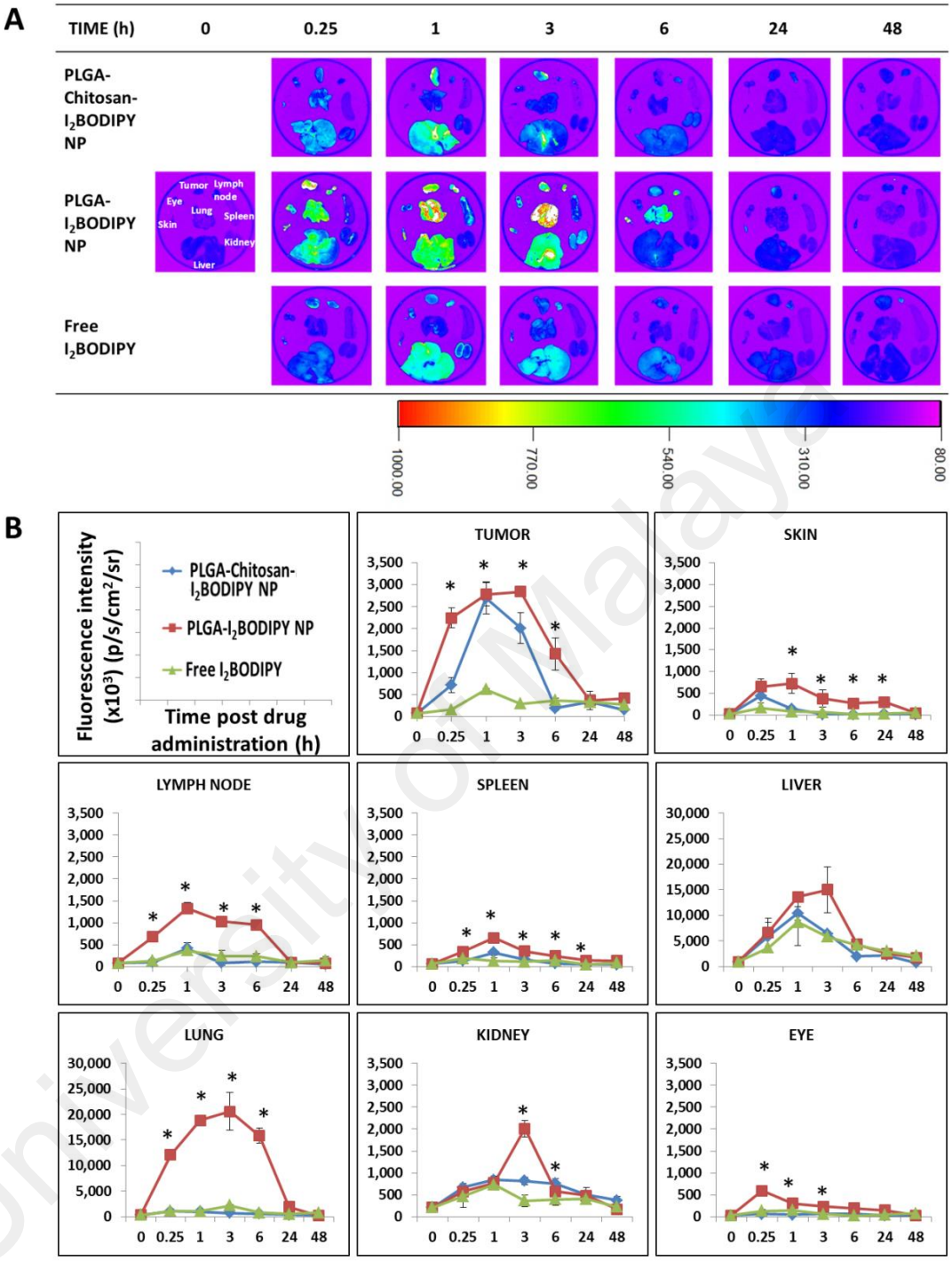

Figure 4.18: *In vivo* biodistribution studies in 4T1 tumour-bearing mice

4T1-tumour-bearing female BALB/c mice were treated with a 10 mg/kg equivalent of I_2BODIPY via the tail vein. Mice (n = 3) were sacrificed at 0, 0.25, 1, 3, 6, 24, 48 h. (A) Organs and tissues (tumour, draining lymph nodes, spleen, kidney, liver, lung, skin, and eye) were harvested, and (B) fluorescence intensities per centimeter square per steradian

(p/s/cm^2/sr) of each organ were recorded using an *in vivo* imager. PLGA-Chitosan-I_2BODIPY and PLGA-I_2BODIPY NP demonstrated prolonged accumulation in tumour tissues for up to 3 h and cleared from the body 48 h post administration. PLGA-Chitosan-I_2BODIPY NP also exhibited "stealth" effects and avoided accumulation in RES organs (lymph node, spleen and liver) compared to PLGA-I_2BODIPY NP and free I_2BODIPY. Data represents mean ± SD (n=3) at each time point. * $p < 0.05$ using One-Way ANOVA. (NP = nanoparticles)

4.8.3 *In vivo* PDT antitumour efficacy studies in 4T1 tumour-bearing mice

The PDT antitumour efficacies of PLGA-Chitosan-I_2BODIPY and PLGA-I_2BODIPY nanoparticles compared with free I_2BODIPY were assessed in 4T1-tumour bearing female BALB/c mice. The 4T1 breast carcinoma (Pulaski & Ostrand-Rosenberg, 1998) was subcutaneously injected into the murine mammary fat pad. When the tumour size reached approximately 150 mm^3, mice were then administered with PLGA-Chitosan-I_2BODIPY and PLGA-I_2BODIPY nanoparticles (10 mg/kg of I_2BODIPY equivalent) in saline via tail vein intravenous injection. Meanwhile, the controls were administered with free I_2BODIPY (10 mg/kg), blank PLGA-Chitosan, PLGA nanoparticles and saline. The mice treated with free I_2BODIPY, PLGA-Chitosan-I_2BODIPY and PLGA-I_2BODIPY nanoparticles were divided into groups with 1 or 3 h drug-light interval (DLI). Treated mice were irradiated with 100 J/cm^2 of light emitting at 530 nm. A set of dark controls without irradiation was performed concurrently.

Tumour growth was completely suppressed (0 mm^3 tumour volume) at 2 – 4 days post-treatment in the mice treated with PLGA-Chitosan-I_2BODIPY and PLGA-I_2BODIPY nanoparticles irradiated at DLI of 1 h (Figure 4.20). This phenomenon caused by direct tumor cell destruction by singlet oxygen, and it has also been reported in other PDT studies (Fadel *et al.*, 2010; Idris *et al.*, 2012; Kue *et al.*, 2015).

Inflammation, haemorrhage with necrosis and eschar were observed at the irradiated tumour area. On day 12, tumour regrowth was detected at peripheral necrotic tissue of the mice. Meanwhile, total tumour suppression until day 6 post treatment was observed in mice treated with PLGA-Chitosan-I_2BODIPY and PLGA-I_2BODIPY nanoparticles photo-irradiated at DLI of 3 h; however, tumour regrowth at the original site was observed at day 9 (Figure 4.20). Mice treated with free I_2BODIPY and a DLI of 1 h did not show complete tumour growth suppression. A mean tumour volume reduction to 25 mm^3 at day 3 was observed but was found to increase from day 6 onwards. Free I_2BODIPY with a DLI of 3 h gave no antitumour response and the tumour growth rate was similar with mice in control groups treated with blank nanoparticles or saline only with irradiation (Figure 4.20). The control group that was treated with a mixture of saline and a cocktail of 2.5% ethanol and 2.5% Cremophor EL gave similar results to those in the mice treated with saline (data not shown). These results support the biodistribution data and indicate that PLGA-Chitosan-I_2BODIPY and PLGA-I_2BODIPY nanoparticles were localized and retained in tumours for up to 3 h following administration, and caused damage to tumour upon photo-irradiation. In comparison, free I_2BODIPY demonstrated weak therapeutic efficacy probably due to its shorter retention time and lower accumulation at tumour tissue.

Mice treated with PLGA-Chitosan-I_2BODIPY and PLGA-I_2BODIPY nanoparticles at a DLI of 1 h showed more effective tumour growth suppression of 4T1 tumour than those treated with nanoparticles at a DLI of 3 h and free I_2BODIPY at DLI of 1 h (Figure 4.20). On day 14, the tumour growth in mice receiving the chitosan-coated and uncoated PLGA-I_2BODIPY nanoparticles at DLI of 1 h were suppressed by 97.2% ($p < 0.05$, One-Way ANOVA) and 97.7% ($p < 0.05$, One-Way ANOVA), respectively, compared to the carrier control group. When irradiated at DLI of 3 h, approximately 89.9% ($p < 0.05$, One-Way ANOVA) and 93.1% ($p < 0.05$, One-Way ANOVA) of

tumour growth suppression was observed for the PLGA-Chitosan-I_2BODIPY and PLGA-I_2BODIPY nanoparticle treatment groups, compared to their respective drug free nanoparticles. Mice treated with free I_2BODIPY at a DLI of 1 h showed 65.8% of tumour growth suppression ($p < 0.05$, One-Way ANOVA) compared to the control group receiving irradiation only. None of the mice treated with free I_2BODIPY irradiated at a DLI of 3 h, blank PLGA-Chitosan nanoparticles or blank PLGA nanoparticles showed suppression of tumour growth. Dark controls without irradiation also failed to show any tumour growth suppression (data not shown).

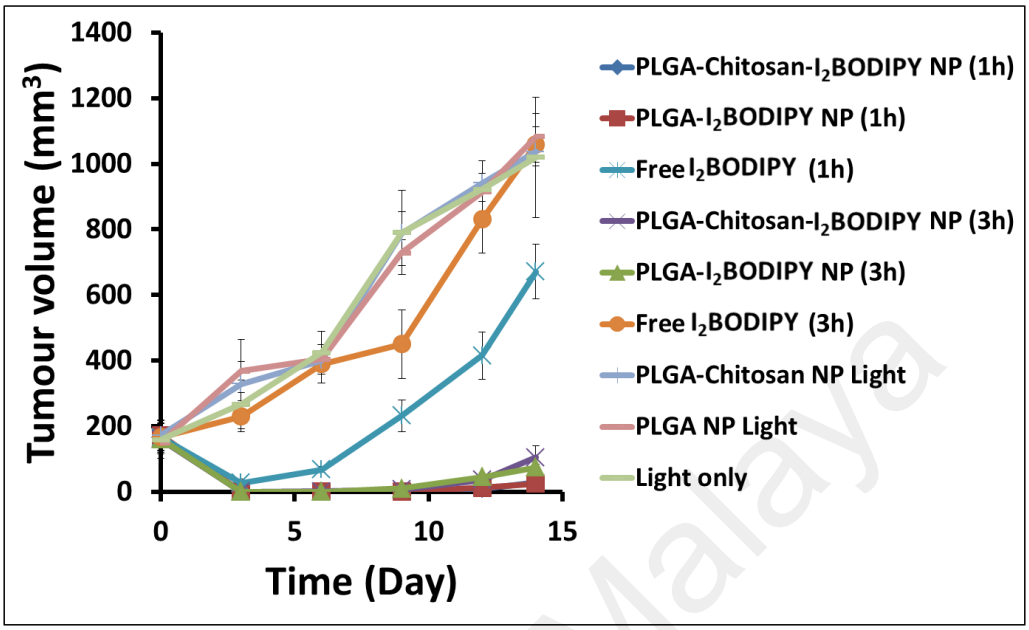

Figure 4.19: *In vivo* PDT efficacy studies in 4T1 tumour-bearing mice

PLGA-Chitosan-I_2BODIPY and PLGA-I_2BODIPY NP effectively suppressed 4T1 tumour growth in BALB/c mice at DLI of 1 and 3 h. Significant tumour volume reduction and delayed tumour regrowth were observed in 4T1 tumour bearing mice receiving PLGA-Chitosan-I_2BODIPY and PLGA-I_2BODIPY NP (10 mg/kg equivalent of I_2BODIPY) at DLIs of 1 and 3 h but not in free I_2BODIPY at a DLI of 1 h. Tumour regrowth was observed at day 12 for mice treated with PLGA-Chitosan-I_2BODIPY and PLGA-I_2BODIPY NP with DLI of 1 h and at day 9 with DLI of 3 h. In mice treated with free I_2BODIPY with a DLI of 1 h, tumour regrowth was observed at day 6. Rapid tumour growth is shown in mice receiving free I_2BODIPY at a DLI of 3 h and the control samples. Photoactivation was conducted at 100 J/cm^2 with a fluence rate of 160 mW/cm^2 (DLI = 1 and 3 h, respectively) after intravenous injection of the samples. Data represents the mean tumour volume ± SEM (n=7) for each group. (NP = nanoparticles)

CHAPTER 5: DISCUSSION

This study suggests that the low molecular weight chitosan (25 kDa) coating on PLGA nanoparticles is able to give stealth properties by evading the macrophage uptake and RES, and also selectively deliver I_2BODIPY and accumulate at tumour site for photodynamic cancer therapy. The nanoparticles were designed with an average size of around 150 nm, which is suitable for systemic administration and optimal for EPR effect (Acharya & Sahoo, 2011; Fang *et al.*, 2011; L. Zhang *et al.*, 2008b). Although nanoparticles at this size might have high possibilities of being recognised and uptaken by the macrophages as demonstrated by the PLGA-I_2BODIPY nanoparticles, stealthing the nanoparticles with low molecular weight chitosan coating was able to help the nanoparticles to evade the RES, as demonstrated in the *in vivo* biodistribution results for the liver, spleen and lymph node organs, and uptake studies in RAW246.7 macrophages. The changes on the particle surface to become more hydrophilic and neutral charged by coating with low molecular weight chitosan could have reduced the process of opsonization and thereby prevented premature clearance by the RES.

The designed nanoparticles in this study had an average zeta potential of -5 mV after they were coated with 0.5 % (w/w) 25 kDa chitosan. This value is desirable because it is close to neutral which is necessary for successful evasion of RES and renal elimination (Acharya & Sahoo, 2011; Salmaso & Caliceti, 2013). Moreover, cationic particles tend to bind to other normal cells in the body which are negatively charged, including endothelial cells before arriving at targeted tumour site (Acharya & Sahoo, 2011; H. Maeda, 2001; Matsumura & Maeda, 1986; Noguchi *et al.*, 1998). Therefore, the degree of chitosan coating was not increased further, despite positively-charged chitosan-coated nanoparticles have been reported to improve cellular uptake *in vitro* compared to uncoated nanoparticles (Chronopoulou *et al.*, 2013; Kim *et al.*, 2008).

Haemolysis study was conducted to evaluate the use of PLGA-Chitosan nanoparticles for systemic administration. The chitosan (5, 10 and 25 kDa) coated-PLGA nanoparticles studied are non-haemolytic up to 10 mg/ml upon incubation up to 5 h. Richardson *et al.* also reported that low molecular weight chitosans of more than 10 kDa were neither toxic nor haemolytic over 5 h of incubation and was administered intravenously as a synthetic gene delivery system (Richardson *et al.*, 1999). Furthermore, the amount of PLGA-Chitosan nanoparticle used in the animal study was only approximately 2 mg per mouse, and this amount of nanoparticles would be rapidly diluted by the total blood volume in circulation which is estimated to be 2 ml (Perrault & Chan, 2010). Thus, the degree of haemolysis that is caused by this minute amount of chitosan is expected to be negligible, at approximately 2%, as indicated in Figure 4.7.

The free I_2BODIPY and I_2BODIPY extracted from PLGA-Chitosan and PLGA nanoparticles in acetone and methanol exhibited a strong absorbance peak at 532 nm with the same fluorescence emission peak. These suggest that the extracted I_2BODIPY did not form aggregation and the process of encapsulation did not alter its photophysical properties. This finding is consistent with Ricci-Júnior and Marchetti (2006) (Ricci-Junior & Marchetti, 2006) where the extracted zinc phthalocyanine from PLGA nanoparticles in ethanol did not form dimer aggregation. Furthermore, encapsulation of I_2BODIPY into the chitosan-coated and uncoated PLGA nanoparticles prevented I_2BODIPY aggregation in PBS as shown in the absorbance spectra of the nanoparticle-photosensitiser constructs. These indicate that the chitosan-coated and uncoated PLGA nanoparticles are able to deliver I_2BODIPY to the tumour site without affecting its photophysical and phototoxic properties.

The singlet oxygen generation ability of I_2BODIPY entrapped in PLGA-Chitosan and PLGA nanoparticles was evaluated by a chemical detection method using ADPA as

a chemical detector. Hydrophobic I_2BODIPY did not produce singlet oxygen in aqueous D_2O due to aggregation but with the aid of surfactant, SDS or Tween 80, a rapid generation of singlet oxygen over time was observed. Meanwhile, PLGA-Chitosan-I_2BODIPY and PLGA-I_2BODIPY nanoparticles in D_2O generated singlet oxygen at 30% less and at a slower rate at the end of the study compared to free I_2BODIPY in surfactant. This may be because some I_2BODIPY have been released from the nanoparticles and formed self-quenched aggregates in D_2O, which led to a slower and reduced singlet oxygen generation. This observation is consistent with published reports that other nanoparticle systems entrapped with photosensitisers also showed reduced singlet oxygen generation characteristic (Chen *et al.*, 2005; Lee *et al.*, 2009; Peng *et al.*, 2008; Sortino *et al.*, 2006).

The initial burst release of I_2BODIPY in PBS at physiological pH was reduced by 2-fold when the PLGA-I_2BODIPY nanoparticles were coated with chitosan, which acted as a protective physical barrier. This system was comparatively more stable than other chitosan-coated nanoparticles reported due to its lesser amount of burst release (Chakravarthi & Robinson, 2011; Chronopoulou *et al.*, 2013; Kim *et al.*, 2008; Norman *et al.*, 1992). A much slower and more sustained release of I_2BODIPY from chitosan-coated PLGA nanoparticles in plasma and PBS at pH 7.4 was also observed compared to uncoated PLGA-I_2BODIPY nanoparticles. Conversely, in acidic pH of 4.8, the amount of I_2BODIPY released from chitosan-coated PLGA-I_2BODIPY nanoparticles was significantly higher than that from uncoated PLGA-I_2BODIPY nanoparticles. The increased rate and amount of I_2BODIPY release may be due to the protonation and dissolution of chitosan layer in the acidic environment. This suggests that I_2BODIPY release may be enhanced upon cellular uptake PLGA-Chitosan-I_2BODIPY nanoparticles in the lysosomes which has an acidic environment, but not for the uncoated PLGA-I_2BODIPY nanoparticles. These findings are in agreement with previous published

reports where coating with chitosan induced a slower sustained drug release in physiological buffer but when in acidic environment, the rate of drug release increased (Chronopoulou *et al.*, 2013; Kim *et al.*, 2008; Tahara *et al.*, 2009). This characteristic of differential release rate is desirable to minimize leakage during systemic circulation and to enhance release in acid tumour environment, adding another level of targeted delivery to cancer.

Chitosan-coated PLGA-I_2BODIPY nanoparticles showed higher photocytotoxicity in 4T1 and MDA-MB-231 tumour-cell viability tests compared to the uncoated PLGA-I_2BODIPY nanoparticles and free I_2BODIPY. The higher potency of chitosan-coated nanoparticles is in good agreement with the higher cellular uptake of I_2BODIPY than the uncoated nanoparticles. These uptake results concurs with previous studies in which enhanced intracellular uptake was reported for chitosan-coated nanoparticles loaded with 6-coumarin compared to the uncoated nanoparticles in human lung adenocarcinoma cells (A549), lung cancer cells (H157) and hepatocarcinoma cells (HepG2/C3A) (Chronopoulou *et al.*, 2013; Kim *et al.*, 2008; Tahara *et al.*, 2009). PEGylation of PLGA nanoparticles loaded with 6-coumarin also reduced the zeta potential to -2.8 mV and exhibited significantly higher cellular uptake in 4T1 cells compared to the non-PEGylated nanoparticles (-26.2 mV) (Pamujula *et al.*, 2012). Reduced intracellular uptake of I_2BODIPY from PLGA-I_2BODIPY nanoparticles may be due to its negative zeta potential that caused electrostatic repulsion with the negatively charged cell membrane.

Cellular internalisation of nanoparticles occurred via the clathrin-mediated endocytic pathway for both chitosan-coated and uncoated PLGA nanoparticles, as postulated by Frohlich (2012) and Tahara *et al*. (2009). Kuhn *et al.* also reported that the cellular uptake of nanoparticles involves a combination of caveolin-mediated and clathrin-

mediated endocytic mechanisms. Nevertheless, some of the I_2BODIPY loaded in the nanoparticles could also be delivered to cancer cells via contact-based transfer as suggested by Snipstad *et al.* (2014), Xu *et al*. (2009) and Chen *et al*. (2008). Conversely, macrophage uptake of nanoparticles involved macropinocytosis and phagocytosis in addition to clathrin-mediated endocytosis (Frohlich, 2012; Kuhn *et al.*, 2014). From the data of *in vitro* release experiment, the time duration used in reaching uptake saturation in cells (after 1 h) had only approximately 11% and 8% of I_2BODIPY was released in plasma for chitosan-coated and uncoated PLGA nanoparticles, respectively. Besides, the cellular uptake of free I_2BODIPY was found to be comparatively lower. Hence, these findings suggest that the cellular uptake of I_2BODIPY in the current study occurred mostly when I_2BODIPY was still entrapped within the nanoparticles.

Furthermore, both the PLGA-Chitosan-I_2BODIPY and PLGA I_2BODIPY nanoparticles were found to localize predominantly at lysosomes, which is the last compartment of the endocytic pathway. This finding suggests that the cellular uptake of nanoparticles was probably via endocytosis. This is in agreement with a study in which 1,2-dioleoyl-sn-glycero-3-phosphoethanolamine (DOPE)/PLGA nanoparticles, ligand modified-PEG-poly(ε-caprolactone) nanoparticles and hyper-branched dendritic-linear-based nanoparticles were reported to localize mainly to endosomes and lysosomes (Chhabra *et al.*, 2014; Gao *et al.*, 2013; Zeng *et al.*, 2014). The release of I_2BODIPY from the nanoparticles was induced in the acidic environment of the lysosome (approximately pH 4.8) and the presence of lysosomal hydrolases. The released I_2BODIPY may have been transferred to membranous organelles, such as mitochondria, due to its lipophilic nature. This explanation is evidenced by the localization of free I_2BODIPY to mitochondria apart from lysosomes. Previous studies reported that photosensitisers with high lipophilicity tend to accumulate in cellular compartments

with high lipid bilayer content, such as the mitochondria and endoplasmic reticulum, and amplify their cellular toxicity in PDT that way (Kessel & Reiners, 2007).

The "stealth" properties of the PLGA nanoparticles were achieved using the low molecular weight-chitosan coating strategy (Figure 5.1). The stealth effect was demonstrated in this study in the low molecular weight chitosan-coated sample in several ways. Firstly, the chitosan-coated sample resisted protein adsorption, by 2-fold compared to the uncoated nanoparticles. This will in turn, reduced surface opsonization that leads to RES uptake and premature clearance of nanoparticles from circulation (Owens & Peppas, 2006; Salmaso & Caliceti, 2013). Secondly, the chitosan-coated PLGA-I_2BODIPY nanoparticles effectively reduced macrophages uptake by approximately 4-fold, compared to PLGA-I_2BODIPY nanoparticles without chitosan coating. As compared to other published literature, the chitosan-coated system in this study exhibited a better stealth effect as only 12% of the initial amount added was uptaken by the macrophages compared to 24% of the rhodamine-loaded PEGylated PLGA nanoparticles after 1 h of incubation (Wang *et al.*, 2007). Thirdly, the *in vivo* biodistribution study in 4T1 tumour-bearing mice showed that the PLGA-Chitosan-I_2BODIPY nanoparticles accumulated to a lesser extent than the uncoated counterpart to RES organs, by 10.2, 2.1 and 1.3 times lower in the lymph node, spleen and liver at the peak levels. These findings indicate that chitosan-coated PLGA nanoparticles were able to evade RES, which consists of primarily monocytes and macrophages that accumulate mainly in lymph node and spleen and Kupffer cells in the liver.

In comparison to PLGA nanoparticles, the chitosan-coated particles also highly accumulated in liver. No statistical difference was observed in between the coated and uncoated nanoparticles but the amount of chitosan coated PLGA nanoparticles was 2.3-fold lower than uncoated nanoparticles at 3 h post-administration. The high

accumulation of particles in liver is because the hepatobiliary system is the primary route of excretion for particles that do not undergo renal clearance. The liver provides the critical function of catabolism and biliary excretion of blood-borne particles and also, eliminates foreign particles through phagocytosis (Michelle Longmire *et al.*, 2008). Kupffer cells in the liver are part of the RES and rely on intracellular degradation for particle removal (Sadauskas *et al.*, 2007). Accumulation of nanoparticles at lymph node is possible after they passage from endothelium (Garnett & Kallinteri, 2006). The dextran-coated superparamagnetic iron oxide nanoparticles with relatively large sizes, approximately 90 nm, were shown to accumulate in lymph node (Lind *et al.*, 2002).

The chitosan-coated PLGA nanoparticles in this study effectively decreased their accumulation in spleen by approximately 3-fold compared to the uncoated ones. This shows a stronger stealth effects to that reported by Stolnik *et al.*, (1994) where the PEGylated PLGA and poloxamine 908 coated-PLGA nanoparticles were accumulated almost 5- and 6-fold higher than the uncoated PLGA nanoparticles, respectively. While, Li *et al.* (2001) reported similar amounts of PEGylated and non-PEGylated PLGA nanoparticles accumulated in spleen and Rojnik *et al.* (2012) reported that the RES tissue distribution differed only slightly between the temoporfin-loaded PEGylated and non-PEGylated PLGA nanoparticles. These indicate that chitosan-coated PLGA nanoparticles may constitute a better nanocarrier alternative for photodynamic cancer therapy in terms of their significant stealth effect compared to the PEGylated PLGA nanoparticles.

Besides, the coating of PLGA nanoparticles with chitosan also demonstrated better tumour selectivity with lower detectable levels in normal tissues such as the lung, skin, eye and kidney compared to uncoated PLGA-I_2BODIPY nanoparticles, even though their accumulation levels in the tumour were similar. This may be due to the similarity

in the size of both types of nanoparticles that confer similar EPR-based tumour accumulation properties. This result also indicates that the tumour accumulation of PLGA nanoparticles was based on the EPR effect and was not affected by the addition of a stealth layer. This finding concurs with Rojnik *et al*. that the PEGylated PLGA nanoparticles also exhibited tumour selectivity with a higher tumour-to-skin ratio and showed decreased accumulation in lung compared to the non-PEGylated PLGA nanoparticles (Rojnik *et al.*, 2012).

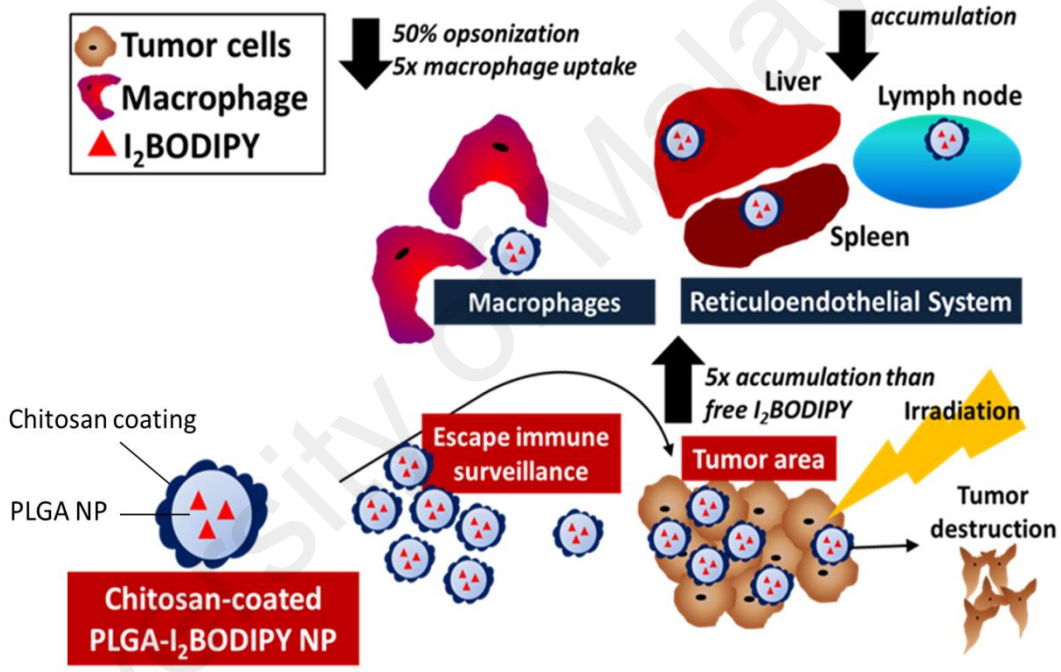

Figure 5.1: Summary of the stealth properties of chitosan coating on PLGA-I2BODIPY that improved tumour selectivity in photodynamic cancer therapy

The *in vivo* biodistribution data is further supported by the results of PDT antitumour efficacy, in which no significant statistical difference was observed throughout the duration of tumour suppression and regrowth between chitosan-coated and uncoated PLGA-I_2BODIPY nanoparticles when treated at a DLI of 1 h or 3 h. A better antitumour effect from PLGA-Chitosan-I_2BODIPY and PLGA-I_2BODIPY nanoparticles is

expected with higher doses and multiple dose treatments. The *in vivo* PDT outcome was slightly better with a DLI of 1 h compared to 3 h possibly because the antitumour PDT efficacy relies mainly on the tumour-associated vascular damage caused by activation of photosensitiser present in the endothelial cells of the tumour vasculature (Voon *et al.*, 2014) and the majority of photosensitiser still remained in vasculature at 1 h DLI. Visudyne, a commercially available liposomal formulation of benzoporphyrin derivative monoacid ring A (BPDMA), and temocene-loaded micelles also showed greater antitumour response with a shorter DLI (Garcı́a-Dı́az *et al.*, 2012; Ichikawa *et al.*, 2004).

CHAPTER 6: CONCLUSION, GENERAL LIMITATIONS AND FUTURE PERSPECTIVES

6.1 Conclusion

In conclusion, this study showed that PLGA-I_2BODIPY nanoparticles stealth coated with low molecular weight chitosan had selective accumulation at tumour site and reduced macrophage uptake by the RES. The hydrophilic coating with near neutral surface charge reduced surface recognition by opsonins to evade immune surveillance by the RES. This helps to prevent premature clearance of the nanoparticles and improved the selective delivery of I_2BODIPY to tumour site by EPR effect. Selective tumour accumulation and reduced random tissue accumulation of the PLGA-Chitosan-I_2BODIPY nanoparticles construct was very useful to prevent generalised photosensitivity especially in the skin and eyes, thereby enhancing the anticancer efficacy of I_2BODIPY when used for photodynamic cancer therapy.

6.2 General limitations

Complete tumour regression could be achieved by multiple PDT. Unlike chemotherapy and radiotherapy, PDT has no cumulative toxicity and does not cause the development of resistance subtypes. Furthermore, the PDT efficiency of the PLGA-Chitosan-I_2BODIPY nanocarrier systems can be further evaluated using different animal models induced with other superficial embedded tumours. For instance, the dimethylbenz[a]anthracene (DBMA)-induced hamster cheek pouch tumour model which is a well-characterised squamous cell carcinoma model that mimics human oral cancer, could be of use. The cheek pouch can be inverted for irradiation and macroscopic evaluation.

6.3 Future perspectives

A variety of alternative stealth polymer can also be investigated and compared their stealth properties with low molecular weight chitosan. This includes polyoxazolines (Lee *et al.*, 2003; von Erlach *et al.*, 2011), poly(amino acids) (Metselaar *et al.*, 2003), polybetaines (Cao *et al.*, 2010; Zhang *et al.*, 2008), polyglycerols (Kainthan & Brooks, 2007; Siegers *et al.*, 2004) and acyclic polyacetals (Papisov, 2001). These polymers have advantages over PEG as they are biodegradable and have abundant of functional groups amenable to multivalent conjugations which can be conjugated to drugs or targeting ligands.

The possibility of conjugating of tumour targeting ligands to the free amine groups on chitosan which could provide the PLGA-Chitosan nanoparticles with active targeting properties are yet to be explored. Active targeting involves drug delivery to the specific target sites based on molecular recognition, whereas passive targeting is promoting of drug entry into the tumour cells determined by physicochemical factors of drug carrier, such as material composition, size and surface properties (*e.g.* surface charge) and by pathophysiological factors of the organism, such as tumour microenvironment as well as EPR effect. For instance, the tropomyosin receptor kinase C (TrkC) targeting ligands, which have been used to successfully eradicate the TrkC-expressing tumours via PDT when conjugated to BODIPY photosensitiser would be potential candidates to evaluate (Kue *et al.*, 2015). It can be attached to the nanoparticles to specifically transport the photosensitisers to the target sites.

Besides, the PLGA-Chitosan-I_2BODIPY nanoparticles are also capable to be further developed into a "theranostic" agent, for example in photoacoustic imaging (Ho *et al.*, 2014; Mehrmohammadi *et al.*, 2013; Zhang *et al.*, 2009). Photoacoustic imaging is a novel hybrid imaging modality combining the high spatial resolution of optical imaging with the high penetration depth of ultrasound imaging (Ho *et al.*, 2014). Preferential

tumour uptake of the fluorescent and photocytotoxic PLGA-Chitosan-I_2BODIPY nanoparticles can be combined with ultrasound imaging for monitoring of cancer progression and therapy outcome *in vivo*. This also could be very useful in clinical PDT to detect tumour location and perform irradiation at the specific site for optimal PDT effect.

REFERENCES

Abuchowski, A., McCoy, J. R., Palczuk, N. C., van Es, T., & Davis, F. F. (1977). Effect of covalent attachment of polyethylene glycol on immunogenicity and circulating life of bovine liver catalase. *Journal of Biological Chemistry, 252*(11), 3582-3586.

Acharya, S., & Sahoo, S. K. (2011). PLGA nanoparticles containing various anticancer agents and tumour delivery by EPR effect. *Adv Drug Deliv Rev, 63*(3), 170-183.

Agostinis, P., Berg, K., Cengel, K. A., Foster, T. H., Girotti, A. W., Gollnick, S. O., . . . Golab, J. (2011). Photodynamic therapy of cancer: an update. *CA: A Cancer Journal for Clinicians, 61*(4), 250-281.

Allen, T. M., & Hansen, C. (1991). Pharmacokinetics of stealth versus conventional liposomes: effect of dose. *Biochimica et Biophysica Acta, 1068*(2), 133-141.

Allen, T. M., Hansen, C. B., & de Menezes, D. E. L. (1995). Pharmacokinetics of long-circulating liposomes. *Advanced Drug Delivery Reviews, 16*(2–3), 267-284.

Altinoglu, E. I., Russin, T. J., Kaiser, J. M., Barth, B. M., Eklund, P. C., Kester, M., & Adair, J. H. (2008). Near-infrared emitting fluorophore-doped calcium phosphate nanoparticles for *in vivo* imaging of human breast cancer. *ACS Nano, 2*(10), 2075-2084.

Amoozgar, Z., Park, J., Lin, Q., & Yeo, Y. (2012). Low molecular-weight chitosan as a pH-sensitive stealth coating for tumor-specific drug delivery. *Molecular Pharmaceutics, 9*(5), 1262-1270.

Anderson, P. M., Tomaras, M., & McConnell, K. (2010). Mifamurtide in osteosarcoma--a practical review. *Drugs Today (Barc), 46*(5), 327-337.

Awuah, S. G., & You, Y. (2012). Boron dipyrromethene (BODIPY)-based photosensitizers for photodynamic therapy. *RSC Advances, 2*(30), 11169-11183.

Bala, I., Hariharan, S., & Kumar, M. N. (2004). PLGA nanoparticles in drug delivery: the state of the art. *Critical Reviews in Therapeutic Drug Carrier Systems, 21*(5), 387-422.

Barth, B. M., E, I. A., Shanmugavelandy, S. S., Kaiser, J. M., Crespo-Gonzalez, D., DiVittore, N. A., . . . Kester, M. (2011). Targeted indocyanine-green-loaded calcium phosphosilicate nanoparticles for *in vivo* photodynamic therapy of leukemia. *ACS Nano, 5*(7), 5325-5337.

Barth, B. M., Sharma, R., Altinoglu, E. I., Morgan, T. T., Shanmugavelandy, S. S., Kaiser, J. M., . . . Adair, J. H. (2010). Bioconjugation of calcium phosphosilicate composite nanoparticles for selective targeting of human breast and pancreatic cancers *in vivo*. *ACS Nano, 4*(3), 1279-1287.

Bartneck, M., Keul, H. A., Zwadlo-Klarwasser, G., & Groll, J. (2010). Phagocytosis Independent Extracellular Nanoparticle Clearance by Human Immune Cells. *Nano Letters, 10*(1), 59-63.

Bates, D. O., Hillman, N. J., Williams, B., Neal, C. R., & Pocock, T. M. (2002). Regulation of microvascular permeability by vascular endothelial growth factors. *Journal of Anatomy, 200*(6), 581-597.

Bendele, A., Seely, J., Richey, C., Sennello, G., & Shopp, G. (1998). Short communication: renal tubular vacuolation in animals treated with polyethylene-glycol-conjugated proteins. *Toxicological Sciences, 42*(2), 152-157.

Bertrand, N., Wu, J., Xu, X., Kamaly, N., & Farokhzad, O. C. (2014). Cancer nanotechnology: the impact of passive and active targeting in the era of modern cancer biology. *Adv Drug Deliv Rev, 66*, 2-25.

Bhattarai, N., Bhattarai, S. R., Khil, M. S., Lee, D. R., & Kim, H. Y. (2003). Aqueous solution properties of amphiphilic triblock copolymer poly(p-dioxanone-co-l-lactide)-block-poly(ethylene glycol). *European Polymer Journal, 39*(8), 1603-1608.

Bissery, M. C., Nohynek, G., Sanderink, G. J., & Lavelle, F. (1995). Docetaxel (Taxotere): a review of preclinical and clinical experience. Part I: Preclinical experience. *Anti-Cancer Drugs, 6*(3), 339-355, 363-338.

Boas, U., & Heegaard, P. M. (2004). Dendrimers in drug research. *Chemical Society Reviews, 33*(1), 43-63.

Breskey, J. D., Lacey, S. E., Vesper, B. J., Paradise, W. A., Radosevich, J. A., & Colvard, M. D. (2013). Photodynamic therapy: occupational hazards and preventative recommendations for clinical administration by healthcare providers. *Photomedicine and Laser Surgery, 31*(8), 398-407.

Bugaj, A. M. (2011). Targeted photodynamic therapy - a promising strategy of tumor treatment. *Photochemical and Photobiological Sciences, 10*(7), 1097-1109.

Bukowski, R., Ernstoff, M. S., Gore, M. E., Nemunaitis, J. J., Amato, R., Gupta, S. K., & Tendler, C. L. (2002). Pegylated interferon alfa-2b treatment for patients with solid tumors: a phase I/II study. *Journal of Clinical Oncology, 20*(18), 3841-3849.

Buyuktimkin, B., Wang, Q., Kiptoo, P., Stewart, J. M., Berkland, C., & Siahaan, T. J. (2012). Vaccine-like controlled-release delivery of an immunomodulating peptide to treat experimental autoimmune encephalomyelitis. *Molecular Pharmaceutics, 9*(4), 979-985.

Byrne, A. T., O'Connor, A. E., Hall, M., Murtagh, J., O'Neill, K., Curran, K. M., . . . Gallagher, W. M. (2009). Vascular-targeted photodynamic therapy with BF2-chelated Tetraaryl-Azadipyrromethene agents: a multi-modality molecular imaging approach to therapeutic assessment. *British Journal of Cancer, 101*(9), 1565-1573.

Campbell, R. B., Fukumura, D., Brown, E. B., Mazzola, L. M., Izumi, Y., Jain, R. K., . . . Munn, L. L. (2002). Cationic charge determines the distribution of liposomes between the vascular and extravascular compartments of tumors. *Cancer Research, 62*(23), 6831-6836.

Cao, Z., Yu, Q., Xue, H., Cheng, G., & Jiang, S. (2010). Nanoparticles for Drug Delivery Prepared from Amphiphilic PLGA Zwitterionic Block Copolymers with Sharp Contrast in Polarity between Two Blocks. *Angewandte Chemie International Edition, 49*(22), 3771-3776.

Carmeliet, P., & Jain, R. K. (2011). Principles and mechanisms of vessel normalization for cancer and other angiogenic diseases. *Nature Reviews. Drug Discovery, 10*(6), 417-427.

Carrstensen, H., Muller, R. H., & Muller, B. W. (1992). Particle size, surface hydrophobicity and interaction with serum of parenteral fat emulsions and model drug carriers as parameters related to RES uptake. *Clinical Nutrition, 11*(5), 289-297.

Casas, A., Battah, S., Di Venosa, G., Dobbin, P., Rodriguez, L., Fukuda, H., . . . MacRobert, A. J. (2009). Sustained and efficient porphyrin generation *in vivo* using dendrimer conjugates of 5-ALA for photodynamic therapy. *Journal of Controlled Release, 135*(2), 136-143.

Castano, A. P., Demidova, T. N., & Hamblin, M. R. (2004). Mechanisms in photodynamic therapy: part one-photosensitizers, photochemistry and cellular localization. *Photodiagnosis and Photodynamic Therapy, 1*(4), 279-293.

Chakravarthi, S. S., & Robinson, D. H. (2011). Enhanced cellular association of paclitaxel delivered in chitosan-PLGA particles. *International Journal of Pharmaceutics, 409*(1-2), 111-120.

Chatterjee, D. K., Fong, L. S., & Zhang, Y. (2008). Nanoparticles in photodynamic therapy: an emerging paradigm. *Advanced Drug Delivery Reviews, 60*(15), 1627-1637.

Chatterjee, D. K., & Yong, Z. (2008). Upconverting nanoparticles as nanotransducers for photodynamic therapy in cancer cells. *Nanomedicine, 3*(1), 73-82.

Chen, B., Pogue, B. W., & Hasan, T. (2005). Liposomal delivery of photosensitising agents. *Expert Opinion on Drug Delivery, 2*(3), 477-487.

Chen, B., Pogue, B. W., Luna, J. M., Hardman, R. L., Hoopes, P. J., & Hasan, T. (2006). Tumor vascular permeabilization by vascular-targeting photosensitization: effects, mechanism, and therapeutic implications. *Clinical Cancer Research, 12*(3 Pt 1), 917-923.

Chen, H., Kim, S., He, W., Wang, H., Low, P. S., Park, K., & Cheng, J.-X. (2008). Fast release of lipophilic agents from circulating PEG-PDLLA micelles revealed by *in vivo* förster resonance energy transfer imaging. *Langmuir, 24*(10), 5213-5217.

Chen, R. H., & Tsaih, M. L. (1998). Effect of temperature on the intrinsic viscosity and conformation of chitosans in dilute HCl solution. *International Journal of Biological Macromolecules, 23*(2), 135-141.

Chen, W., & Zhang, J. (2006). Using nanoparticles to enable simultaneous radiation and photodynamic therapies for cancer treatment. *Journal of Nanoscience and Nanotechnology, 6*(4), 1159-1166.

Cheng, X., Zhang, F., Zhou, G., Gao, S., Dong, L., Jiang, W., . . . Zhang, J. (2009). DNA/chitosan nanocomplex as a novel drug carrier for doxorubicin. *Drug Delivery, 16*(3), 135-144.

Cheng, Y., C. Samia, A., Meyers, J. D., Panagopoulos, I., Fei, B., & Burda, C. (2008). Highly efficient drug delivery with gold nanoparticle vectors for in vivo photodynamic therapy of cancer. *Journal of the American Chemical Society, 130*(32), 10643-10647.

Cheon Lee, S., Kim, C., Chan Kwon, I., Chung, H., & Young Jeong, S. (2003). Polymeric micelles of poly(2-ethyl-2-oxazoline)-block-poly(epsilon-caprolactone) copolymer as a carrier for paclitaxel. *Journal of Controlled Release, 89*(3), 437-446.

Chhabra, R., Grabrucker, A. M., Veratti, P., Belletti, D., Boeckers, T. M., Vandelli, M. A., . . . Ruozi, B. (2014). Characterization of lysosome-destabilizing DOPE/PLGA nanoparticles designed for cytoplasmic drug release. *International Journal of Pharmaceutics, 471*(1-2), 349-357.

Chronopoulou, L., Massimi, M., Giardi, M. F., Cametti, C., Devirgiliis, L. C., Dentini, M., & Palocci, C. (2013). Chitosan-coated PLGA nanoparticles: a sustained drug release strategy for cell cultures. *Colloids and Surfaces. B, Biointerfaces, 103*, 310-317.

Corbin, I. R., & Zheng, G. (2007). Mimicking nature's nanocarrier: synthetic low-density lipoprotein-like nanoparticles for cancer-drug delivery. *Nanomedicine, 2*(3), 375-380.

Dash, M., Chiellini, F., Ottenbrite, R. M., & Chiellini, E. (2011). Chitosan—A versatile semi-synthetic polymer in biomedical applications. *Progress in Polymer Science, 36*(8), 981-1014.

Demberelnyamba, D., Ariunaa, M., & Shim, Y. K. (2008). Newly synthesized water soluble cholinium-purpurin photosensitizers and their stabilized gold nanoparticles as promising anticancer agents. *International Journal of Molecular Sciences, 9*(5), 864-871.

Ding, F., Deng, H., Du, Y., Shi, X., & Wang, Q. (2014). Emerging chitin and chitosan nanofibrous materials for biomedical applications. *Nanoscale, 6*(16), 9477-9493.

Dobrovolskaia, M. A., Aggarwal, P., Hall, J. B., & McNeil, S. E. (2008). Preclinical studies to understand nanoparticle interaction with the immune system and its potential effects on nanoparticle biodistribution. *Molecular Pharmaceutics, 5*(4), 487-495.

Dolmans, D. E., Fukumura, D., & Jain, R. K. (2003). Photodynamic therapy for cancer. *Nature Reviews. Cancer, 3*(5), 380-387.

Dougherty, T. J., Gomer, C. J., Henderson, B. W., Jori, G., Kessel, D., Korbelik, M., . . . Peng, Q. (1998). Photodynamic therapy. *Journal of the National Cancer Institute, 90*(12), 889-905.

Dougherty, T. J., Grindey, G. B., Fiel, R., Weishaupt, K. R., & Boyle, D. G. (1975). Photoradiation therapy. II. Cure of animal tumors with hematoporphyrin and light. *Journal of the National Cancer Institute, 55*(1), 115-121.

Dougherty, T. J., Kaufman, J. E., Goldfarb, A., Weishaupt, K. R., Boyle, D., & Mittleman, A. (1978). Photoradiation therapy for the treatment of malignant tumors. *Cancer Research, 38*(8), 2628-2635.

Dreher, M. R., Liu, W., Michelich, C. R., Dewhirst, M. W., Yuan, F., & Chilkoti, A. (2006). Tumor vascular permeability, accumulation, and penetration of macromolecular drug carriers. *Journal of the National Cancer Institute, 98*(5), 335-344.

Drobek, T., Spencer, N. D., & Heuberger, M. (2005). Compressing PEG Brushes. *Macromolecules, 38*(12), 5254-5259.

Duncan, R. (2003). The dawning era of polymer therapeutics. *Nature Reviews. Drug Discovery, 2*(5), 347-360.

Dysart, J. S., & Patterson, M. S. (2005). Characterization of Photofrin photobleaching for singlet oxygen dose estimation during photodynamic therapy of MLL cells in vitro. *Physics in Medicine and Biology, 50*(11), 2597-2616.

Ebrahimnejad, P., Dinarvand, R., Jafari, M. R., Tabasi, S. A., & Atyabi, F. (2011). Characterization, blood profile and biodistribution properties of surface modified PLGA nanoparticles of SN-38. *International Journal of Pharmaceutics, 406*(1-2), 122-127.

Eisenberg, S., Windmueller, H. G., & Levy, R. I. (1973). Metabolic fate of rat and human lipoprotein apoproteins in the rat. *Journal of Lipid Research, 14*(4), 446-458.

Essa, S., Rabanel, J. M., & Hildgen, P. (2011). Characterization of rhodamine loaded PEG-g-PLA nanoparticles (NPs): effect of poly(ethylene glycol) grafting density. *International Journal of Pharmaceutics, 411*(1-2), 178-187.

Fadel, M., Kassab, K., & Abdel Fadeel, D. (2010). Zinc phthalocyanine-loaded PLGA biodegradable nanoparticles for photodynamic therapy in tumor-bearing mice. *Lasers in Medical Science, 25*(2), 283-292.

Fang, J., Nakamura, H., & Maeda, H. (2011). The EPR effect: Unique features of tumor blood vessels for drug delivery, factors involved, and limitations and augmentation of the effect. *Adv Drug Deliv Rev, 63*(3), 136-151.

Fang, J., Sawa, T., & Maeda, H. (2003). Factors and mechanism of "EPR" effect and the enhanced antitumor effects of macromolecular drugs including SMANCS. *Advances in Experimental Medicine and Biology, 519*, 29-49.

Fayter, D., Corbett, M., Heirs, M., Fox, D., & Eastwood, A. (2010). A systematic review of photodynamic therapy in the treatment of pre-cancerous skin conditions, Barrett's oesophagus and cancers of the biliary tract, brain, head and neck, lung, oesophagus and skin. *Health Technology Assessment, 14*(37), 1-288.

Fella, C., Walker, G. F., Ogris, M., & Wagner, E. (2008). Amine-reactive pyridylhydrazone-based PEG reagents for pH-reversible PEI polyplex shielding. *European Journal of Pharmaceutical Sciences, 34*(4-5), 309-320.

Felt, O., Buri, P., & Gurny, R. (1998). Chitosan: A Unique Polysaccharide for Drug Delivery. *Drug Development and Industrial Pharmacy, 24*(11), 979-993.

Frank, M. M., & Fries, L. F. (1991). The role of complement in inflammation and phagocytosis. *Immunology Today, 12*(9), 322-326.

Frohlich, E. (2012). The role of surface charge in cellular uptake and cytotoxicity of medical nanoparticles. *International Journal of Nanomedicine, 7*, 5577-5591.

Gamaleia, N. F., Shishko, E. D., Dolinsky, G. A., Shcherbakov, A. B., Usatenko, A. V., & Kholin, V. V. (2010). Photodynamic activity of hematoporphyrin conjugates with gold nanoparticles: experiments *in vitro*. *Experimental Oncology, 32*(1), 44-47.

Gao, F., Bai, Y., Ma, S. R., Liu, F., & Li, Z. S. (2010). Systematic review: photodynamic therapy for unresectable cholangiocarcinoma. *Journal of Hepato-Biliary-Pancreatic Sciences, 17*(2), 125-131.

Gao, H., Yang, Z., Zhang, S., Cao, S., Shen, S., Pang, Z., & Jiang, X. (2013). Ligand modified nanoparticles increases cell uptake, alters endocytosis and elevates glioma distribution and internalization. *Scientific Reports, 3*, 2534.

Garc á-D áz, M., Kawakubo, M., Mroz, P., Sagrist à, M. L., Mora, M., Nonell, S., & Hamblin, M. R. (2012). Cellular and vascular effects of the photodynamic agent temocene are modulated by the delivery vehicle. *Journal of Controlled Release, 162*(2), 355-363.

Garnett, M. C., & Kallinteri, P. (2006). Nanomedicines and nanotoxicology: some physiological principles. *Occupational Medicine (Oxford, England), 56*(5), 307-311.

Gary-Bobo, M., Mir, Y., Rouxel, C., Brevet, D., Basile, I., Maynadier, M., . . . Raehm, L. (2011). Mannose-functionalized mesoporous silica nanoparticles for efficient two-photon photodynamic therapy of solid tumors. *Angewandte Chemie International Edition, 50*(48), 11425-11429.

Gelderblom, H., Verweij, J., Nooter, K., & Sparreboom, A. (2001). Cremophor EL: the drawbacks and advantages of vehicle selection for drug formulation. *European journal of cancer (Oxford, England : 1990), 37*(13), 1590-1598.

Gijsens, A., Derycke, A., Missiaen, L., De Vos, D., Huwyler, J., Eberle, A., & de Witte, P. (2002). Targeting of the photocytotoxic compound AlPcS4 to hela cells by transferrin conjugated peg-liposomes. *International Journal of Cancer, 101*(1), 78-85.

Gilding, D. K., & Reed, A. M. (1979). Biodegradable polymers for use in surgery - polyglycolic/poly(actic acid) homo- and copolymers: 1. *Polymer, 20*(12), 1459-1464.

Glantz, M. J., LaFollette, S., Jaeckle, K. A., Shapiro, W., Swinnen, L., Rozental, J. R., . . . Howell, S. B. (1999). Randomized trial of a slow-release versus a standard formulation of cytarabine for the intrathecal treatment of lymphomatous meningitis. *Journal of Clinical Oncology, 17*(10), 3110-3116.

Govender, T., Stolnik, S., Garnett, M. C., Illum, L., & Davis, S. S. (1999). PLGA nanoparticles prepared by nanoprecipitation: drug loading and release studies of a water soluble drug. *Journal of Controlled Release, 57*(2), 171-185.

Greenwald, R. B., Choe, Y. H., McGuire, J., & Conover, C. D. (2003). Effective drug delivery by PEGylated drug conjugates. *Advanced Drug Delivery Reviews, 55*(2), 217-250.

Gregoriadis, G., Jain, S., Papaioannou, I., & Laing, P. (2005). Improving the therapeutic efficacy of peptides and proteins: a role for polysialic acids. *International Journal of Pharmaceutics, 300*(1-2), 125-130.

Greish, K., Nagamitsu, A., Fang, J., & Maeda, H. (2005). Copoly(styrene-maleic acid)-pirarubicin micelles: high tumor-targeting efficiency with little toxicity. *Bioconjugate Chemistry, 16*(1), 230-236.

Greish, K., Sawa, T., Fang, J., Akaike, T., & Maeda, H. (2004). SMA-doxorubicin, a new polymeric micellar drug for effective targeting to solid tumours. *Journal of Controlled Release, 97*(2), 219-230.

Gu, Z., Aimetti, A. A., Wang, Q., Dang, T. T., Zhang, Y., Veiseh, O., . . . Anderson, D. G. (2013). Injectable Nano-Network for Glucose-Mediated Insulin Delivery. *ACS Nano, 7*(5), 4194-4201.

Hamad, I., Hunter, A. C., Szebeni, J., & Moghimi, S. M. (2008). Poly(ethylene glycol)s generate complement activation products in human serum through increased alternative pathway turnover and a MASP-2-dependent process. *Molecular Immunology, 46*(2), 225-232.

Hans, M. L., & Lowman, A. M. (2002). Biodegradable nanoparticles for drug delivery and targeting. *Current Opinion in Solid State and Materials Science, 6*(4), 319-327.

Harush-Frenkel, O., Debotton, N., Benita, S., & Altschuler, Y. (2007). Targeting of nanoparticles to the clathrin-mediated endocytic pathway. *Biochemical and Biophysical Research Communications, 353*(1), 26-32.

Hatakeyama, H., Akita, H., & Harashima, H. (2011). A multifunctional envelope type nano device (MEND) for gene delivery to tumours based on the EPR effect: a strategy for overcoming the PEG dilemma. *Adv Drug Deliv Rev, 63*(3), 152-160.

He, X., Wu, X., Wang, K., Shi, B., & Hai, L. (2009). Methylene blue-encapsulated phosphonate-terminated silica nanoparticles for simultaneous *in vivo* imaging and photodynamic therapy. *Biomaterials, 30*(29), 5601-5609.

Heidel, J. D., & Davis, M. E. (2011). Clinical developments in nanotechnology for cancer therapy. *Pharmaceutical Research, 28*(2), 187-199.

Herborn, C. U., Barkhausen, J., Paetsch, I., Hunold, P., Mahler, M., Shamsi, K., & Nagel, E. (2003). Coronary Arteries: Contrast-enhanced MR Imaging with SH L 643A—Experience in 12 Volunteers. *Radiology, 229*(1), 217-223.

Ho, C. J., Balasundaram, G., Driessen, W., McLaren, R., Wong, C. L., Dinish, U. S., . . . Olivo, M. (2014). Multifunctional photosensitizer-based contrast agents for photoacoustic imaging. *Scientific Reports, 4*, 5342.

Hobbs, S. K., Monsky, W. L., Yuan, F., Roberts, W. G., Griffith, L., Torchilin, V. P., & Jain, R. K. (1998). Regulation of transport pathways in tumor vessels: role of tumor type and microenvironment. *Proceedings of the National Academy of Sciences of the United States of America, 95*(8), 4607-4612.

Hong, R. L., Huang, C. J., Tseng, Y. L., Pang, V. F., Chen, S. T., Liu, J. J., & Chang, F. H. (1999). Direct comparison of liposomal doxorubicin with or without polyethylene glycol coating in C-26 tumor-bearing mice: is surface coating with polyethylene glycol beneficial? *Clinical Cancer Research, 5*(11), 3645-3652.

Hopper, C., Niziol, C., & Sidhu, M. (2004). The cost-effectiveness of Foscan mediated photodynamic therapy (Foscan-PDT) compared with extensive palliative surgery and palliative chemotherapy for patients with advanced head and neck cancer in the UK. *Oral Oncology, 40*(4), 372-382.

Hudson, R., Carcenac, M., Smith, K., Madden, L., Clarke, O. J., Pelegrin, A., . . . Boyle, R. W. (2005). The development and characterisation of porphyrin isothiocyanate-monoclonal antibody conjugates for photoimmunotherapy. *British Journal of Cancer, 92*(8), 1442-1449.

Hur, C., Nishioka, N. S., & Gazelle, G. S. (2003). Cost-effectiveness of photodynamic therapy for treatment of Barrett's esophagus with high grade dysplasia. *Digestive Diseases and Sciences, 48*(7), 1273-1283.

Huwyler, J., Drewe, J., & Krahenbuhl, S. (2008). Tumor targeting using liposomal antineoplastic drugs. *International Journal of Nanomedicine, 3*(1), 21-29.

Ichikawa, K., Takeuchi, Y., Yonezawa, S., Hikita, T., Kurohane, K., Namba, Y., & Oku, N. (2004). Antiangiogenic photodynamic therapy (PDT) using Visudyne causes effective suppression of tumor growth. *Cancer Letters, 205*(1), 39-48.

Idris, N. M., Gnanasammandhan, M. K., Zhang, J., Ho, P. C., Mahendran, R., & Zhang, Y. (2012). *In vivo* photodynamic therapy using upconversion nanoparticles as remote-controlled nanotransducers. *Nature Medicine, 18*(10), 1580-1585.

Ilium, L. (1998). Chitosan and its use as a pharmaceutical excipient. *Pharmaceutical Research, 15*(9), 1326-1331.

Isele, U., van Hoogevest, P., Leuenberger, H., Capraro, H.-G., & Schieweck, K. (1994). Pharmaceutical development of CGP 55847: a liposomal Zn-phthalocyanine formulation using a controlled organic solvent dilution method. *SPIE Proceedings* 2078. doi: 10.1117/12.168680.

Ishida, T., Atobe, K., Wang, X., & Kiwada, H. (2006). Accelerated blood clearance of PEGylated liposomes upon repeated injections: effect of doxorubicin-encapsulation and high-dose first injection. *Journal of Controlled Release, 115*(3), 251-258.

Ishida, T., Harada, M., Wang, X. Y., Ichihara, M., Irimura, K., & Kiwada, H. (2005). Accelerated blood clearance of PEGylated liposomes following preceding liposome injection: effects of lipid dose and PEG surface-density and chain length of the first-dose liposomes. *Journal of Controlled Release, 105*(3), 305-317.

Ishida, T., Harashima, H., & Kiwada, H. (2002). Liposome clearance. *Bioscience Reports, 22*(2), 197-224.

Ishida, T., Ichihara, M., Wang, X., Yamamoto, K., Kimura, J., Majima, E., & Kiwada, H. (2006). Injection of PEGylated liposomes in rats elicits PEG-specific IgM, which is responsible for rapid elimination of a second dose of PEGylated liposomes. *Journal of Controlled Release, 112*(1), 15-25.

Ishida, T., Kashima, S., & Kiwada, H. (2008). The contribution of phagocytic activity of liver macrophages to the accelerated blood clearance (ABC) phenomenon of PEGylated liposomes in rats. *Journal of Controlled Release, 126*(2), 162-165.

Ishida, T., & Kiwada, H. (2008). Accelerated blood clearance (ABC) phenomenon upon repeated injection of PEGylated liposomes. *International Journal of Pharmaceutics, 354*(1-2), 56-62.

Ishida, T., Wang, X., Shimizu, T., Nawata, K., & Kiwada, H. (2007). PEGylated liposomes elicit an anti-PEG IgM response in a T cell-independent manner. *Journal of Controlled Release, 122*(3), 349-355.

Ivanov, S., Zhuravsky, S., Yukina, G., Tomson, V., Korolev, D., & Galagudza, M. (2012). In Vivo Toxicity of Intravenously Administered Silica and Silicon Nanoparticles. *Materials, 5*(10), 1873-1889.

Jain, R. A. (2000). The manufacturing techniques of various drug loaded biodegradable poly(lactide-co-glycolide) (PLGA) devices. *Biomaterials, 21*(23), 2475-2490.

Jain, R. K. (1987). Transport of molecules across tumor vasculature. *Cancer and Metastasis Reviews, 6*(4), 559-593.

Jain, R. K. (1998). The next frontier of molecular medicine: delivery of therapeutics. *Nature Medicine, 4*(6), 655-657.

Jain, R. K., & Stylianopoulos, T. (2010). Delivering nanomedicine to solid tumors. *Nature Reviews. Clinical Oncology, 7*(11), 653-664.

Jain, S., Hirst, D. G., & O'Sullivan, J. M. (2012). Gold nanoparticles as novel agents for cancer therapy. *British Journal of Radiology, 85*(1010), 101-113.

Ji, R. C. (2005). Characteristics of lymphatic endothelial cells in physiological and pathological conditions. *Histology and Histopathology, 20*(1), 155-175.

Jiang, F., Lilge, L., Grenier, J., Li, Y., Wilson, M. D., & Chopp, M. (1998). Photodynamic therapy of U87 human glioma in nude rat using liposome-delivered photofrin. *Lasers in Surgery and Medicine, 22*(2), 74-80.

Jiang, F., Lilge, L., Logie, B., Li, Y., & Chopp, M. (1997). Photodynamic therapy of 9L gliosarcoma with liposome-delivered photofrin. *Photochemistry and Photobiology, 65*(4), 701-706.

John, F., & George, J. Curcumin Encapsulated Alginate/Pluronic Block Copolymer Micelles as a Promising Therapeutic Agent.

Jones, M.-C., & Leroux, J.-C. (1999). Polymeric micelles – a new generation of colloidal drug carriers. *European Journal of Pharmaceutics and Biopharmaceutics, 48*(2), 101-111.

Josefsen, L. B., & Boyle, R. W. (2008a). Photodynamic therapy and the development of metal-based photosensitisers. *Met Based Drugs, 2008*, 276109.

Josefsen, L. B., & Boyle, R. W. (2008b). Photodynamic therapy: novel third-generation photosensitizers one step closer? *British Journal of Pharmacology, 154*(1), 1-3.

Juarranz, A., Jaen, P., Sanz-Rodriguez, F., Cuevas, J., & Gonzalez, S. (2008). Photodynamic therapy of cancer. Basic principles and applications. *Clinical and Translational Oncology, 10*(3), 148-154.

Kafshgari, M., Delalat, B., Tong, W., Harding, F., Kaasalainen, M., Salonen, J., & Voelcker, N. (2015). Oligonucleotide delivery by chitosan-functionalized porous silicon nanoparticles. *Nano Research, 8*(6), 2033-2046.

Kainthan, R. K., & Brooks, D. E. (2007). In vivo biological evaluation of high molecular weight hyperbranched polyglycerols. *Biomaterials, 28*(32), 4779-4787.

Kamkaew, A., Lim, S. H., Lee, H. B., Kiew, L. V., Chung, L. Y., & Burgess, K. (2013). BODIPY dyes in photodynamic therapy. *Chemical Society Reviews, 42*(1), 77-88.

Kao, Y. J., & Juliano, R. L. (1981). Interactions of liposomes with the reticuloendothelial system. Effects of reticuloendothelial blockade on the

clearance of large unilamellar vesicles. *Biochimica et Biophysica Acta, 677*(3-4), 453-461.

Karnik, R., Gu, F., Basto, P., Cannizzaro, C., Dean, L., Kyei-Manu, W., . . . Farokhzad, O. C. (2008). Microfluidic Platform for Controlled Synthesis of Polymeric Nanoparticles. *Nano Letters, 8*(9), 2906-2912.

Kataoka, K., Harada, A., & Nagasaki, Y. (2001). Block copolymer micelles for drug delivery: design, characterization and biological significance. *Advanced Drug Delivery Reviews, 47*(1), 113-131.

Kato, H. (1998). Photodynamic therapy for lung cancer--a review of 19 years' experience. *Journal of Photochemistry and Photobiology. B, Biology, 42*(2), 96-99.

Kean, T., Roth, S., & Thanou, M. (2005). Trimethylated chitosans as non-viral gene delivery vectors: cytotoxicity and transfection efficiency. *Journal of Controlled Release, 103*(3), 643-653.

Kean, T., & Thanou, M. (2010). Biodegradation, biodistribution and toxicity of chitosan. *Adv Drug Deliv Rev, 62*(1), 3-11.

Kenausis, G. L., Vörös, J., Elbert, D. L., Huang, N., Hofer, R., Ruiz-Taylor, L., . . . Spencer, N. D. (2000). Poly(l-lysine)-g-Poly(ethylene glycol) Layers on Metal Oxide Surfaces: Attachment Mechanism and Effects of Polymer Architecture on Resistance to Protein Adsorption†. *The Journal of Physical Chemistry B, 104*(14), 3298-3309.

Kessel, D. (1989). Determinants of photosensitization by purpurins. *Photochemistry and Photobiology, 50*(2), 169-174.

Kessel, D. (1992). Properties of cremophor el micelles probed by fluorescence. *Photochemistry and Photobiology, 56*(4), 447-451.

Kessel, D., & Reiners, J. J., Jr. (2007). Apoptosis and autophagy after mitochondrial or endoplasmic reticulum photodamage. *Photochemistry and Photobiology, 83*(5), 1024-1028.

Khan, T. A., Peh, K. K., & Ch'ng, H. S. (2002). Reporting degree of deacetylation values of chitosan: the influence of analytical methods. *Journal of Pharmacy and Pharmaceutical Sciences, 5*(3), 205-212.

Kiew, L. V., Cheong, S. K., Sidik, K., & Chung, L. Y. (2010). Improved plasma stability and sustained release profile of gemcitabine via polypeptide conjugation. *International Journal of Pharmaceutics, 391*(1-2), 212-220.

Kim, B. S., Kim, C. S., & Lee, K. M. (2008). The intracellular uptake ability of chitosan-coated Poly (D,L-lactide-co-glycolide) nanoparticles. *Archives of Pharmacal Research, 31*(8), 1050-1054.

Kim, K., Kim, J. H., Park, H., Kim, Y.-S., Park, K., Nam, H., . . . Kwon, I. C. (2010). Tumor-homing multifunctional nanoparticles for cancer theragnosis:

simultaneous diagnosis, drug delivery, and therapeutic monitoring. *Journal of Controlled Release, 146*(2), 219-227.

Kinsella, T. J., Baron, E. D., Colussi, V. C., Cooper, K. D., Hoppel, C. L., Ingalls, S. T., . . . Remick, S. C. (2011). Preliminary clinical and pharmacologic investigation of photodynamic therapy with the silicon phthalocyanine photosensitizer pc 4 for primary or metastatic cutaneous cancers. *Frontiers in Oncology, 1,* 14.

Klibanov, A. L., Maruyama, K., Torchilin, V. P., & Huang, L. (1990). Amphipathic polyethyleneglycols effectively prolong the circulation time of liposomes. *FEBS Letters, 268*(1), 235-237.

Konan-Kouakou, Y. N., Boch, R., Gurny, R., & Allémann, E. (2005). *In vitro* and *in vivo* activities of verteporfin-loaded nanoparticles. *Journal of Controlled Release, 103*(1), 83-91.

Konsoula, R., & Jung, M. (2008). In vitro plasma stability, permeability and solubility of mercaptoacetamide histone deacetylase inhibitors. *International Journal of Pharmaceutics, 361*(1-2), 19-25.

Koo, H., Lee, H., Lee, S., Min, K. H., Kim, M. S., Lee, D. S., . . . Jeong, S. Y. (2010). *In vivo* tumor diagnosis and photodynamic therapy via tumoral pH-responsive polymeric micelles. *Chemical Communications, 46*(31), 5668-5670.

Kopelman, R., Lee Koo, Y.-E., Philbert, M., Moffat, B. A., Ramachandra Reddy, G., McConville, P., . . . Ross, B. D. (2005). Multifunctional nanoparticle platforms for *in vivo* MRI enhancement and photodynamic therapy of a rat brain cancer. *Journal of Magnetism and Magnetic Materials, 293*(1), 404-410.

Koudelka, S., Turanek-Knotigova, P., Masek, J., Korvasova, Z., Skrabalova, M., Plockova, J., . . . Turanek, J. (2010). Liposomes with high encapsulation capacity for paclitaxel: Preparation, characterisation and in vivo anticancer effect. *Journal of Pharmaceutical Sciences, 99*(5), 2309-2319.

Kozlowska, D., Foran, P., MacMahon, P., Shelly, M. J., Eustace, S., & O'Kennedy, R. (2009). Molecular and magnetic resonance imaging: the value of immunoliposomes. *Advanced Drug Delivery Reviews, 61*(15), 1402-1411.

Kue, C. S., Kamkaew, A., Lee, H. B., Chung, L. Y., Kiew, L. V., & Burgess, K. (2015). Targeted PDT agent eradicates TrkC expressing tumors via photodynamic therapy (PDT). *Molecular Pharmaceutics, 12*(1), 212-222.

Kuhn, D. A., Vanhecke, D., Michen, B., Blank, F., Gehr, P., Petri-Fink, A., & Rothen-Rutishauser, B. (2014). Different endocytotic uptake mechanisms for nanoparticles in epithelial cells and macrophages. *Beilstein J Nanotechnol, 5*, 1625-1636.

Kumar, M. N. V. R., Muzzarelli, R. A. A., Muzzarelli, C., Sashiwa, H., & Domb, A. J. (2004). Chitosan chemistry and pharmaceutical perspectives. *Chemical Reviews, 104*(12), 6017-6084.

Kumar, R., Roy, I., Ohulchanskky, T. Y., Vathy, L. A., Bergey, E. J., Sajjad, M., & Prasad, P. N. (2010). In vivo biodistribution and clearance studies using multimodal organically modified silica nanoparticles. *ACS Nano, 4*(2), 699-708.

Kumari, A., Yadav, S. K., & Yadav, S. C. (2010). Biodegradable polymeric nanoparticles based drug delivery systems. *Colloids and Surfaces B: Biointerfaces, 75*(1), 1-18.

Kuznetsova, N. A., Gretsova, N. S., Derkacheva, V. M., Kaliya, O. L., & Lukyanets, E. A. (2003). Sulfonated phthalocyanines: aggregation and singlet oxygen quantum yield in aqueous solutions. *Journal of Porphyrins and Phthalocyanines, 7*(3), 147-154.

Kwan, B. C., Kronenberg, F., Beddhu, S., & Cheung, A. K. (2007). Lipoprotein metabolism and lipid management in chronic kidney disease. *Journal of the American Society of Nephrology, 18*(4), 1246-1261.

Kwon, G. S., & Okano, T. (1996). Polymeric micelles as new drug carriers. *Advanced Drug Delivery Reviews, 21*(2), 107-116.

Lasic, D. D., Martin, F. J., Gabizon, A., Huang, S. K., & Papahadjopoulos, D. (1991). Sterically stabilized liposomes: a hypothesis on the molecular origin of the extended circulation times. *Biochimica et Biophysica Acta (BBA) - Biomembranes, 1070*(1), 187-192.

Lassalle, H.-P., Dumas, D., Gräfe, S., D'Hallewin, M.-A., Guillemin, F., & Bezdetnaya, L. (2009). Correlation between in vivo pharmacokinetics, intratumoral distribution and photodynamic efficiency of liposomal mTHPC. *Journal of Controlled Release, 134*(2), 118-124.

Le Garrec, D., Taillefer, J., Van Lier, J. E., Lenaerts, V., & Leroux, J.-C. (2002). Optimizing pH-responsive polymeric micelles for drug delivery in a cancer photodynamic therapy model. *Journal of Drug Targeting, 10*(5), 429-437.

Lee, C. C., MacKay, J. A., Fréchet, J. M., & Szoka, F. C. (2005). Designing dendrimers for biological applications. *Nature Biotechnology, 23*(12), 1517-1526.

Lee, S. C. (2002). Dendrimers in nanobiological devices *Dendrimers and Other Dendritic Polymers* (pp. 547-557): John Wiley & Sons, Ltd.

Lee, S. J., Koo, H., Jeong, H., Huh, M. S., Choi, Y., Jeong, S. Y., . . . Kwon, I. C. (2011). Comparative study of photosensitizer loaded and conjugated glycol chitosan nanoparticles for cancer therapy. *Journal of Controlled Release, 152*(1), 21-29.

Lee, S. J., Koo, H., Lee, D.-E., Min, S., Lee, S., Chen, X., . . . Choi, K. (2011). Tumor-homing photosensitizer-conjugated glycol chitosan nanoparticles for synchronous photodynamic imaging and therapy based on cellular on/off system. *Biomaterials, 32*(16), 4021-4029.

Lee, S. J., Park, K., Oh, Y.-K., Kwon, S.-H., Her, S., Kim, I.-S., . . . Kwon, I. C. (2009). Tumor specificity and therapeutic efficacy of photosensitizer-encapsulated

glycol chitosan-based nanoparticles in tumor-bearing mice. *Biomaterials, 30*(15), 2929-2939.

Lee, S. W., Yun, M. H., Jeong, S. W., In, C. H., Kim, J. Y., Seo, M. H., . . . Kim, S. O. (2011). Development of docetaxel-loaded intravenous formulation, Nanoxel-PM using polymer-based delivery system. *Journal of Controlled Release, 155*(2), 262-271.

Levine, B., & Deretic, V. (2007). Unveiling the roles of autophagy in innate and adaptive immunity. *Nature Reviews. Immunology, 7*(10), 767-777.

Li, S. D., & Huang, L. (2008). Pharmacokinetics and biodistribution of nanoparticles. *Molecular Pharmaceutics, 5*(4), 496-504.

Li, Y., Pei, Y., Zhang, X., Gu, Z., Zhou, Z., Yuan, W., . . . Gao, X. (2001). PEGylated PLGA nanoparticles as protein carriers: synthesis, preparation and biodistribution in rats. *Journal of Controlled Release, 71*(2), 203-211.

Lim, S. H., Thivierge, C., Nowak-Sliwinska, P., Han, J., van den Bergh, H., Wagnieres, G., . . . Lee, H. B. (2010). In vitro and in vivo photocytotoxicity of boron dipyrromethene derivatives for photodynamic therapy. *Journal of Medicinal Chemistry, 53*(7), 2865-2874.

Lim, S. H., Yam, M. L., Lam, M. L., Kamarulzaman, F. A., Samat, N., Kiew, L. V., . . . Lee, H. B. (2014). Photodynamic Characterization of Amino Acid Conjugated 151-Hydroxypurpurin-7-lactone for Cancer Treatment. *Molecular Pharmaceutics, 11*(9), 3164-3173.

Lind, K., Kresse, M., Debus, N. P., & Muller, R. H. (2002). A novel formulation for superparamagnetic iron oxide (SPIO) particles enhancing MR lymphography: comparison of physicochemical properties and the in vivo behaviour. *Journal of Drug Targeting, 10*(3), 221-230.

Liu, Y., Shipton, M. K., Ryan, J., Kaufman, E. D., Franzen, S., & Feldheim, D. L. (2007). Synthesis, stability, and cellular internalization of gold nanoparticles containing mixed peptide−poly(ethylene glycol) monolayers. *Analytical Chemistry, 79*(6), 2221-2229.

Longmire, M., Choyke, P. L., & Kobayashi, H. (2008). Clearance Properties of Nano-sized Particles and Molecules as Imaging Agents: Considerations and Caveats. *Nanomedicine, 3*(5), 703-717.

Longmire, M., Choyke, P. L., & Kobayashi, H. (2008). Clearance properties of nano-sized particles and molecules as imaging agents: considerations and caveats. *Nanomedicine (Lond), 3*(5), 703-717.

Loudet, A., & Burgess, K. (2007). BODIPY Dyes and Their Derivatives: Syntheses and Spectroscopic Properties. *Chemical Reviews, 107*(11), 4891-4932.

Lowe, C. E. (1954). Preparation of high molecular weight polyhydroxyacetic ester: Google Patents.

Lu, J., Liong, M., Li, Z., Zink, J. I., & Tamanoi, F. (2010). Biocompatibility, biodistribution, and drug-delivery efficiency of mesoporous silica nanoparticles for cancer therapy in animals. *Small, 6*(16), 1794-1805.

Lu, J. M., Wang, X., Marin-Muller, C., Wang, H., Lin, P. H., Yao, Q., & Chen, C. (2009). Current advances in research and clinical applications of PLGA-based nanotechnology. *Expert Review of Molecular Diagnostics, 9*(4), 325-341.

Lukyanov, A. N., & Torchilin, V. P. (2004). Micelles from lipid derivatives of water-soluble polymers as delivery systems for poorly soluble drugs. *Advanced Drug Delivery Reviews, 56*(9), 1273-1289.

Maeda, H. (2001). The enhanced permeability and retention (EPR) effect in tumor vasculature: the key role of tumor-selective macromolecular drug targeting. *Advances in Enzyme Regulation, 41*(1), 189-207.

Maeda, H. (2001). SMANCS and polymer-conjugated macromolecular drugs: advantages in cancer chemotherapy. *Adv Drug Deliv Rev, 46*(1-3), 169-185.

Maeda, H., Matsumoto, T., Konno, T., Iwai, K., & Ueda, M. (1984). Tailor-making of protein drugs by polymer conjugation for tumor targeting: A brief review on smancs. *Journal of Protein Chemistry, 3*(2), 181-193.

Maeda, H., Takeshita, J., & Kanamaru, R. (1979). A lipophilic derivative of neocarzinostatin. A polymer conjugation of an antitumor protein antibiotic. *International Journal of Peptide and Protein Research, 14*(2), 81-87.

Makadia, H. K., & Siegel, S. J. (2011). Poly Lactic-co-Glycolic Acid (PLGA) as Biodegradable Controlled Drug Delivery Carrier. *Polymers (Basel), 3*(3), 1377-1397.

Markovsky, E., Baabur-Cohen, H., Eldar-Boock, A., Omer, L., Tiram, G., Ferber, S., . . . Satchi-Fainaro, R. (2012). Administration, distribution, metabolism and elimination of polymer therapeutics. *Journal of Controlled Release, 161*(2), 446-460.

Marotta, D. E., Cao, W., Wileyto, E. P., Li, H., Corbin, I., Rickter, E., . . . Busch, T. M. (2011). Evaluation of bacteriochlorophyll-reconstituted low-density lipoprotein nanoparticles for photodynamic therapy efficacy *in vivo*. *Nanomedicine, 6*(3), 475-487.

Master, A., Livingston, M., & Sen Gupta, A. (2013). Photodynamic nanomedicine in the treatment of solid tumors: perspectives and challenges. *Journal of Controlled Release, 168*(1), 88-102.

Matsumura, Y., & Maeda, H. (1986). A new concept for macromolecular therapeutics in cancer chemotherapy: mechanism of tumoritropic accumulation of proteins and the antitumor agent smancs. *Cancer Research, 46*(12 Pt 1), 6387-6392.

McCarthy, T. D., Karellas, P., Henderson, S. A., Giannis, M., O'Keefe, D. F., Heery, G., . . . Holan, G. (2005). Dendrimers as drugs: discovery and preclinical and

clinical development of dendrimer-based microbicides for HIV and STI prevention. *Molecular Pharmaceutics, 2*(4), 312-318.

McNeil, S. E. (2009). Nanoparticle therapeutics: a personal perspective. *Wiley Interdisciplinary Reviews: Nanomedicine and Nanobiotechnology, 1*(3), 264-271.

Mehrmohammadi, M., Yoon, S. J., Yeager, D., & Emelianov, S. Y. (2013). Photoacoustic Imaging for Cancer Detection and Staging. *Curr Mol Imaging, 2*(1), 89-105.

Metselaar, J. M., Bruin, P., de Boer, L. W., de Vringer, T., Snel, C., Oussoren, C., . . . Hennink, W. E. (2003). A novel family of L-amino acid-based biodegradable polymer-lipid conjugates for the development of long-circulating liposomes with effective drug-targeting capacity. *Bioconjugate Chemistry, 14*(6), 1156-1164.

Mishra, S., Webster, P., & Davis, M. E. (2004). PEGylation significantly affects cellular uptake and intracellular trafficking of non-viral gene delivery particles. *European Journal of Cell Biology, 83*(3), 97-111.

Misra, R., Acharya, S., & Sahoo, S. K. (2010). Cancer nanotechnology: application of nanotechnology in cancer therapy. *Drug Discovery Today, 15*(19–20), 842-850.

Moan, J., & Berg, K. (1991). The photodegradation of porphyrins in cells can be used to estimate the lifetime of singlet oxygen. *Photochemistry and Photobiology, 53*(4), 549-553.

Moffatt, S., & Cristiano, R. J. (2006). Uptake characteristics of NGR-coupled stealth PEI/pDNA nanoparticles loaded with PLGA-PEG-PLGA tri-block copolymer for targeted delivery to human monocyte-derived dendritic cells. *International Journal of Pharmaceutics, 321*(1-2), 143-154.

Moghimi, S. M. (1998). Opsono-recognition of liposomes by tissue macrophages. *International Journal of Pharmaceutics, 162*(1–2), 11-18.

Moghimi, S. M., & Hamad, I. (2008). Liposome-mediated triggering of complement cascade. *Journal of Liposome Research, 18*(3), 195-209.

Moghimi, S. M., Hunter, A. C., & Murray, J. C. (2001). Long-circulating and target-specific nanoparticles: theory to practice. *Pharmacological Reviews, 53*(2), 283-318.

Mora-Huertas, C. E., Fessi, H., & Elaissari, A. (2010). Polymer-based nanocapsules for drug delivery. *International Journal of Pharmaceutics, 385*(1–2), 113-142.

Müller, R. H., Wallis, K. H., Tröster, S. D., & Kreuter, J. (1992). In vitro characterization of poly(methyl-methacrylate) nanoparticles and correlation to their in vivo fate. *Journal of Controlled Release, 20*(3), 237-246.

Muthu, M. (2009). Nanoparticles based on PLGA and its co-polymer: an overview. *Asian Journal of Pharmaceutics, 3*(4), 266-273.

Nakamura, M., Davila-Zavala, P., Tokuda, H., Takakura, Y., & Hashida, M. (1998). Uptake and gene expression of naked plasmid DNA in cultured brain microvessel endothelial cells. *Biochemical and Biophysical Research Communications, 245*(1), 235-239.

Ng, K. K., Lovell, J. F., & Zheng, G. (2011). Lipoprotein-inspired nanoparticles for cancer theranostics. *Accounts of Chemical Research, 44*(10), 1105-1113.

Nishiyama, N., Nakagishi, Y., Morimoto, Y., Lai, P.-S., Miyazaki, K., Urano, K., . . . Kataoka, K. (2009). Enhanced photodynamic cancer treatment by supramolecular nanocarriers charged with dendrimer phthalocyanine. *Journal of Controlled Release, 133*(3), 245-251.

Noguchi, Y., Wu, J., Duncan, R., Strohalm, J., Ulbrich, K., Akaike, T., & Maeda, H. (1998). Early phase tumor accumulation of macromolecules: a great difference in clearance rate between tumor and normal tissues. *Japanese Journal of Cancer Research, 89*(3), 307-314.

Norman, M. E., Williams, P., & Illum, L. (1992). Human serum albumin as a probe for surface conditioning (opsonization) of block copolymer-coated microspheres. *Biomaterials, 13*(12), 841-849.

O'Neal, D. P., Hirsch, L. R., Halas, N. J., Payne, J. D., & West, J. L. (2004). Photo-thermal tumor ablation in mice using near infrared-absorbing nanoparticles. *Cancer Letters, 209*(2), 171-176.

Ochsner, M. (1996). Light scattering of human skin: a comparison between zinc (II)-phthalocyanine and photofrin II. *Journal of Photochemistry and Photobiology. B, Biology, 32*(1-2), 3-9.

Owens, D. E., 3rd, & Peppas, N. A. (2006). Opsonization, biodistribution, and pharmacokinetics of polymeric nanoparticles. *International Journal of Pharmaceutics, 307*(1), 93-102.

Padera, T. P., Stoll, B. R., Tooredman, J. B., Capen, D., di Tomaso, E., & Jain, R. K. (2004). Pathology: cancer cells compress intratumour vessels. *Nature, 427*(6976), 695.

Pamujula, S., Hazari, S., Bolden, G., Graves, R. A., Chinta, D. D., Dash, S., . . . Mandal, T. K. (2012). Cellular delivery of PEGylated PLGA nanoparticles. *Journal of Pharmacy and Pharmacology, 64*(1), 61-67.

Papisov, M. I. (2001). Acyclic Polyacetals from Polysaccharides: Biomimetic Biomedical "Stealth" Polymers *Biopolymers from Polysaccharides and Agroproteins* (Vol. 786, pp. 301-314): American Chemical Society.

Park, J. H., Saravanakumar, G., Kim, K., & Kwon, I. C. (2010). Targeted delivery of low molecular drugs using chitosan and its derivatives. *Advanced Drug Delivery Reviews, 62*(1), 28-41.

Patel, H. M., & Moghimi, S. M. (1998). Serum-mediated recognition of liposomes by phagocytic cells of the reticuloendothelial system - The concept of tissue specificity. *Adv Drug Deliv Rev, 32*(1-2), 45-60.

Peng, C. L., Shieh, M. J., Tsai, M. H., Chang, C. C., & Lai, P. S. (2008). Self-assembled star-shaped chlorin-core poly(epsilon-caprolactone)-poly(ethylene glycol) diblock copolymer micelles for dual chemo-photodynamic therapies. *Biomaterials, 29*(26), 3599-3608.

Perrault, S. D., & Chan, W. C. W. (2010). In vivo assembly of nanoparticle components to improve targeted cancer imaging. *Proceedings of the National Academy of Sciences, 107*(25), 11194-11199.

Petersen, H., Fechner, P. M., Martin, A. L., Kunath, K., Stolnik, S., Roberts, C. J., . . . Kissel, T. (2002). Polyethylenimine-graft-poly(ethylene glycol) copolymers: influence of copolymer block structure on DNA complexation and biological activities as gene delivery system. *Bioconjugate Chemistry, 13*(4), 845-854.

Prabhakar, U., Maeda, H., Jain, R. K., Sevick-Muraca, E. M., Zamboni, W., Farokhzad, O. C., . . . Blakey, D. C. (2013). Challenges and key considerations of the enhanced permeability and retention effect for nanomedicine drug delivery in oncology. *Cancer Research, 73*(8), 2412-2417.

Pratten, M. K., & Lloyd, J. B. (1986). Pinocytosis and phagocytosis: the effect of size of a particulate substrate on its mode of capture by rat peritoneal macrophages cultured in vitro. *Biochimica et Biophysica Acta, 881*(3), 307-313.

Prokop, A., & Davidson, J. M. (2008). Nanovehicular intracellular delivery systems. *Journal of Pharmaceutical Sciences, 97*(9), 3518-3590.

Pulaski, B. A., & Ostrand-Rosenberg, S. (1998). Reduction of established spontaneous mammary carcinoma metastases following immunotherapy with major histocompatibility complex class II and B7.1 cell-based tumor vaccines. *Cancer Research, 58*(7), 1486-1493.

Rao, C. N. R., Ramakrishna Matte, H. S. S., Voggu, R., & Govindaraj, A. (2012). Recent progress in the synthesis of inorganic nanoparticles. *Dalton Transactions, 41*(17), 5089-5120.

Reddy, G. R., Bhojani, M. S., McConville, P., Moody, J., Moffat, B. A., Hall, D. E., . . . Ross, B. D. (2006). Vascular targeted nanoparticles for imaging and treatment of brain tumors. *Clinical Cancer Research, 12*(22), 6677-6686.

Remaut, K., Lucas, B., Braeckmans, K., Demeester, J., & De Smedt, S. C. (2007). Pegylation of liposomes favours the endosomal degradation of the delivered phosphodiester oligonucleotides. *Journal of Controlled Release, 117*(2), 256-266.

Rezanka, P., Záruba, K., & Král, V. (2008). A change in nucleotide selectivity pattern of porphyrin derivatives after immobilization on gold nanoparticles. *Tetrahedron Letters, 49*(45), 6448-6453.

Rhodes, L. E., de Rie, M., Enstrom, Y., Groves, R., Morken, T., Goulden, V., . . . Wolf, P. (2004). Photodynamic therapy using topical methyl aminolevulinate vs surgery for nodular basal cell carcinoma: results of a multicenter randomized prospective trial. *Archives of Dermatology, 140*(1), 17-23.

Ricci-Junior, E., & Marchetti, J. M. (2006). Zinc(II) phthalocyanine loaded PLGA nanoparticles for photodynamic therapy use. *International Journal of Pharmaceutics, 310*(1-2), 187-195.

Richardson, S. C., Kolbe, H. V., & Duncan, R. (1999). Potential of low molecular mass chitosan as a DNA delivery system: biocompatibility, body distribution and ability to complex and protect DNA. *International Journal of Pharmaceutics, 178*(2), 231-243.

Richter, A. M., Yip, S., Waterfield, E., Logan, P. M., Slonecker, C. E., & Levy, J. G. (1991). Mouse skin photosensitization with benzoporphyrin derivatives and photofrin®: Macroscopic and microscopic evaluation. *Photochemistry and Photobiology, 53*(2), 281-286.

Roby, A., Erdogan, S., & Torchilin, V. P. (2006). Solubilization of poorly soluble PDT agent, meso-tetraphenylporphin, in plain or immunotargeted PEG-PE micelles results in dramatically improved cancer cell killing *in vitro*. *European Journal of Pharmaceutics and Biopharmaceutics, 62*(3), 235-240.

Roby, A., Erdogan, S., & Torchilin, V. P. (2007). Enhanced *in vivo* antitumor efficacy of poorly soluble PDT agent, meso-tetraphenylporphine, in PEG-PE-based tumor-targeted immunomicelles. *Cancer Biology & Therapy, 6*(7), 1136-1142.

Rodriguez, M. A., Pytlik, R., Kozak, T., Chhanabhai, M., Gascoyne, R., Lu, B., . . . Winter, J. N. (2009). Vincristine sulfate liposomes injection (Marqibo) in heavily pretreated patients with refractory aggressive non-Hodgkin lymphoma: report of the pivotal phase 2 study. *Cancer, 115*(15), 3475-3482.

Rojnik, M., Kocbek, P., Moret, F., Compagnin, C., Celotti, L., Bovis, M. J., . . . Kos, J. (2012). In vitro and in vivo characterization of temoporfin-loaded PEGylated PLGA nanoparticles for use in photodynamic therapy. *Nanomedicine (Lond), 7*(5), 663-677.

Roser, M., Fischer, D., & Kissel, T. (1998). Surface-modified biodegradable albumin nano- and microspheres. II: effect of surface charges on in vitro phagocytosis and biodistribution in rats. *European Journal of Pharmaceutics and Biopharmaceutics, 46*(3), 255-263.

Roy, I., Ohulchanskyy, T. Y., Pudavar, H. E., Bergey, E. J., Oseroff, A. R., Morgan, J., . . . Prasad, P. N. (2003). Ceramic-based nanoparticles entrapping water-insoluble photosensitizing anticancer drugs: a novel drug-carrier system for photodynamic therapy. *Journal of the American Chemical Society, 125*(26), 7860-7865.

Rück, A., Böhmler, A., & Steiner, R. (2005). PDT with TOOKAD® studied in the chorioallantoic membrane of fertilized eggs. *Photodiagnosis and Photodynamic Therapy, 2*(1), 79-90.

Sadauskas, E., Wallin, H., Stoltenberg, M., Vogel, U., Doering, P., Larsen, A., & Danscher, G. (2007). Kupffer cells are central in the removal of nanoparticles from the organism. *Particle and Fibre Toxicology, 4*(1), 1-7.

Salmaso, S., & Caliceti, P. (2013). Stealth Properties to Improve Therapeutic Efficacy of Drug Nanocarriers. *Journal of Drug Delivery, 2013*, 19.

Samad, A., Sultana, Y., & Aqil, M. (2007). Liposomal drug delivery systems: an update review. *Current Drug Delivery, 4*(4), 297-305.

Schipper, N. G., Varum, K. M., Stenberg, P., Ocklind, G., Lennernas, H., & Artursson, P. (1999). Chitosans as absorption enhancers of poorly absorbable drugs. 3: Influence of mucus on absorption enhancement. *European Journal of Pharmaceutical Sciences, 8*(4), 335-343.

Schmid, F.-X. (2001). Biological Macromolecules: UV-visible Spectrophotometry *eLS*: John Wiley & Sons, Ltd.

Scholes, P. D., Coombes, A. G. A., Illum, L., Daviz, S. S., Vert, M., & Davies, M. C. (1993). The preparation of sub-200 nm poly(lactide-co-glycolide) microspheres for site-specific drug delivery. *Journal of Controlled Release, 25*(1–2), 145-153.

Schuller, D. E., McCaughan, J. S., Jr., & Rock, R. P. (1985). Photodynamic therapy in head and neck cancer. *Archives of Otolaryngology, 111*(6), 351-355.

Semple, S. C., Chonn, A., & Cullis, P. R. (1998). Interactions of liposomes and lipid-based carrier systems with blood proteins: Relation to clearance behaviour in vivo. *Advanced Drug Delivery Reviews, 32*(1–2), 3-17.

Senior, J., Delgado, C., Fisher, D., Tilcock, C., & Gregoriadis, G. (1991). Influence of surface hydrophilicity of liposomes on their interaction with plasma protein and clearance from the circulation: studies with poly(ethylene glycol)-coated vesicles. *Biochimica et Biophysica Acta (BBA) - Biomembranes, 1062*(1), 77-82.

Senior, J. H. (1987). Fate and behavior of liposomes in vivo: a review of controlling factors. *Critical Reviews in Therapeutic Drug Carrier Systems, 3*(2), 123-193.

Shan, X., Liu, C., Yuan, Y., Xu, F., Tao, X., Sheng, Y., & Zhou, H. (2009). In vitro macrophage uptake and in vivo biodistribution of long-circulation nanoparticles with poly(ethylene-glycol)-modified PLA (BAB type) triblock copolymer. *Colloids and Surfaces. B, Biointerfaces, 72*(2), 303-311.

Sheng, Y., Yuan, Y., Liu, C., Tao, X., Shan, X., & Xu, F. (2009). In vitro macrophage uptake and in vivo biodistribution of PLA-PEG nanoparticles loaded with hemoglobin as blood substitutes: effect of PEG content. *Journal of Materials Science. Materials in Medicine, 20*(9), 1881-1891.

Siegers, C., Biesalski, M., & Haag, R. (2004). Self-assembled monolayers of dendritic polyglycerol derivatives on gold that resist the adsorption of proteins. *Chemistry, 10*(11), 2831-2838.

Simon, V., Devaux, C., Darmon, A., Donnet, T., Thiénot, E., Germain, M., . . . Marill, J. (2010). Pp IX silica nanoparticles demonstrate differential interactions with *in vitro* tumor cell lines and *in vivo* mouse models of human cancers. *Photochemistry and Photobiology, 86*(1), 213-222.

Skidan, I., Dholakia, P., & Torchilin, V. (2008). Photodynamic therapy of experimental B-16 melanoma in mice with tumor-targeted 5,10,15,20-tetraphenylporphin-loaded PEG-PE micelles. *Journal of Drug Targeting, 16*(6), 486-493.

Skyrme, R. J., French, A. J., Datta, S. N., Allman, R., Mason, M. D., & Matthews, P. N. (2005). A phase-1 study of sequential mitomycin C and 5-aminolaevulinic acid-mediated photodynamic therapy in recurrent superficial bladder carcinoma. *BJU International, 95*(9), 1206-1210.

Snipstad, S., Westrøm, S., Mørch, Y., Afadzi, M., Åslund, A., & de Lange Davies, C. (2014). Contact-mediated intracellular delivery of hydrophobic drugs from polymeric nanoparticles. *Cancer Nanotechnology, 5*(1), 1-18.

Solban, N., Rizvi, I., & Hasan, T. (2006). Targeted photodynamic therapy. *Lasers in Surgery and Medicine, 38*(5), 522-531.

Soo Choi, H., Liu, W., Misra, P., Tanaka, E., Zimmer, J. P., Itty Ipe, B., . . . Frangioni, J. V. (2007). Renal clearance of quantum dots. *Nat Biotech, 25*(10), 1165-1170.

Sortino, S., Mazzaglia, A., Monsu Scolaro, L., Marino Merlo, F., Valveri, V., & Sciortino, M. T. (2006). Nanoparticles of cationic amphiphilic cyclodextrins entangling anionic porphyrins as carrier-sensitizer system in photodynamic cancer therapy. *Biomaterials, 27*(23), 4256-4265.

Stevanovic, M., & Uskokovic, D. (2009). Poly(lactide-co-glycolide)-based micro and nanoparticles for the controlled drug delivery of vitamins. *Current Nanoscience, 5*(1), 1-14.

Stolnik, S., Dunn, S. E., Garnett, M. C., Davies, M. C., Coombes, A. G., Taylor, D. C., . . . et al. (1994). Surface modification of poly(lactide-co-glycolide) nanospheres by biodegradable poly(lactide)-poly(ethylene glycol) copolymers. *Pharmaceutical Research, 11*(12), 1800-1808.

Storm, G., Belliot, S. O., Daemen, T., & Lasic, D. D. (1995). Surface modification of nanoparticles to oppose uptake by the mononuclear phagocyte system. *Advanced Drug Delivery Reviews, 17*(1), 31-48.

Swartz, M. A. (2001). The physiology of the lymphatic system. *Adv Drug Deliv Rev, 50*(1-2), 3-20.

Swartz, M. A., & Fleury, M. E. (2007). Interstitial flow and its effects in soft tissues. *Annual Review of Biomedical Engineering, 9*, 229-256.

Tahara, K., Sakai, T., Yamamoto, H., Takeuchi, H., Hirashima, N., & Kawashima, Y. (2009). Improved cellular uptake of chitosan-modified PLGA nanospheres by A549 cells. *International Journal of Pharmaceutics, 382*(1-2), 198-204.

Tan, H. W., & Misran, M. (2013). Polysaccharide-anchored fatty acid liposome. *International Journal of Pharmaceutics, 441*(1-2), 414-423.

Tarn, D., Ashley, C. E., Xue, M., Carnes, E. C., Zink, J. I., & Brinker, C. J. (2013). Mesoporous silica nanoparticle nanocarriers: biofunctionality and biocompatibility. *Accounts of Chemical Research, 46*(3), 792-801.

Tomayko, M. M., & Reynolds, C. P. (1989). Determination of subcutaneous tumor size in athymic (nude) mice. *Cancer Chemotherapy and Pharmacology, 24*(3), 148-154.

Torchilin, V. P. (2004). Targeted polymeric micelles for delivery of poorly soluble drugs. *Cellular and Molecular Life Sciences CMLS, 61*(19-20), 2549-2559.

Triesscheijn, M., Baas, P., Schellens, J. H., & Stewart, F. A. (2006). Photodynamic therapy in oncology. *Oncologist, 11*(9), 1034-1044.

Trindade, T., O'Brien, P., & Pickett, N. L. (2001). Nanocrystalline semiconductors: synthesis, properties, and perspectives. *Chemistry of Materials, 13*(11), 3843-3858.

Tu, J., Wang, T., Shi, W., Wu, G., Tian, X., Wang, Y., . . . Ren, L. (2012). Multifunctional ZnPc-loaded mesoporous silica nanoparticles for enhancement of photodynamic therapy efficacy by endolysosomal escape. *Biomaterials, 33*(31), 7903-7914.

Ullal, A. V., Reiner, T., Yang, K. S., Gorbatov, R., Min, C., Issadore, D., . . . Weissleder, R. (2011). Nanoparticle-Mediated Measurement of Target–Drug Binding in Cancer Cells. *ACS Nano, 5*(11), 9216-9224.

Valle, J. W., Armstrong, A., Newman, C., Alakhov, V., Pietrzynski, G., Brewer, J., . . . Ranson, M. (2011). A phase 2 study of SP1049C, doxorubicin in P-glycoprotein-targeting pluronics, in patients with advanced adenocarcinoma of the esophagus and gastroesophageal junction. *Investigational New Drugs, 29*(5), 1029-1037.

van Nostrum, C. F. (2004). Polymeric micelles to deliver photosensitizers for photodynamic therapy. *Advanced Drug Delivery Reviews, 56*(1), 9-16.

Vargas, A., Pegaz, B., Debefve, E., Konan-Kouakou, Y., Lange, N., Ballini, J. P., . . . Delie, F. (2004). Improved photodynamic activity of porphyrin loaded into nanoparticles: an in vivo evaluation using chick embryos. *International Journal of Pharmaceutics, 286*(1-2), 131-145.

Vasir, J. K., & Labhasetwar, V. (2008). Quantification of the force of nanoparticle-cell membrane interactions and its influence on intracellular trafficking of nanoparticles. *Biomaterials, 29*(31), 4244-4252.

Verma, S., Watt, G. M., Mai, Z., & Hasan, T. (2007). Strategies for enhanced photodynamic therapy effects. *Photochemistry and Photobiology, 83*(5), 996-1005.

Verrecchia, T., Spenlehauer, G., Bazile, D. V., Murry-Brelier, A., Archimbaud, Y., & Veillard, M. (1995). Non-stealth (poly(lactic acid/albumin)) and stealth (poly(lactic acid-polyethylene glycol)) nanoparticles as injectable drug carriers. *Journal of Controlled Release, 36*(1–2), 49-61.

Vert, M., Mauduit, J., & Li, S. (1994). Biodegradation of PLA/GA polymers: increasing complexity. *Biomaterials, 15*(15), 1209-1213.

Vicent, M. J., Ringsdorf, H., & Duncan, R. (2009). Polymer therapeutics: clinical applications and challenges for development. *Adv Drug Deliv Rev, 61*(13), 1117-1120.

von Erlach, T., Zwicker, S., Pidhatika, B., Konradi, R., Textor, M., Hall, H., & Luhmann, T. (2011). Formation and characterization of DNA-polymer-condensates based on poly(2-methyl-2-oxazoline) grafted poly(L-lysine) for non-viral delivery of therapeutic DNA. *Biomaterials, 32*(22), 5291-5303.

Voon, S. H., Kiew, L. V., Lee, H. B., Lim, S. H., Noordin, M. I., Kamkaew, A., . . . Chung, L. Y. (2014). In vivo studies of nanostructure-based photosensitizers for photodynamic cancer therapy. *Small, 10*(24), 4993-5013.

Wang, Q., Du, Y.-M., Fan, L.-H., Liu, H., & Wang, X.-H. (2003). Structures and Properties of Chitosan-Starch-Sodium Benzoate Blend Films. *Wuhan University Journal (Natural Science Edition), 6*, 013.

Wang, S., Fan, W., Kim, G., Hah, H. J., Lee, Y. E., Kopelman, R., . . . Pandey, R. K. (2011a). Novel methods to incorporate photosensitizers into nanocarriers for cancer treatment by photodynamic therapy. *Lasers in Surgery and Medicine, 43*(7), 686-695.

Wang, Q., Gu, Z., Jamal, S., Detamore, M. S., & Berkland, C. (2013a). Hybrid hydroxyapatite nanoparticle colloidal gels are injectable fillers for bone tissue engineering. *Tissue Engineering. Part A, 19*(23-24), 2586-2593.

Wang, S., Gao, R., Zhou, F., & Selke, M. (2004). Nanomaterials and singlet oxygen photosensitizers: potential applications in photodynamic therapy. *Journal of Materials Chemistry, 14*(4), 487-493.

Wang, Z.-J., He, Y.-Y., Huang, C.-G., Huang, J.-S., Huang, Y.-C., An, J.-Y., . . . Jiang, L.-J. (1999). Pharmacokinetics, tissue distribution and photodynamic therapy efficacy of liposomal-delivered hypocrellin A, a potential photosensitizer for tumor therapy. *Photochemistry and Photobiology, 70*(5), 773-780.

Wang, S., Huang, P., Nie, L., Xing, R., Liu, D., Wang, Z., . . . Chen, X. (2013b). Single continuous wave laser induced photodynamic/plasmonic photothermal therapy using photosensitizer-functionalized gold nanostars. *Advanced Materials, 25*(22), 3055-3061.

Wang, Q., Jamal, S., Detamore, M. S., & Berkland, C. (2011b). PLGA-chitosan/PLGA-alginate nanoparticle blends as biodegradable colloidal gels for seeding human umbilical cord mesenchymal stem cells. *Journal of Biomedical Materials Research. Part A, 96*(3), 520-527.

Wang, A. Z., Langer, R., & Farokhzad, O. C. (2012). Nanoparticle delivery of cancer drugs. *Annual Review of Medicine, 63*, 185-198.

Wang, Z., Liu, W., Xu, H., & Yang, X. (2007). Preparation and in vitro Studies of Stealth PEGylated PLGA Nanoparticles as Carriers for Arsenic Trioxide*. *Chinese Journal of Chemical Engineering, 15*(6), 795-801.

Weersink, R. A., Bogaards, A., Gertner, M., Davidson, S. R., Zhang, K., Netchev, G., . . . Wilson, B. C. (2005). Techniques for delivery and monitoring of TOOKAD (WST09)-mediated photodynamic therapy of the prostate: clinical experience and practicalities. *Journal of Photochemistry and Photobiology. B, Biology, 79*(3), 211-222.

Whitacre, C. M., Feyes, D. K., Satoh, T., Grossmann, J., Mulvihill, J. W., Mukhtar, H., & Oleinick, N. L. (2000). Photodynamic therapy with the phthalocyanine photosensitizer Pc 4 of SW480 human colon cancer xenografts in athymic mice. *Clinical Cancer Research, 6*(5), 2021-2027.

Wolinsky, J. B., & Grinstaff, M. W. (2008). Therapeutic and diagnostic applications of dendrimers for cancer treatment. *Advanced Drug Delivery Reviews, 60*(9), 1037-1055.

Wu, L., & Burgess, K. (2008). A new synthesis of symmetric boraindacene (BODIPY) dyes. *Chemical Communications*(40), 4933-4935.

Xu, P., Gullotti, E., Tong, L., Highley, C. B., Errabelli, D. R., Hasan, T., . . . Yeo, Y. (2009). Intracellular drug delivery by poly(lactic-co-glycolic acid) nanoparticles, revisited. *Molecular Pharmaceutics, 6*(1), 190-201.

Yallapu, M. M., Gupta, B. K., Jaggi, M., & Chauhan, S. C. (2010). Fabrication of curcumin encapsulated PLGA nanoparticles for improved therapeutic effects in metastatic cancer cells. *Journal of Colloid and Interface Science, 351*(1), 19-29.

Yamamoto, Y., Nagasaki, Y., Kato, Y., Sugiyama, Y., & Kataoka, K. (2001). Long-circulating poly(ethylene glycol)–poly(d,l-lactide) block copolymer micelles with modulated surface charge. *Journal of Controlled Release, 77*(1–2), 27-38.

Yamaoka, T., Tabata, Y., & Ikada, Y. (1994). Distribution and tissue uptake of poly(ethylene glycol) with different molecular weights after intravenous administration to mice. *Journal of Pharmaceutical Sciences, 83*(4), 601-606.

Yameen, B., Choi, W. I., Vilos, C., Swami, A., Shi, J., & Farokhzad, O. C. (2014). Insight into nanoparticle cellular uptake and intracellular targeting. *Journal of Controlled Release*.

Yang, Y., Wang, S., Wang, Y., Wang, X., Wang, Q., & Chen, M. (2014). Advances in self-assembled chitosan nanomaterials for drug delivery. *Biotechnology Advances, 32*(7), 1301-1316.

Yogo, T., Urano, Y., Ishitsuka, Y., Maniwa, F., & Nagano, T. (2005). Highly Efficient and Photostable Photosensitizer Based on BODIPY Chromophore. *Journal of the American Chemical Society, 127*(35), 12162-12163.

Yokoyama, M. (2011). Clinical Applications of Polymeric Micelle Carrier Systems in Chemotherapy and Image Diagnosis of Solid Tumors. *Journal of Experimental & Clinical Medicine, 3*(4), 151-158.

Zamboni, W. C. (2008). Concept and clinical evaluation of carrier-mediated anticancer agents. *Oncologist, 13*(3), 248-260.

Zaruba, K., Kralova, J., Rezanka, P., Pouckova, P., Veverkova, L., & Kral, V. (2010). Modified porphyrin-brucine conjugated to gold nanoparticles and their application in photodynamic therapy. *Organic & Biomolecular Chemistry, 8*(14), 3202-3206.

Zeng, X., Morgenstern, R., & Nyström, A. M. (2014). Nanoparticle-directed sub-cellular localization of doxorubicin and the sensitization breast cancer cells by circumventing GST-Mediated drug resistance. *Biomaterials, 35*(4), 1227-1239.

Zhang, F., Liu, M. R., & Wan, H. T. (2014). Discussion about several potential drawbacks of PEGylated therapeutic proteins. *Biological and Pharmaceutical Bulletin, 37*(3), 335-339.

Zhang, J. X., Hansen, C. B., Allen, T. M., Boey, A., & Boch, R. (2003). Lipid-derivatized poly(ethylene glycol) micellar formulations of benzoporphyrin derivatives. *Journal of Controlled Release, 86*(2–3), 323-338.

Zhang, L., Gu, F. X., Chan, J. M., Wang, A. Z., Langer, R. S., & Farokhzad, O. C. (2008a). Nanoparticles in medicine: therapeutic applications and developments. *Clinical Pharmacology and Therapeutics, 83*(5), 761-769.

Zhang, P., Steelant, W., Kumar, M., & Scholfield, M. (2007). Versatile photosensitizers for photodynamic therapy at infrared excitation. *Journal of the American Chemical Society, 129*(15), 4526-4527.

Zhang, Q., Iwakuma, N., Sharma, P., Moudgil, B. M., Wu, C., McNeill, J., . . . Grobmyer, S. R. (2009). Gold nanoparticles as a contrast agent for in vivo tumor imaging with photoacoustic tomography. *Nanotechnology, 20*(39), 395102.

Zhang, X. Q., Xu, X., Bertrand, N., Pridgen, E., Swami, A., & Farokhzad, O. C. (2012). Interactions of nanomaterials and biological systems: Implications to personalized nanomedicine. *Adv Drug Deliv Rev, 64*(13), 1363-1384.

Zhang, Z., Vaisocherová, H., Cheng, G., Yang, W., Xue, H., & Jiang, S. (2008b). Nonfouling Behavior of Polycarboxybetaine-Grafted Surfaces: Structural and Environmental Effects. *Biomacromolecules, 9*(10), 2686-2692.

Zheng, X., Baker, H., Hancock, W. S., Fawaz, F., McCaman, M., & Pungor, E., Jr. (2006). Proteomic analysis for the assessment of different lots of fetal bovine serum as a raw material for cell culture. Part IV. Application of proteomics to the manufacture of biological drugs. *Biotechnology Progress, 22*(5), 1294-1300.

LIST OF PUBLICATIONS AND PAPERS PRESENTED

A) Research Presentations

i. **Poster presentation at Faculty of Medicine Research Week (FOMRW) 2015: From Powder to Pill & Pill to Heal, University Malaya, Kuala Lumpur Malaysia, 11th – 15th May 2015.**

Chitosan decorated poly(lactic-co-glycolic acid)-diiodinated boron dipyrromethene nanoparticles improved stealth properties and tumor selectivity in photodynamic cancer therapy (Awarded 3rd Prize as the Best Poster Presenter)

[1]Voon, S-H; [2]Tiew, S-X; [1]Kue, C-S; [3]Lee, H-B; [1]Kiew, L-V; [2]Misran, M; [4]Kamkaew, A; [4]Burgess, K; [3]Chung, L-Y

[1]Department of Pharmacology, Faculty of Medicine, University Malaya, Lembah Pantai, Kuala Lumpur, 50603, Malaysia

[2]Department of Chemistry, Faculty of Science, University of Malaya, Lembah Pantai, Kuala Lumpur, 50603, Malaysia

[3]Department of Pharmacy, Faculty of Medicine, University of Malaya, Lembah Pantai, Kuala Lumpur, 50603, Malaysia

[4]Department of Chemistry, Texas A&M University, College Station Texas 77842, United States

ii. Oral presentation at Controlled Release & Drug Delivery Symposium (CRDDS) 2015 in conjunction with The 1st MyCRS Scientific Conference: Targeted Delivery – Translating Ideas into New Technology, Kuala Lumpur, Malaysia, 15th – 16th August 2015.

Chitosan Decorated Polymeric Nanoparticles Improved Stealth Properties and Tumor Selectivity in Photodynamic Cancer Therapy *In Vitro* and *In Vivo*

S. H. Voon[1], S. X. Tiew[2], C. S. Kue[1], H. B. Lee[3], L. V. Kiew[1], M. Misran[2], A. Kamkaew[4], K. Burgess[4], and L. Y. Chung[3]

[1]Department of Pharmacology, Faculty of Medicine, University Malaya, Lembah Pantai, Kuala Lumpur, 50603, Malaysia

[2]Department of Chemistry, Faculty of Science, University of Malaya, Lembah Pantai, Kuala Lumpur, 50603, Malaysia

[3]Department of Pharmacy, Faculty of Medicine, University of Malaya, Lembah Pantai, Kuala Lumpur, 50603, Malaysia

[4]Department of Chemistry, Texas A&M University, College Station Texas 77842, United States

B) Publications

i. SH Voon, LV Kiew, HB Lee, SH Lim, MI Noordin, A Kamkaew, K Burgess, LY Chung. 2014. ***In vivo*** **studies of nanostructure-based photosensitisers for photodynamic cancer therapy.** Small. 10(24): 4993 – 5013. (IF: 8.368)

ii. SH Voon, SX Tiew, CS Kue, HB Lee, LV Kiew, M Misran, A Kamkaew, K Burgess, and LY Chung. 2015. **Chitosan-coated poly(lactic-co-glycolic acid)-diiodinated boron-dipyrromethene nanoparticles improve tumor selectivity and stealth properties in photodynamic cancer therapy.** Journal of Biomedical Nanotechnology. 12(7): 1431-1452.

APPENDICES

Appendix A. Synthesis and Characterisation of Diiodinated-Boron Dipyrromethene

3,5-Dimethyl-1H-pyrrole-2-carbaldehyde **1** (246 mg, 2 mmol) was dissolved in 10 ml CH_2Cl_2 and POCl3 (0.22 ml, 2.4 mmol) was added dropwise over 1 min at 0 ℃. The solution was then warmed to room temperature slowly and stirred for 12 h. Subesequently, the mixture was cooled to 0 ℃ and Et_3N (1.4 ml, 10 mmol) was added dropwise over 5 min. After stirring for 15 min, BF_3OEt_2 (2.0 ml, 16 mmol) was added dropwise to the solution over 5 min. The reaction mixture was then warmed to room temperature and stirred for 12 h. To remove the polar impurities, the mixture was passed through a short pad of silica gel eluting with CH_2Cl_2. The solvents were removed under reduced pressure. The residue was dissolved in CH_2Cl_2 and water was added, and the mixture was stirred at room temperature overnight (to decompose excess BF_3OEt_2 and other impurities). The organic layer was washed with water, brine and dried over Na_2SO_4. The solvent was removed under reduced pressure and the residue was purified by flash chromatography (5 % EtOAc/hexanes) to give the pure product **2** (229 mg, 92 %) as a red solid. ^{1}H NMR ($CDCl_3$, 500 MHz) δ 7.01 (s, 1H), 6.02 (s, 2H), 2.51 (s, 6H), 2.22 (s, 6H); ^{13}C NMR ($CDCl_3$, 125 MHz) δ 156.7, 141.2, 133.4, 120.0, 119.0, 14.6, 11.2; ^{19}F NMR ($CDCl_3$, 282 MHz) δ 30.68 (q, *J* = 33.5 Hz). HRMS (ESI) m/z calcd for $(M+H)^+$ $C_{13}H_{16}BF_2N_2$ 249.1375; found 249.1373 (Wu & Burgess, 2008).

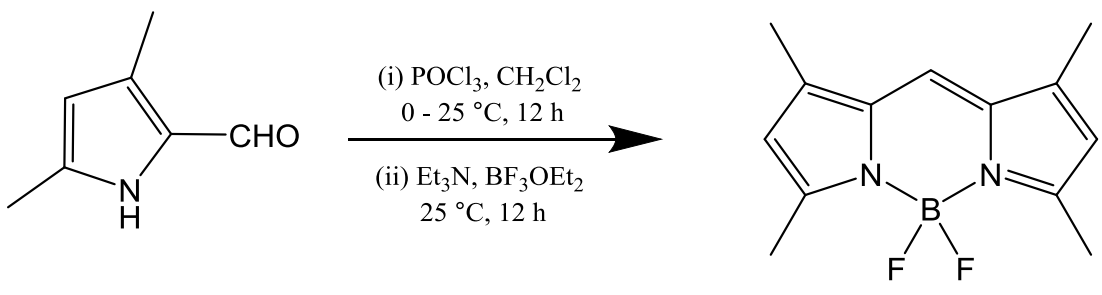

1 **2**

Iodic acid (2.0 eq.) dissolved in a minimum amount of water was added dropwise over 20 min to a solution of 4,4-difluoro-1,3,5,7-tetramethyl-4-bora-3a,4a-diaza-*s*-indacene **3** (1.0 eq.) and iodine (2.5 eq.) in EtOH. This mixture was then warmed for 20 min at 60 ℃. After cooling, the mixture was evaporated under vacuum. The crude product was purified by silica gel chromatography and recrystallized from chloroform and *n*-hexane to afford diiodinated-boron dipyrromethene **4** (yield 83 %) (Loudet & Burgess, 2007; T. Yogo *et al.*, 2005). ^{1}H-NMR ($CDCl_3$, 300 MHz): δ 2.22 (s, 6H); 2.54 (s, 6H); 7.10 (s, 1H). ^{13}C-NMR ($CDCl_3$, 75 MHz): δ 13.75, 15.68, 82.00, 120.22, 132.81, 144.35, 157.70. HRMS (ESI-): calcd for $[M - 1]^{-1}$; Found. 498.9186. Anal. Calcd for $C_{13}H_{13}BF_2I_2N_2$:N, 5.60; C, 31.24; H, 2.62. Found: N, 5.42; C, 31.39; H, 2.76 (T. Yogo *et al.*, 2005).

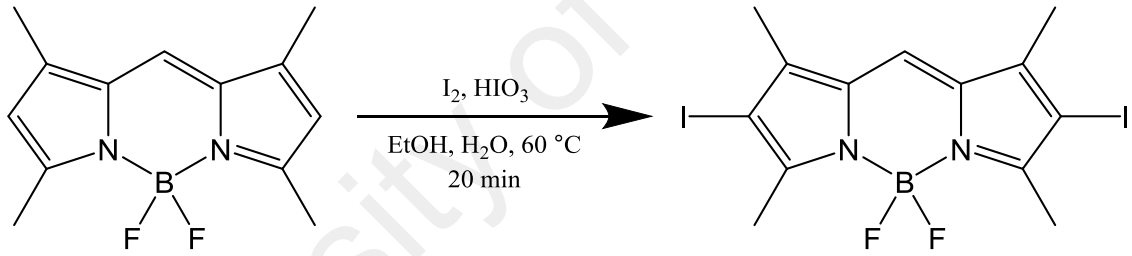

MeOH
ϕ 0.02 (0.1% (v/v) DMF as cosolvent)
λmax abs 534 nm
λmax emiss 548 nm

Appendix B. Animal ethics approval letter

UNIVERSITY OF MALAYA
KUALA LUMPUR

19th September 2014

Voon Siew Hui
Department of Pharmacology
Faculty of Medicine

Dear Researcher,

Evaluation of maximal tolerated dose (MTD) and efficacies of photosensitizers encapsulated with polymeric nano-carrier in targeting tumours

This is to inform you that the FOM Institutional Animal Care and Use Committee, University of Malaya (FOM IACUC) has approved your Animal Use Protocol with the above mentioned title for a duration of three (3) years until **September 2017.**

Please be advised that should you require changes to be made to the approved protocol, you are responsible to submit an application for amendments. Failure to do so may result in the Approval of your Animal Research Protocol be withdrawn by FOM IACUC.

Your Ethics Reference no. : **2014-09-11/PHAR/R/VSH**

Thank you.

Yours sincerely,

Professor Dr. Sim Si Mui
Chairperson
Faculty of Medicine Institutional Animal Care and Use Committee (FOM IACUC)

Faculty of Medicine Institutional Animal Care and Use Committee (FOM IACUC)
Deputy Dean (Research), Faculty of Medicine, University of Malaya, 50603, Kuala Lumpur, MALAYSIA
Tel: (603) 7967 7515 • Fax: (603) 7956 6941• E-mail: [illegible]
• Website: http://www.reform.com